BMU
BAKI MÜHƏNDİSLİK UNİVERSİTETİ

ISSN 2521-6317

Journal of Baku Engineering University

ADVANCES in CHEMISTRY and CHEMICAL ENGINEERING

Volume 9
Number 1
2025

Journal is published twice a year
Number - 1. June, Number - 2. December

An International Journal

http://journal.beu.edu.az

Contact address

Journal of Baku Engineering University
AZ0101, Khirdalan city, Hasan Aliyev str. 120, Absheron, Baku, Azerbaijan
Tel: *00 994 12 - 349 99 95* ***Fax:*** *00 994 12 349-99-90/91*
e-mail: *chemstrybiology@beu.edu.az,* *journal@beu.edu.az*
web: *http://journal.beu.edu.az*
facebook: *Journal Of Baku Engineering University*

ISSN 2521-6317

ISSN 2521-6317

Journal of Baku Engineering University

ADVANCES IN CHEMISTRY AND CHEMICAL ENGINEERING

Baku - AZERBAIJAN

J O U R N A L O F B A K U E N G I N E E R I N G U N I V E R S I T Y
ADVANCES IN CHEMISTRY AND CHEMICAL ENGINEERING
2025. Volume 9, Number 1

CONTENTS

UDC: 547.13
DOI: https://doi.org/10.30546/2521-6317.2025.01.489

SYNTHESIS OF Fe METAL COMPLEX BASED ON A TRIAZAPENTADIENE-TYPE LIGAND DERIVED FROM A PYRAZOLE SUBSTRUCTURE

Gamza YAHYAYEVA*[1,2], İbadulla MAHMUDOV[3,4], Abel MAHARRAMOV[1], Sara HASANOVA[2], Victor N. KHRUSTALEV[5], Namiq SHIKHALIYEV[3]

[1] *Organic Chemistry Department, Baku State University, Z. Khalilov str. 23, AZ 1148, Baku, Azerbaijan,*

[2] *Chemistry and physics Department, Azerbaijan University of Architecture and Construction, Ayna Sultanova str, Baku, Azerbaijan,*

[3] *Department of Chemical Engineering, Baku Engineering University, Hasan Aliyev str, AZ0101, Baku, Azerbaijan,*

[4]*Institute of Chemistry of Additives name of A.M. Guliyev, Beyukshor Highway, Block 2062, Baku, AZ 1029, Baku, Azerbaijan*

[5]*RUDN University, Moscow, Russian Federation*

ARTICLE INFO

Article history
Received:2025-12-04
Received in revised form:2025-12-08
Accepted:2025-12-14
Available online

Keywords:
Pyrazole,
Metal complexes,
N-ligands

ABSTRACT

Three-component reactions are often characterized by complex mechanistic pathways, and the identification of intermediate species is essential for understanding their progression. In this study, a pyrazole-based ligand was synthesized, and its reaction with malononitrile and o-tolualdehyde was examined with the aim of obtaining triazine-containing heterocycles. Two products were detected by TLC and their structures were confirmed by single-crystal X-ray diffraction. The desired triazine derivative was successfully obtained; however, the formation of (2-methylbenzylidene) propanedinitrile—arising from a Knoevenagel condensation between malononitrile and o-tolualdehyde—was also observed. Although initially detected as an unexpected by-product of the three-component reaction, its appearance is fully consistent with the well-known propensity of malononitrile to readily condense with aromatic aldehydes. The reduced reactivity of the imine functionality, attributed to the ligand being present in its salt form, was identified as the key factor limiting full conversion toward the triazine scaffold. Considering the coordination ability of triazapentadiene-type ligands, an Fe(III) complex of the pyrazole-derived ligand was also synthesized within the scope of this work.

* *Corresponding author.*
E-mail addresses: gamza.yahyayeva@azmiu.edu.az (Gamza Y.Yahyayeva).

1. Introduction

Determining the course of three-component reactions is one of the major challenges in modern organic synthesis. These types of reactions are generally studied using DFT methods. However, in some cases, elucidating the structures of intermediates formed at early stages can greatly facilitate understanding the direction in which the reaction proceeds. The reaction between dicyandiamide and pyrazole has been shown to afford (E) 1-(amino(1H-pyrazol-1-yl) methylene) guanidine [1], demonstrating that this transformation can occur under typical condensation conditions. Recent studies have emphasized that pyrazole-based aza-heterocycles are highly

versatile pharmacophores with broad therapeutic relevance, extensive reactivity, and widespread applications in synthetic and medicinal chemistry. Biguanides are a versatile class of compounds with broad applications in catalysis, metal complexation, organic synthesis, and medicinal chemistry, including well-known examples such as metformin and chlorhexidine, highlighting both their historical importance and renewed interest in developing new synthetic methodologies to expand their chemical diversity [2]. Efficient and environmentally friendly methods have been established for synthesizing monosubstituted biguanides from amines, utilizing high-yielding, chromatography-free, and water-compatible protocols, which are particularly effective for challenging aliphatic amines [3]. Incorporation of guanidine and biguanidine groups into chlorin derivatives enables the design of targeted photosensitizers with high photodynamic efficiency, offering a versatile platform for multifunctional drug development and improved selectivity in cancer therapy [4]. Comprehensive reviews further demonstrate that modern methodologies enable the efficient preparation of functionalized pyrazole derivatives from numerous precursors while revealing their notable anti-cancer, anti-inflammatory, anti-bacterial, and anti-viral activities [5]. Metal complexes of pyrazoles and other nitrogen-based heterocycles have attracted growing attention due to their diverse bioactivities, and understanding the relationship between their structural features and biological effects is essential for designing more effective and less toxic therapeutic agents [6]. Recent findings on azo dye–based pyrazole ligands and their transition-metal complexes demonstrate that such systems can be synthesized and structurally validated through comprehensive spectroscopic, thermal, and computational analyses, typically forming paramagnetic octahedral geometries. Moreover, these studies show that both the free ligands and their metal complexes exhibit notable antimicrobial and cytotoxic activities, with certain Fe(II) and Co(II) complexes displaying particularly enhanced biological efficacy [7]. Computational analyses, including NBO, QTAIM, and molecular docking, have additionally shown that pyrazole-based systems often possess favorable electronic distributions and strong biomolecular interactions, supporting their therapeutic potential [8]. In parallel, biguanide derivatives have demonstrated promising applications as organic linkers in coordination polymers and metal–organic frameworks, facilitating structural tunability and selective gas adsorption [9]. Recent mechanistic investigations revealed that substituent effects, solvent polarity, and acid–base properties strongly influence the reactivity of dicyandiamide-based condensation systems, enabling controlled access to structurally diverse heterocycles [10]. Advances in catalyst-assisted synthetic strategies, including transition-metal catalysis and organocatalysis, have further expanded the chemical space of pyrazole-containing frameworks under milder and more sustainable reaction conditions [11]. The pharmaceutical relevance of pyrazole derivatives continues to grow, with several compounds progressing into clinical evaluation for metabolic, neurological, and inflammatory disorders [12]. Additionally, multi-component reactions involving amidines, malononitrile, and aromatic aldehydes have emerged as powerful tools for rapidly constructing nitrogen-rich scaffolds with high atom economy and structural diversity [13]. Structure–activity relationship (SAR) studies have shown that introducing electron-withdrawing substituents or heteroaromatic fragments into pyrazole or biguanide cores can significantly enhance antimicrobial, antioxidant, and enzyme-inhibitory properties [14]. Recent studies demonstrated that pyrazole-based thiocarbohydrazide Schiff bases exhibit strong COX-2 binding affinity, supported by spectroscopic characterization and molecular docking analyses, suggesting their potential as promising anti-inflammatory agents. [15].

2. Experimental part

Materials and methods

All reagents — including the pyrazole derivatives, malononitrile, *o*-tolualdehyde, and iron (III) chloride hydrate — were purchased from commercial suppliers and used without further purification unless otherwise stated. The solvents were of analytical grade and employed as received. Infrared spectra were recorded using a standard FT-IR spectrometer, and elemental analyses were carried out at an accredited analytical laboratory. Single-crystal X-ray diffraction data were collected on a modern diffractometer equipped with a CCD detector.

2.1 Synthesis of pyrazole-based ligand ((E)-1-[amino(1H-pyrazol-1-yl)methylene]guanidinium chloride)

The ligand derived from pyrazole was synthesized by heating a mixture of pyrazole (12 mmol), cyanoguanidine (12 mmol), hydrochloric acid (12 mmol), and 3 ml of deionized water at 80 °C for 30 minutes. After the reaction mixture was cooled to room temperature, white crystalline products formed, which were subsequently filtered and collected. The obtained ligand was characterized using various analytical techniques, including FT-IR spectroscopy and single-crystal X-ray diffraction.

2.2 Three-component reaction

A mixture of (E)-1-[amino(1H-pyrazol-1-yl)methylene]guanidinium chloride (188 mg, 1 mmol), o-tolualdehyde (120 mg, 1 mmol) and malononitrile (66 mg, 1 mmol) was refluxed in methanol for 5 h. The solvent was subsequently removed in vacuo, and the residue was recrystallized from methanol using charcoal.Although the main goal was to obtain a triazine-based product, the reaction did not proceed through a single, clean pathway.

Alongside the expected heterocyclic compound, we also detected a second product**-(2-methylbenzylidene) propanedinitrile**. This by-product formed independently through a typical **Knoevenagel condensation** between malononitrile and *o*-tolualdehyde. Its appearance can be explained by the high reactivity of malononitrile toward aldehydes and by the fact that the ligand, present in its salt form, shows reduced nucleophilicity, limiting its involvement in the cyclization process.

As a result, the three-component reaction produced both the desired triazine-containing compound and the Knoevenagel condensation product, providing additional insight into the competitive pathways operating within the reaction mixture.

2.3 Synthesis of (2-methylbenzylidene)propanedinitrile via Knoevenagel Condensation

The compound (2-methylbenzylidene) propanedinitrile was formed through a classical Knoevenagel condensation between malononitrile and o-tolualdehyde. Although it first emerged as an unexpected side product during the three-component reaction, its appearance is fully in line with the well-known tendency of malononitrile to readily condense with aromatic aldehydes. During purification, the compound was isolated in a stable, crystalline form, and **high-quality single crystals suitable for X-ray diffraction were successfully obtained**, enabling precise structural verification. The identification of this product not only confirmed the presence of competing reaction pathways under the applied conditions but also provided a clearer picture of how these parallel processes influence the overall product distribution.

2.4 Synthesis of Fe (III) Complex of a Pyrazole-Based Ligand

The ligand and metal salt were separately dissolved in 3–4 ml of methanol and then combined at room temperature. Afterward, an additional small portion of the metal salt was dissolved in methanol (3–4 ml) and added to the mixture. Once the reaction had finished, 2–3 drops of sodium hydroxide were introduced, and the solution was allowed to recrystallize from methanol. The resulting metal complex was thoroughly characterized using infrared spectroscopy and elemental analysis.

3. Result and discussion

3.1 Reaction and X-ray images of (E)-N`-(diaminomethyl)-1H-pyrazole-carboximidamide

Considering the biological importance of pyrazole and its derivatives, we prepared pyrazole-based ligands derived from cyanoguanidine and pyrazole, as outlined in Scheme 1.

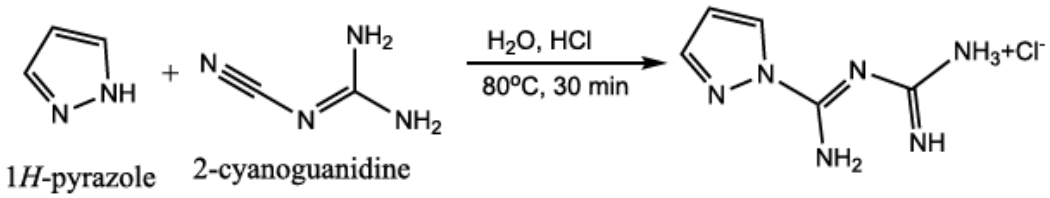

Scheme 1. Synthesis of pyrazole-based ((E)-N′-(diaminomethyl) 1H-pyrazole-1-carboximidamide).

The ligand (E)-1-(amino(1H-pyrazol-1-yl)methylene) guanidinium chloride was synthesized through a nucleophilic addition reaction, in which the amine nitrogen of pyrazole attacks the cyano group of dicyandiamide under acidic conditions. When the same transformation is attempted under basic conditions—using sodium hydroxide instead of hydrochloric acid—the reaction yields complex product mixtures that are difficult to isolate and characterize. Owing to continuous protonation, all five nitrogen atoms within the (E)-1-(amino(1H-pyrazol-1-yl)methylene) guanidinium chloride framework are capable of coordinating to metal centers. The cationic structure of the (E)-1-(amino(1H-pyrazol-1-yl)methylene) guanidine unit is illustrated in Figure 1.

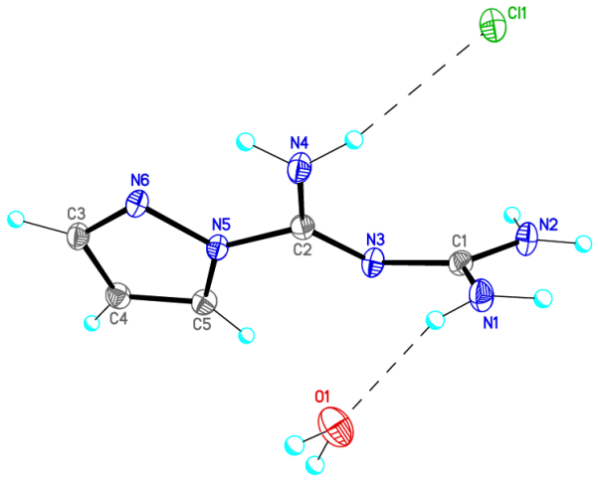

Figure 1. X-ray images of (E)-1-(amino(1H-pyrazol-1-yl)methylene)guanidine.

3.2 **X-ray images *of (2-methylbenzylidene)propanedinitrile***

As shown in **Figure 2,** single-crystal X-ray analysis confirms that the (2-methylbenzylidene) propanedinitrile molecule adopts the expected E-configuration around the C=C double bond. The dinitrile fragment (C1–C10–N1 and C1–C11–N2) is almost linear relative to the benzylidene moiety, which is typical for C≡N groups. The aromatic ring (C3–C9) is planar, with the o-methyl substituent (C8–C7–C6 direction) causing a slight, noticeable deviation from the ring plane. The geometry around C2 supports effective π-conjugation across the molecule, consistent with the electron-withdrawing nature of the cyano groups. Overall, **Figure 2** illustrates the structural integrity and electronic characteristics of the synthesized compound.

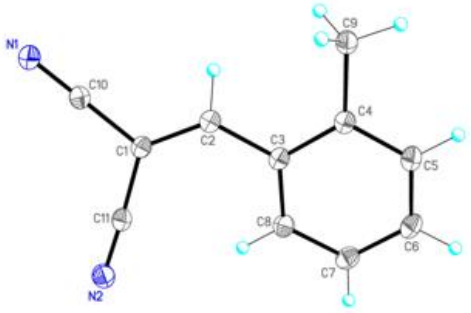

Figure 2. X-ray images of (2-methylbenzylidene) propanedinitrile.

3.3 ***Synthesis reaction of Fe(III) complex of a Pyrazole-Based Ligand***

As illustrated in **Scheme 2**, the complex with the formula ($C_{36}H_{81}Cl_9Fe_8N_{36}O_{21}$) was prepared by reacting the H_5L•HCl ligand with $FeCl_3{\cdot}6H_2O$ in methanol.

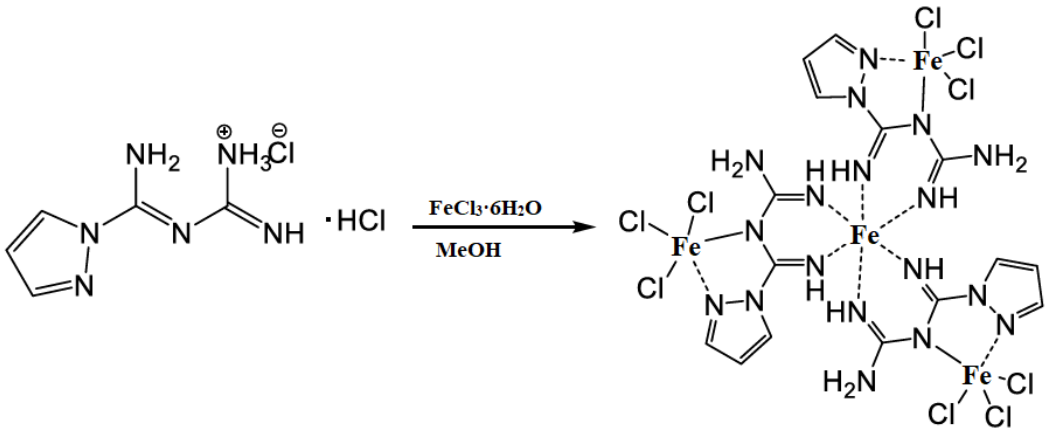

Scheme 2. Synthesis of Fe (III) metal complex of pyrazole-based ligand.

Yield of the reaction 85,7 per cent, conversion 90 percent and analytic values given below.

The average atomic masses employed in the calculations were: C 12.011, H 1.008, N 14.007, O 15.999, Cl 35.453, and Fe 55.845. Based on these values, the molecular weight of the complex was calculated as M_r = 2120.112 g·mol^{-1} (36×12.011 + 81×1.008 + 9×35.453 + 8×55.845 + 36×14.007 + 21×15.999 = 2120.112).

The calculated elemental composition of the complex is as follows:
C 20.39 %, H 3.85 %, N 23.78 %, Cl 15.05 %, Fe 21.07 %, and O 15.85 %.

FT-IR analysis reveals that the characteristic ligand-based vibrational modes—ν(O–H), ν(N–H), ν(C=O), and ν(C=N)—are retained upon coordination, appearing in their typical regions (approximately 3270–3380, 2950, 1620, and 1585 cm^{-1}, respectively). In contrast, metal-centered vibrations attributable to Fe–Cl and Fe–N bonding emerge in the lower-frequency domain (ca. 250–600 cm^{-1}), consistent with the formation of the corresponding coordination environment.

4. Conclusion

Pyrazole-based ligands were successfully synthesized from pyrazole and cyanoguanidine and fully characterized using single-crystal X-ray diffraction. The three-component reaction with o-tolualdehyde and malononitrile produced both the target triazine compound and the Knoevenagel condensation by-product, (2-methylbenzylidene) propanedinitrile, revealing competing reaction pathways. The Fe(III) complex of the pyrazole-based ligand was prepared in methanol and confirmed by elemental analysis. Overall, these results demonstrate that the ligand efficiently forms stable metal complexes with precise molecular architectures. This study provides a clear foundation for exploring the biological activity of these complexes, including their potential as enzyme inhibitors.

It is easy to transfer electron bridge between Fe-S in the natural proteins and electron and magnetic interaction via bridges between Fe-Fe. The value of metal Fe is increase because of its amount, price and eco- friendly last and catalytic and electrochemistry usage. Same complex has various properties like magnetic, catalytic and electrochemical and it is possible use multiple areas. Pyrazole based ligand carry out easy electron and steric change properties and it makes easy to control magnet changes around it.

Potential application Fe based pyrazole ligand is also possible to make oxidation reduction processes, various magnet materials, for enzyme change reaction and also specific bridge interaction.

REFERENCES

1. Mahmudov, I., Atioğlu, Z., Akkurt, M., Abdullayev, Y., Sujayev, A., & Bhattarai, A. (2022). *Crystal structure and Hirshfeld surface analysis of 2-(4-amino-6-phenyl-1,2,5,6-tetrahydro-1,3,5-triazin-2-ylidene) malononitrile dimethylformamide hemisolvate*. *Acta Crystallographica Section E: Crystallographic Communications, 78*, 691–695. https://doi.org/10.1107/S2056989022006910
2. *Grytsai, O., Ronco, C., & Benhida, R. (2021). Synthetic accesses to biguanide compounds. Organic & Biomolecular Chemistry, 19(20), 4441–4458.* https://doi.org/10.*3762/bjoc.17.82*
3. *Bardovskyi, R., Fabre, M., Ronco, C., & Benhida, R. (2021). Mild Biamidine-Transfer Conditions for the Synthesis of Aliphatic Biguanides. SynOpen, 5(4), 314–320.* https://doi.org/10.1055/a-1681-4544
4. Ostroverkhov, P. V., Kirin, N. S., Tikhonov, S. I., Usachev, M. N., Abramova, O. B., Kaplan, M. A., Mironov, A. F., & Grina, M. A. (2021). *Guanidine and biguanidine derivatives of natural chlorins: Synthesis and biological assessment*. **Journal of Porphyrins and Phthalocyanines, 25**(12), 1390–1403. https://doi.org/10.6060/mhc224071o
5. Moussa, Z., Ramanathan, M., Alharmoozi, S. M., Alkaabi, S. A. S., Al Aryani, S. H. M., Ahmed, S. A., & Al-Masri, H. T. (2024). *Recent highlights in the synthesis and biological significance of pyrazole derivatives*. *Heliyon, 10*(20), e38894. https://doi.org/10.1016/j.heliyon.2024.e38894
6. Malinowska, K., Lorenz, I.–P., Sadowska, B., & Mucha, P. (2019). *Metal ion complexes with pyrazoles, aziridines and diaziridines – synthesis and biological activity*. *Current Medicinal Chemistry, 26*(4), 648–663. https://doi.org/10.2174/0929867325666180221124447
7. Alkurdi, A. F., AlJahdali, M. Sh., & Alshehri, A. A. (2022). *Synthesis, characterization, DFT calculation, and biological activity of pyrazole-based azo-metal(II) complexes*. *Results in Chemistry, 4*, Article 100457. https://doi.org/10.1016/j.rechem.2022.100566

8. Ebenezer, O., Singh-Pillay, A., Koorbanally, N. A., & Singh, P. (2020). *Antibacterial evaluation and molecular docking studies of pyrazole-thiosemicarbazones and their pyrazole-thiazolidinone conjugates*. **Medicinal Chemistry Research**. Advance online publication. https://doi.org/10.1007/s11030-020-10046-w
9. Veisi, H., Abrifam, M., Kamangar, S. A., Pirhayati, M., Saremi, S. G., Noroozi, M., … & Karmakar, B. (2021). Pd immobilization on biguanidine-modified Zr-UiO-66 MOF: synthesis, characterization, and application as a reusable heterogeneous catalyst. *Scientific Reports, 11*, 21883. https://doi.org/10.1038/s41598-021-00991-3
10. Kunishima, M., Kitamura, M., Tanaka, H., Nakakura, I., Moriya, T., & Hioki, K. (2013). Study of 1,3,5-triazine-based catalytic amide-forming reactions: Effect of solvents and basicity of reactants. *Chemical & Pharmaceutical Bulletin, 61*(8), 882–886. https://doi.org/10.1248/cpb.c13-00368
11. Lin, W.-S., & Kuwata, S. (2023). Recent developments in reactions and catalysis of protic pyrazole complexes. *Molecules, 28*(8), 3529. https://doi.org/10.3390/molecules28083529
12. Ahmed, A., Zaib, S., Bhat, M. A., Saeed, A., Altaf, M. Z., Zahra, F. T., Shabir, G., Rana, N., & Khan, I. (2024). Acyl pyrazole sulfonamides as new antidiabetic agents: Synthesis, glucosidase inhibition studies, and molecular docking analysis. *Frontiers in Chemistry, 12*, Article 1380523. https://doi.org/10.3389/fchem.2024.1380523
13. Liu, Y., & Wheeler, S. E. (2024). Impact of solvent dielectric and protonation state on rotational barriers in protonated 1,3,5-triazines. *Journal of Organic Chemistry, 89*(8), 5480–5484. https://doi.org/10.1021/acs.joc.3c02918
14. Bhagwat, S. K., Pawar, T. J., Kulkarni, S. A., Patil, A. A., More, R. A., Jimenez-Halla, J. O. C., Alvarado-Salazar, J. A., Olivares-Romero, J. L., Muteeb, G., Delgado-Alvarado, E., & Patil, S. V. (2024). *Synthesis, characterization, biological activities, and computational studies of pyrazolyl–thiazole derivatives of thiophene*. *RSC Advances, 14*, 39004–39016. https://doi.org/10.1039/D4RA06228K
15. Abdul-Malik, M. A., Abdou, A., Fouad, M. R., Alkamali, A. S. N., & Abdel-Rahee, S. A. A. (2024). Synthesis, spectral characterization and molecular docking studies of some thiocarbohydrazide-based Schiff bases with pyrazole moiety as potential anti-inflammatory agents. *Current Chemistry Letters, 13*(4), 683–694. https://doi.org/10.5267/j.ccl.2024.5.002

UDC: 678.56+620.3
DOI: https://doi.org/10.30546/2521-6317.2025.01.463

INTEGRATION OF ASPEN PLUS AND NAMD FOR THE DESIGN AND OPTIMIZATION OF CHITOSAN-GRAPHENE OXIDE COMPOSITE HYDROGELS

Nizami AKBAROV[1], Narmina GULIYEVA[2]*, Elsun AZIZOV[3], Rasul RAHIMOV[2], Zulfiya JAVADOVA[2], Narmin ISMAYILOVA[2]

Department of Analytical and Organic Chemistry, Azerbaijan State Pedagogical University, Baku, Azerbaijan

[2]Department of Chemical Engineering, Baku Engineering University, Baku, Azerbaijan
[3]Institute for Chemistry and Processes for Energy, the Environment and Health (ICPEES), University of Strasbourg, Strasbourg, France

ARTICLE INFO

Article history:
Received:2025-10-27
Received in revised form:2025-10-27
Accepted:2025-12-16
Available online

Keywords:
chitosan, Aspen Plus, NAMD, graphene oxide, nanomaterials, water purification, membranes, chemical engineering, environmental applications.

ABSTRACT

This study explores the use of Aspen Plus and NAMD as powerful tools for the simulation and design of processes using chitosan as a component and its functionalized derivatives. By employing these digital platforms, researchers can effectively analyze and predict the performance potential of chitosan-derived systems, especially in applications related to bioengineering and environmental science. Their implementation significantly reduces the risk of errors during synthesis and structuring, improves product yield, and facilitates further functionalization of materials. Particular attention is given to the utilization of (GO) graphene oxide in water treatment technologies. The paper outlines a method for synthesizing GO and investigates the structural and functional characteristics of its surface layers. It also discusses the integration of GO into chitosan-based matrices for the development of advanced membrane systems showing enhanced ability to filter impurities. Empirical evidence proves that the application of digital modeling tools contributes to the optimization of research and development processes involving chitosan and (GO) graphene oxide, supporting the creation of innovative materials for environmental engineering purposes.

**Corresponding author:*
Narmina A. Guliyeva, e-mail: nquliyeva@beu.edu.az

INTRODUCTION

Aspen Plus is widely used in engineering and industry for optimization and design of chemical processes. Its capabilities include: process design, equipment modeling and simulation, environmental analysis, big data integration [1]. Aspen Plus is ideal for solving large-scale problems that require the consideration of aggregated properties of materials and systems [2]. NAMD ("Nanoscale Molecular Dynamics") is used in molecular dynamics to simulate the behavior of atoms and molecules. Key capabilities of NAMD include: biomolecular research, materials science, high performance computing, integration with visualizers [3]. NAMD is in demand in academic research, pharmaceuticals and materials science, where atomic level detail

is important [4]. Despite the differences in modeling scale, Aspen Plus and NAMD can complement each other. The use of Aspen Plus and NAMD continues to expand due to the following trends in biotechnology and organic synthesis to produce composite materials for medical and food engineering applications. Both approaches are crucial in fostering innovation within the field of sustainable materials and environmentally sound technologies. Chitosan, obtained by deacetylation of chitin, is a an altered form of a natural polysaccharide possessing remarkable physical, chemical, and biological characteristics, notably biocompatibility, biodegradability, and fat-binding ability, heavy metals, and other substances [5]. Structurally, chitosan consists of repeating units of 2-amino-2-deoxy-D-glucose linked by β-(1→4)-glycosidic bonds, which forms its polymer framework [6]. The polymer structure of chitosan is due to the presence of amino groups in the C2 position, which, depending on the degree of deacetylation and pH of the medium, can be in a protonated or neutral form. This feature determines such key properties of chitosan as the ability to ion exchange and interact with charged molecules, including proteins, lipids, and organic acids. Additionally, the existence of both amino and hydroxyl groups in the chitosan backbone contributes to its elevated reactivity, positioning it as a versatile platform for functionalization and composite formation. For example, modification of the polymer chain allows obtaining derivatives with specified properties, such as improved solubility, sorption capacity or specific bioactivity.

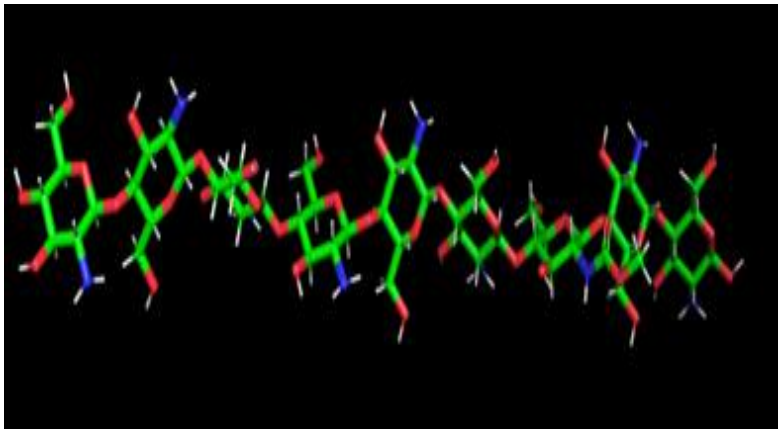

Fig.1. Molecular structure of chitosan visualized using the NAMD program.

The conformational features of chitosan, including the spatial arrangement of acetyl groups in N-acetylglucosamine units, plays an important role in predicting its behavior in various chemical and biological systems [7]. Chitosan possesses distinctive properties that make it increasingly sought after across various industries. Its market potential is expected to expand, driven by global trends such as environmental awareness, the pursuit of healthier lifestyles, and advancements in innovative technologies. In healthcare and medicine, chitosan is gaining traction due to its natural origins and beneficial characteristics.These aspects are the subject of active research in the field of synthesis of new materials, biomedicine and environmental cleaning technologies [8]. As an ingredient in dietary supplements, chitosan is valued for its ability to lower cholesterol, enhance metabolism, and support gut health. Marketing efforts will focus on highlighting its natural composition, safety, and positive effects on overall well-being. Thanks to its antimicrobial, anti-inflammatory, and wound-healing properties, chitosan is also widely applied in medical products, such as dressings, surgical sutures, and antibacterial coatings. The promotion of these materials will underscore their eco-friendly nature, efficiency, and compatibility with biological systems, supported by technologies like ASPEN PLUS and

NAMD. In agriculture, chitosan is utilized as a biopesticide and plant growth enhancer. Its capacity to strengthen plant immunity and increase resilience to stress positions it as a promising tool in promoting organic and sustainable farming practices [9]. Chitosan is very popular in the food industry because it is practically not absorbed in the gastrointestinal tract [10], which makes it a valuable component for the production of low-calorie products, serves as a source of essential substances and improves the technological properties of food products. Its ability to bind and remove fats and toxins from the body, as well as its minimal caloric content, make chitosan indispensable for the creation of healthy food products and health maintenance products [11,12]. The versatility of GO also extends beyond environmental applications. Its layered structure and the potential for functional group modification make it an invaluable material in biomedicine, engineering, and technology. These applications leverage the ability of GO to form a range of covalent and non-covalent bonds through its functional groups, further broadening its utility [13,14]. The oxygen content in graphene oxide, which typically ranges from 3% to 40% by weight, significantly influences its properties. A precise understanding of the oxygen-functional group content is essential for optimizing GO's performance in various applications [15,16]. Furthermore, the composition of GO can vary with changes in its surface area, which directly impacts its adsorption efficiency and reactivity. Research has demonstrated that GO membranes exhibit exceptional water permeability combined with selective ion and molecule transport, making them highly effective in water filtration systems.

In the field of nanotechnology, GO is increasingly recognized as a cost-effective and environmentally friendly material for purifying water from toxic pollutants [17,18]. Its applications range from sewage treatment and CO2 capture to the removal of residual pesticides and pharmaceuticals from water, showcasing its adaptability and effectiveness [19,20]. The continuous exploration of GO's properties and its integration into innovative technologies highlight its potential to transform environmental protection strategies while contributing to sustainable development goals [16,18,20].

EXPERIMENTAL PART

- Preparation of Chitosan-Based Hydrogels Using Different Concentrated Solutions

Chitosan was dissolved in acetic acid solution (0.1%) and stirred for several hours to ensure complete dissolution of chitosan. The prepared gel was then placed in Petri dishes with a thickness of approximately 3-6 mm. NaOH solution (1-5 M) was slowly added to the chitosan solution, forming gels with different textures according to the different concentrations of the solutions.

- Method for Synthesis of Graphene Oxide

For the synthesis of graphene oxide, three plastic containers were prepared, each containing 3 g of graphite and 1 g of sodium nitrate ($NaNO_3$) and 6 g of potassium permanganate ($KMnO_4$), respectively. Separately, 46 ml of concentrated sulfuric acid (95–98% H_2SO_4) was measured out using a graduated cylinder. To monitor the exothermic reaction, the process was carried out in an ice bath using multi-necked flasks equipped with thermometers to maintain precise temperature control. $KMnO_4$ was added slowly over two hours, ensuring that the reaction temperature remained within 20–25 °C. After continuous stirring for four hours, the resulting mixture was filtered, and the resulting solid product was thoroughly washed with distilled water to remove residual sulfuric acid and normalize the medium.

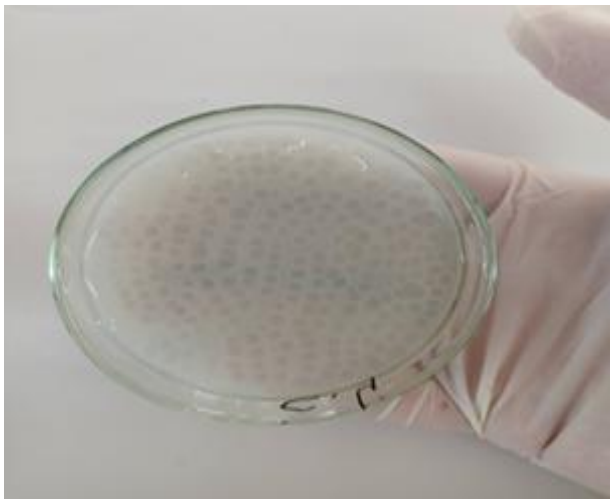

Fig. 2. Obtaining a hydrogel structure of chitosan

Fig. 3. Chitosan-based hydrogel for use in water purification

RESULTS AND DISCUSSION

This study uses an integrated approach combining numerical modeling and laboratory experiment to obtain and analyze a composite hydrogel based on functionalized chitosan and graphene oxide (Ch@GO). Modeling was performed using the Aspen Plus V12 and NAMD 2.14 software packages, which allowed us to cover both the macroscopic and molecular levels of interaction between the components.

- **Modeling in Aspen Plus**

The following parameters were varied during the modeling process: temperature (20–80 °C), pressure (atmospheric and elevated), mass ratio of components (chitosan, graphene oxide, acid solution), and the duration of ultrasonic treatment.

- **Molecular modeling in NAMD**

At the molecular level, the interaction between chitosan and graphene oxide was modeled using the NAMD package to describe the polysaccharide chains of chitosan and the functional groups of graphene oxide. The structures were considered at different pH values. The analysis showed stable formation of hydrogen bonds between the amino groups of chitosan and oxygen-

containing groups of graphene oxide, with an average length of ~2.1 Å. With increasing pH, an increase in the distance between the chitosan chains was observed due to deionization, which potentially affects the degree of swelling and permeability of the hydrogel.

Experimental confirmation

To confirm the model data, laboratory experiments were carried out to synthesize a composite hydrogel. Mixtures of functionalized chitosan and graphene oxide (Ch@GO) were prepared in weight ratios of 1:1, 2:1 and 3:1. Chitosan was dissolved in 0.1% acetic acid solution with stirring, after which graphene oxide was added. The resulting solutions were treated with an ultrasonic device until a homogeneous mass was obtained. The mixtures were poured into Petri dishes and kept at 50 ° C for 3 hours. The obtained samples demonstrated good form-forming properties, a homogeneous structure and high stability. The morphology and distribution of components in the composite corresponded to the structures predicted based on molecular modeling. Thus, the correspondence between the calculations and the actual properties of the synthesized material was experimentally confirmed. The use of numerical modeling made it possible to significantly narrow the range of experimental search and ensure the production of a hydrogel with predicted characteristics, underscoring the role of simulation-based approaches in optimizing all steps of composite biomaterial creation.

Fig.4. Chitosan-based graphene oxide (Ch@GO) hydrogel.

CONCLUSION

Aspen Plus and NAMD are powerful tools for exploring chitosan and its practical applications. The composite material and chitosan-based hydrogels can be used to effectively remove pollutants, which is important for environmental and industrial applications. The successful integration of molecular modeling and experimental methods confirms the promise of the approach for the development of new materials. The results can be scaled up for industrial production of filter systems and purification plants. In this study, we successfully synthesized a composite hydrogel comprising graphene oxide (GO) and chitosan, demonstrating its high potential for addressing water pollution issues. Structural refinement and performance enhancement of the chitosan-GO system were achieved through a combined computational approach using NAMD for molecular-level understanding and Aspen Plus for process-level modeling. This integrative methodology not only provided an optimized material design but also facilitated the evaluation of its scalability for environmental remediation applications. The comparison between these two modeling platforms highlights a promising path for the development and industrialization of advanced filtration materials based on biopolymer composites.

REFERENCES

1. Volin YM, Ostrovskii GM. Three phases in the development of computer simulation of chemical engineering systems. *Theoretical Foundations of Chemical Engineering*. 2006;40:281–290.
2. Shevyrev SA. Application of the Aspen Plus software package for simulation of the synthesis-gas composition in oxygen-free steam gasification of biomass. *Thermal Engineering*. 2021;68(9):698–704.
3. Kale LV, Skeel RD, Bhandarkar M, et al. NAMD: A parallel object-oriented molecular dynamics program. *International Journal of High Performance Computing Applications*. 1999;13(1):61–69.
4. Phillips JC, Braun R, Wang W, et al. Scalable molecular dynamics with NAMD. *Journal of Computational Chemistry*. 2005;26(16):1781–1802.
5. Guliyeva NA. Stability of water HKUST-1 upon mixing with chitosan and graphene oxide. *GFZ Conference Proceedings*. 2022/2025. Available from: https://gfz2025.sciencesconf.org/data/pages/03_Programme_de_taille_2026.pdf
6. Azad AK, Sermsintham N, Chandrkrachang S, Stevens WF. Chitosan membrane as a wound healing dressing: characterization and clinical application. *Journal of Biomedical Materials Research Part B: Applied Biomaterials*. 2004;69B:216–222.
7. Aziz MA, Cabral JD, Brooks HJL, et al. Antimicrobial properties of a chitosan dextran based hydrogel for surgical use. *Antimicrobial Agents and Chemotherapy*. 2012;56:280–287.
8. Arteche Pujana M, Pérez Álvarez L, Cesteros Iturbe LC, Katime I. Biodegradable chitosan nanogels crosslinked with genipin. *Carbohydrate Polymers*. 2013;94:836–842.
9. Kean T, Thanou M. Biodegradation, biodistribution and toxicity of chitosan. *Advanced Drug Delivery Reviews*. 2010;62:3–11.
10. Raafat D, Von Bargen K, Haas A, Sahl HG. Insights into the mode of action of chitosan as an antibacterial compound. *Applied and Environmental Microbiology*. 2008;74:3764–3773.
11. Miguel SP, Ribeiro MP, Brancal H, et al. Thermoresponsive chitosan–agarose hydrogel for skin regeneration. *Carbohydrate Polymers*. 2014;111:366–373.
12. Vissarionov SV, Asadulaev MS, Shabunin AS. Experimental evaluation of the efficiency of chitosan matrixes under conditions of modeling of bone defect in vivo. *Pediatric Traumatology, Orthopaedics and Reconstructive Surgery*. 2020;8(1):53–62. DOI: 10.17816/PTORS16480
13. Devi SC, Khan RA. Effect of graphene oxide on mechanical and durability performance of concrete. *Journal of Building Engineering*. 2020;27:100948.
14. Liu Z. Nonlinear optical properties of graphene oxide in nanosecond and picosecond regimes. *Applied Physics Letters*. 2009;94:021902.
15. Zheng X, Jia B, Chen X, Gu M. In situ third-order non-linear responses during laser reduction of graphene oxide thin films towards on-chip non-linear photonic devices. *Advanced Materials*. 2014;26(17):2699–2703.
16. Guliyeva NA, Abaszadea RG, Khanmammadova EA, Azizov EM. Synthesis and analysis of nanostructured graphene oxide. *Journal of Optoelectronic and Biomedical Materials*. 2023;15(1):23–30.
17. Akbarov NA, Guliyeva NA. Fertilizer based on graphene oxide nanolayers and nutrients from organic waste. *International Scientific Journal "Endless Light in Science"*. 2024:242–245.
18. Guliyeva NA, Azizov EM. Composite based on chitosan and graphene oxide. *International Journal of Sciences: Basic and Applied Research (IJSBAR)*. 2022;65(1):141–147.
19. Murshudov T, Elshan A, Asadov M, Guliyeva N, Rahimov M, Elsun A. Iron nanoparticle-containing graphene oxide: Synthesis and membrane properties. *Journal of Optoelectronic and Biomedical Materials*. 2025;17(2):119–127.
20. Massart R. Preparation of aqueous magnetic liquids in alkaline and acidic media. *IEEE Transactions on Magnetics*. 1981;17(2):1247–1248. DOI: 10.1109/TMAG.1981.1061188

UOT: 547.057+547.2/.4+547.51+547.7/.8
DOI: https://doi.org/10.30546/2521-6317.2025.01.471

NEW SYNTHESIS OF BUTANE AND CYCLOHEXANE COMPOUNDS CONTAINING TWO FURAN FRAGMENTS

E.I. MAMMADOV, G.A. ZAIDOVA

Azerbaijan Technical University
AZ1073, Baku, H. Cavid pr. 25
e-mail: zaida.zaid88@gmail.com
e-mail: mammadov.elman@rambler.ru

ARTICLE INFO

Article history:
Received:2025-12-16
Received in revised form:2025-12-16
Accepted:2025-12-16
Available online

Keywords:
3-chloro- and 2-methyl-3-chloropropenes; adipic and trans-1,4-cyclohexandicarboxylic acid dichlorides; 1,4-di-(2-furyl)- and 1,4-di-[2-(4-methylfuryl)]butanes; trans-1,4-di-(2-furyl)- and trans-1,4-di-[2-(4-methylfuryl)]cyclohexanes; Diels-Alder adducts

ABSTRACT

The reaction of adipic acid with thionyl chloride ($SOCl_2$) yields the dichloride anhydride of the corresponding acid. It has been established that, regardless of whether 1,4-cyclohexanedicarboxylic acid is in the cis- or trans-form, its reaction with PCl_3 produces only the dichloride anhydride of trans-1,4-cyclohexanedicarboxylic acid. In the electrophilic addition of adipic and trans-1,4-cyclohexandicarboxylic acid dichlorides to 3-chloro- and 2-methyl-3-chloropropenes in the presence of $AlCl_3$, 1,2,11,12-tetrachloro-2,11-H(CH_3)dodecane-4,9-diones and trans-1,4-di-[3-H(CH_3)-3,4-dichlorobutanoyl-1]cyclohexanes were obtained, which upon vacuum distillation form 1,4-difuryl derivatives of butane and cyclohexane. Structures of difurans are confirmed by IR and NMR ^1H spectroscopy and chemical transformations. Furan compounds with maleic anhydride form Diels-Alder adducts.

INTRODUCTION

Furan and its derivatives are frequently encountered in the composition of natural compounds, they exhibit physiological activity and are widely used in the development of effective pharmaceuticals as well as chemical agents employed in plant protection [1–5].

The broad range of application fields of furan compounds has provided a strong impetus for research directed toward their synthesis by new methods.

Saturated and unsaturated chloroketones are promising starting materials for the synthesis of heterocyclic compounds containing one or two heteroatoms [6–14]. The electrophilic addition reactions of acid chlorides to unsaturated hydrocarbons, their chloro-substituted derivatives, and allylic-type chlorides represent one of the favorable approaches for the synthesis of saturated and unsaturated chloroketones [6, 9–11, 13–16].

It is known that the electrophilic addition reactions of acid chlorides to 3-chloropropene (allyl chloride) and 2-methyl-3-chloropropene (methallyl chloride) in the presence of $AlCl_3$ proceed according to Markovnikov's rule, and that the nature of the products formed depends on the structure of the corresponding carboxylic acids. Thus, when the acid chlorides of acetic, propionic, and butyric acids are used, a mixture of saturated and unsaturated chloroketones is mainly obtained, whereas higher aliphatic carboxylic acid chlorides ($\geq C_4$) as well as cycloalkane

carboxylic acid chlorides yield 2- and 2,4-substituted furan derivatives [6, 10, 12, 17–19].

In the presented article, valuable heterocyclic compounds containing two furan fragments were obtained by the method described.

EXPERIMENTAL SECTION

IR spectra were recorded on a Thermo Scientific Nicolet IS10 FT-IR spectrophotometer, and ^{1}H NMR spectra were measured on a "Bruker AM-360" instrument using internal standards TMS or HMDC.

The purity of the synthesized furans (4a–d) was determined by thin-layer chromatography (TLC) on "Sulufol UV-254" plates.

Commercial reagents, including 3-chloropropene (2a), 2-methyl-3-chloropropene (2b), adipic acid, and *cis*- and *trans*-1,4-cyclohexanedicarboxylic acids, were used as starting materials.

1. Synthesis of difuran compounds 4a–d.

1.1. 1,4-di-(2-furyl)butane (4a). A mixture of 14.7 g (0.11 mol) $AlCl_3$ and 80 ml of dry dichloroethane was cooled to −20 °C, and then, under stirring, 8.35 g (0.05 mol) of dichloranhydride 1a and 9.2 g (0.12 mol) of 3-chloropropene (2a) were added sequentially. The reaction mixture was stirred until it reached room temperature, quenched with 5% HCl solution, and the organic layer was separated, while the aqueous layer was extracted with ether (2 × 100 ml). The combined organic layer and ether extracts were successively washed with water, 10% $NaHCO_3$ solution, and again with water, and dried over anhydrous $CaCl_2$. The solvents were removed, and the residue was distilled under vacuum in a nitrogen atmosphere. This afforded 4g (42% yield) of 1,4-di-(2-furyl)butane (4a) with the following characteristics: $t_{boil.}$ 108-109 °C/3mm; n_D^{20} 1.4955. IR spectrum (cm^{-1}): 3125, 3155(ν_{CH}); 1517, 1598 ($\nu_{C=C,C=C}$); 880 (δ_{CH}). ^{1}H NMR spectrum(δ, ppm): 1.65 (4H, m, furyl-CH_2-); 2.58 (4H, m, -CH_2-CH_2-); 5.9 (H^3-cyclo, 2H, m); 6.13 (H^4-cyclo, 2H, m); 7.2 (H^5-cyclo, 2H, m). TLC: R_f 0.53, eluent – hexane: benzene 3:1.

1.2. 1,4-di-[2-(4-metylfuryl)]butane (4b). Using the above method 1.1, adipic acid dichloranhydride (1a) and 2-methyl-3-chloropropene (2b) afforded 1,4-di-[2-(4-methylfuryl)]butane (4b): yield 51%; $t_{boil.}$ 117 – 119 °C/3mm; n_D^{20} 1.4930. IR spectrum (cm^{-1}): 3130 (ν_{CH}); 1534, 1610 ($\nu_{C=C,C=C}$); 889 (δ_{CH}). ^{1}H NMR spectrum (δ, ppm): 1.4-1.9 (4H, m, furyl-CH_2-); 1.85 (6H, d, J=8 Hs, 2C^4-CH_3); 2.4-2.9 (4H, m, -CH_2-CH_2-); 5.72 (H^3-cyclo, 2H, m); 6.94 (H^5-cyclo, 2H, m). TLC: R_f 0.61, eluent – hexane: benzene - 3:1.

Using the above method (1.1), difurans 4c and 4d were synthesized from the reaction of *trans*-1,4-cyclohexanedicarboxylic acid dichloranhydride (1b) with 3-chloropropene (2a) or 2-methyl-3-chloropropene (2b).

1.3. Trans-1,4-di-(2-furyl)cyclohexane (4c). Yield 53%; $t_{melting}$ 84-85 °C (CH_3OH). IR spectrum (cm^{-1}): 3130, 3135(ν_{CH}); 1510, 1606 ($\nu_{C=C,C=C}$); 889 (δ_{CH}). ^{1}H NMR spectrum (δ,ppm): 1.1-2.4 (10H-cyclo, m); 5.82 (H^3-cyclo, 2H, m); 6.1 (H^4-cyclo, 2H, m); 7.14 (H^5-cyclo, 2H, m). TLC: R_f 0.56, eluent - $CHCl_3$: hexane - 1:1.

1.4. Trans-1,4-di-[2-(4-metyfuril)]cyclololohexane (4d). Yield 57%; $t_{melting}$ 100-101°C (CH_3OH). IR spectrum (cm^{-1}): 2950(ν_{CH}); 1532, 1606 ($\nu_{C=C,C=C}$); 895 (δ_{CH}). ^{1}H NMR spectrum (δ, ppm): 1.2-2.1 (10H-cyclo, m); 1.8 (6H, d, J=8 Hs, 2C^4-CH_3); 5.6 (H^3-cyclo, s, 2H); 6.8 (H^5-cyclo, 2H, m). TLC: R_f 0.49, eluent - $CHCl_3$:hexane - 1:1.

RESULTS AND DISCUSSION

The dichlorides of adipic and trans-1,4-cyclohexanedicarboxylic acids (1a,b) were taken to synthesize heterocyclic compounds containing two furan rings.

The dichloride of adipic acid (1a) was obtained from the reaction of the acid with thionyl chloride (scheme 1).

Scheme 1.

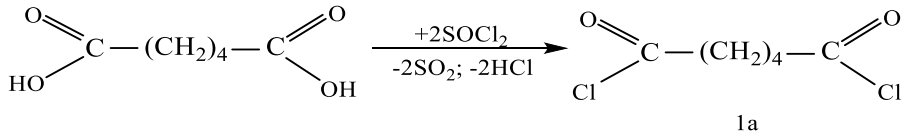

1a

The dichloride (1a) was used without purification, as it readily decomposes upon distillation.

It was determined that, regardless of whether 1,4-cyclohexanedicarboxylic acid is taken in the cis- or trans-form, the reaction with PCl_3 yields only the dichloride of *trans*-1,4-cyclohexane dicarboxylic acid. Hydrolysis of the dichloride (1b) with water affords exclusively *trans*-1,4-cyclohexanedicarboxylic acid (scheme 2).

Scheme 2.

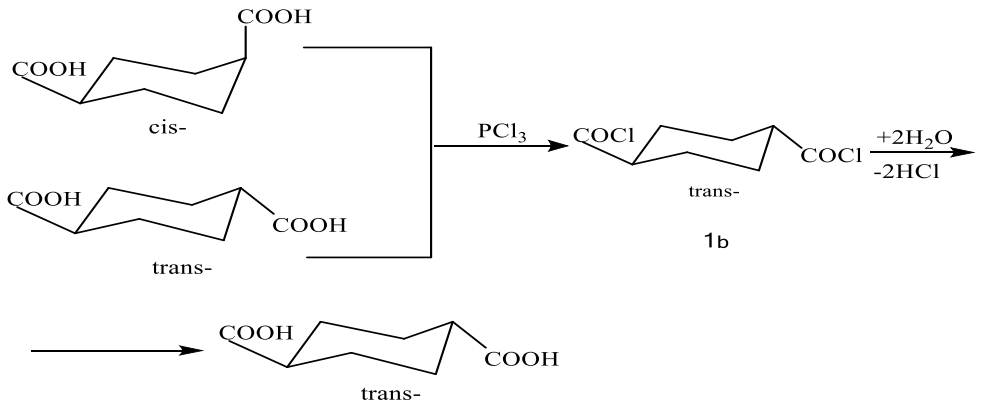

1b

Reaction of the dichlorides 1a,b with 3-chloropropene (2a) and 2-methyl-3-chloropropene (2b) in the presence of $AlCl_3$ afforded 1,2,11,12-tetrachloro-2,11-H(CH_3)-dodecane-4,9-dione (3a,b) and *trans*-1,4-di-[3-H(CH_3)-3,4-dichlorobutanoyl-1]cyclohexane (3c,d) (scheme 3).

Scheme 3.

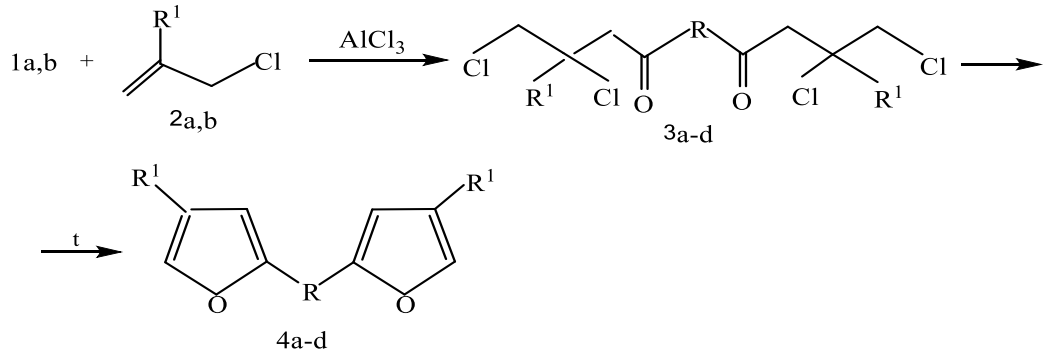

R= −$(CH_2)_4$− (1a; 3a,b; 4a,b); *trans*-1,4-cyclo-C_6H_{10} (1b; 3c,d; 4c,d); R^1 = H (2a; 3a,c; 4a,c); CH_3 (2b; 3b,d; 4b,d).

During vacuum distillation of the tetrachloroketones (3a–d), heterocyclization occurs, leading to the formation of 1,4-difuryl derivatives of butane (4a,b) and cyclohexane (4c,d) (scheme 3).

The structures of the difurans (4a–d) were confirmed based on IR and ^{1}H NMR spectral data as well as chemical transformations.

In the furan compounds 4a–d, the furan rings participate in a Diels–Alder reaction with maleic anhydride, forming the corresponding Diels–Alder adducts (scheme 4) [20].

Scheme 4.

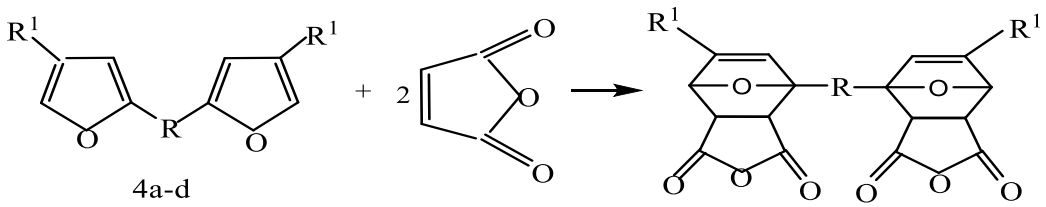

Here, R and R^1 - are the ones shown in the 3rd scheme.

The IR spectra of the difuran compounds (4a–d) exhibit absorption bands characteristic of the furan ring (cm^{-1}): 2950-3150 (ν_{CH}); 1598-1610 ($\nu_{C=C}$); 1510-1534 ($\nu_{C=C}$); 880-895 ($\boldsymbol{\delta}_{CH}$) (experimental section).

In the ^{1}H NMR spectra of compounds 4a–d, the protons of the 1,4-substituted butane (cyclohexane) fragments appear at δ 1.4–2.9 (1.1–2.4) ppm, while the protons of the furan ring are observed as characteristic multiplets at δ 5.6–7.2 ppm (experimental section).

Thus, a two-step, efficient method has been developed for the synthesis of butane and cyclohexane difuryl derivatives based on the reaction of the dichlorides of adipic and *trans*-1,4-cyclohexanedicarboxylic acids with 3-chloropropene and 2-methyl-3-chloropropene.

REFERENCES

1. Mashkovsky, M.D. *Medicinal Products*. Moscow: Novaya Volna, 2021, 1216 pp.
2. Joule, J., Mills, K. *Heterocyclic Chemistry*. Moscow: Mir, 2009, 728 pp.
3. Yurovskaya, M.A. *Chemistry of Aromatic Heterocyclic Compounds*. Moscow: Binom, 2015, 208 pp.
4. Grapov, A.F. New Insecticides and Acaricides // *Uspekhi Khimii* [Russian Chemical Reviews], 1999, Vol. 68(8), pp. 773–784.
5. Kwiesien, H. Five-Membered Ring Systems: Furans and Benzofurans // Progress in Heterocyclics Chemistry, 2020, № 31, pp. 281-323.
6. Guseinova, V.A., Zaidova, G.A., Mammadov, E.İ. Reaction of Chloranhydrides of Cycloalkanecarboxilic Acids with some Allylis Chlorides // Chemical Problems, 2021, № 3 (19), pp. 179-185.
7. Petkovich, S.K., Potkin, V.I., Kaberdin, R.V. Synthesis of 3-Aryl-5-Dichloroethyl-N-Carbonylpyrazoles based on 1-Aryl-3,4,4-Trichloro-3-Buten-1-ones // *Zhurnal Organicheskoi Khimii* [Journal of Organic Chemistry], 2006, Vol. 42, Issue 10, pp. 1496–1499.
8. Bozhenkov, G.V., Savosik, V.A., Klyba, L.V. [et al.]. 1-Alkylpyrazoles and 1-Alkyl-5-Chloropyrazoles from Halogenvinylketones and 1,1-Dialkylhydrazones // *Zhurnal Organicheskoi Khimii* [Journal of Organic Chemistry], 2008, Vol. 44, Issue 8, pp. 1207–1212.
9. Ahmadova, N.Y. Synthesis of 1-Allyl-2-Cycloalkyl-4-H(CH_3)pyrroles from Saturated Dichloroketones and Unsaturated Chloroketones // *News of the Pedagogical University. Series of Mathematics and Natural Sciences*. Baku: ADPU, 2024, Vol. 72, No. 3, pp. 95–101.

10. Ibragimov, I.I., Mamedov, E.I., Ismailov, A.T. [et al.]. Chemistry of Allylic-type Cystems. II. Acylation of 3-Bromo- and 2-Methyl-1-Propenes // *Zhurnal Organicheskoi Khimii* [Journal of Organic Chemistry], 1990, Vol. 26, Issue 8, pp. 1648–1654.
11. Mammadov, E., Mammadov, A., Huseynova, V. [et al.]. Temperature Dependence of the Reaction of Elektrophilic Addition of Acyl Chlorides to Allyl Chloride / 6th İnternational Conference: Thermophysical and Mechanical Properties of Aduanced Materials (Thermam 2019). İzmir, Turkey, 22-24 september, 2019, pp. 54-55.
12. Bozhenkov, G.V., Levkovskaya, G.G., Larina, L.I. [et al.]. Synthesis, Structure, and Properties of 1,2-Dichlorovinylalkylketones // *Zhurnal Organicheskoi Khimii* [Journal of Organic Chemistry], 2004, Vol. 40, Issue 11, pp. 1632–1640.
13. Ahmadova, N.Y., Mammadov, E.I. A New Approach to the Synthesis of Cycloalkyl-Substituted Pyrroles / In *Proceedings of the International Scientific Conference "Monomers and Contemporary Problems of Petrochemistry" Dedicated to the 110th Anniversary of Academician S. Mehdiyev*. Baku, December 19–20, 2024, pp. 86–87.
14. Mammadov, E.İ., Huseynova, V.A., Mekhtiyeva, S.T. [et al.]. New Synthesis of 3- and 1,3- Pyrazole Derivatives based on 1-Cycloalpyl-2,3-dichloro-1-propanones // Azerb. Chem. Journal, 2022, № 4, pp. 89-94.
15. Mammadov, E., Huseynova, V., Yusubov, F. [et al.]. New Way for the Synthesis of 1,3-Pyrazole Derivatives by the Reaction of 1-Alkyl-2,3-dichloropropanones with Phenylhydrazine // Norwegian Journal of development of the International Science. Oslo, Nor-Norway, 2022, № 90, pp. 3-7.
16. Ahmadova, N.Y., Mammadov, E.I. A New Synthesis of 1,2- and 1,2,4-Substituted Pyrroles // *News of the Pedagogical University. Series of Mathematics and Natural Sciences*. Baku: ADPU, 2023, Vol. 71, No. 3, pp. 84–93.
17. Zaidova, Q.Ə., Mammadov, E.I., Ismayilov, S.Q. Study of the Acylation Products of 3-Chloro-, 2-Methyl-3-Chloro- and 2,3-Dichloropropenes // *Azerbaijan Technical University, Scientific Works*, 2019, No. 2, pp. 101–104.
18. Ismailov, A.G., Mamedov, E.I. Synthesis of Furan Derivatives via Condensation of Cycloalkanecarbonyl Chlorides with Allyl Chloride // *Zhurnal Organicheskoi Khimii* [Journal of Organic Chemistry], 1974, Vol. 10, Issue 5, pp. 1129–1130.
19. USSR Author's Certificate 450797. Method for the Preparation of 2-(Chlorocycloalkyl)furans / Ismailov, A.G., Mamedov, E.I. // *Bulletin of Inventions*, 1974, No. 43, p. 57.
20. Joule, J., Smith, G. *Fundamentals of Heterocyclic Chemistry*. Moscow: Mir, 1975, pp. 206–283.

UDC: 547.562.4
DOI: https://doi.org/10.30546/2521-6317.2025.01.494

SYNTHESIS OF *para*-[1(3)-METHYLCYCLOALKYL]PHENOLS: PROPERTIES AND APPLICATIONS

Ulviyya GURBANOVA, Chingiz RASULOV, Günay HEYDARLI, Fatima GASIMOVA

Academician Y.H. Mammadaliyev Institute of Petrochemical Processes of the Ministry of Science and Education of the Republic of Azerbaijan, AZ 1025, Baku, 30 Khojaly Ave

E-mail:ulviyyagurbanova01@gmail.com

ARTICLE INFO

Article history
Received:2025-10-31
Received in revised form:2025-11-01
Accepted:2025-12-18
Available online

Keywords:
phenol, 1(3)-methylcyclohexenes, cycloalkylation, para-[1(3)-methylcycloalkyl]phenols, acylation

ABSTRACT

This research focuses on the cycloalkylation reactions of phenol with 1-methylcyclopentene (MCP) and 1(3)-methylcyclohexenes (MCH) were investigated using a zeolite-based heterogeneous catalyst of both ecological and industrial significance. The reactions were carried out in a continuous-flow pilot plant, and optimal reaction conditions were determined as follows: temperature – 120°C, phenol-to-MCH molar ratio – 1:1, and volumetric flow rate – 0.6 h^{-1}. Under these conditions, the yield of para-(1-methylcyclohexyl)phenol was found to be 73.8% with a selectivity of 92.1%; the yield of para-(3-methylcyclohexyl)phenol was 69.4% with a selectivity of 89.7%; and the yield of para-(1-methylcyclopentyl)phenol reached 68.5% with the same selectivity of 89.2%. The structure and composition of the synthesized products were confirmed by IR spectroscopy (BRUKER ALPHA) and by ^{1}H and ^{13}C NMR spectroscopy (300 MHz). In addition, differential thermal analysis (DTA) and thermogravimetric analysis (TGA) were carried out using a Jupiter STA 449F3 synchronous thermal analyzer (NETZSCH, Germany) under dynamic conditions in an inert nitrogen atmosphere, within the temperature range of 25–650°C and at a heating rate of 10 K/min. Furthermore, the acylation reactions of the synthesized para-methylcycloalkylphenols with acetyl chloride in the presence of a $ZnCl_2/\gamma$-Al_2O_3 catalyst were studied.

1. Introduction

The rapid development of industry leads to an increased demand for chemical compounds and the expansion of their application areas. Simultaneously, pressing global issues such as environmental protection and energy efficiency are gaining increased attention. In this context, the synthesis of chemically efficient and environmentally safe compounds has become a priority in modern research. Among various classes of organic compounds, alkylphenols occupy a prominent position due to their broad applicability and valuable properties [1–5].

Alkylphenols not only serve as corrosion inhibitors, antioxidants, and stabilizers but also act as key components in the production of synthetic lubricants, surfactants, polymer additives, cosmetic products, and pharmaceuticals. The structural diversity and chemical reactivity of these compounds enable their widespread application in petrochemistry, polymer science, and materials engineering [6–10]. In addition to enhancing the thermal and mechanical stability of

end products, alkylphenols contribute to resistance against oxidative degradation, thereby improving the overall efficiency of industrial processes[11–15].

Growing environmental concerns have intensified research into developing more flexible and efficient synthesis methods for alkylphenols, as well as improving their functional characteristics. Consequently, the relevance of these compounds in chemical research and industrial applications has grown significantly. In light of these factors, the present study investigates the synthesis and application potential of industrially significant alkylphenols—namely, 1-methylcyclopentyl- and 1(3)-methylcyclohexylphenols—using an environmentally benign, zeolite-based catalyst KN-30 (containing 96.22% SiO_2), TS 2177-011-07622236-2008, under continuous-flow conditions in a pilot plant. The use of zeolites as catalysts in petrochemical processes is considered one of the major achievements of twentieth-century chemical science. Their large surface area, microporous structure, and intrinsic acidity make zeolites highly efficient heterogeneous catalysts. These properties not only facilitate faster reaction rates but also enhance product yield. Consequently, zeolite-based heterogeneous catalysts are widely employed in oil refining and petrochemical industries [16–20].

2. Experimental Section

Phenol, 1-methylcyclopentene, and 1(3)-methylcyclohexenes were used as starting materials for the alkylation process. Phenol was distilled to ensure purity before the reaction. 1-Methylcyclopentene was obtained via the dehydration of cyclohexanol. 1-Methylcyclohexene (with a purity of 99.8%) was synthesized through the condensation of isoprene with ethylene, while 3-methylcyclohexene (98.6% purity) was produced by the condensation of piperylene with ethylene. The physical properties of the initial compounds are presented in the table below.

Table 1. Physical properties of the raw materials

Properties	**Phenol**	**1-MCP**	**1-MCH**	**3-MCH**
Chemical formula	C_6H_5OH	C_6H_{10}	C_7H_{12}	C_7H_{12}
Molecular weight (g/mol)	94	82	96	96
Melting point (°C)	40-42	-	-	-
Boiling point (°C)	182	75	110-111	103-104
Density (g/cm³, 25°C)	1.071	0.7782	0.8200	0.8142
Refractive index (n_D^{20}, 20°C)	1.4503	1.4347	1.4502	1.4435

The mechanism of the cycloalkylation reaction of phenol with 1-methylcyclopentene and 1(3)-methylcyclohexenes is based on the principles of electrophilic aromatic substitution (EAS). The chemical equation of the reaction is presented below.

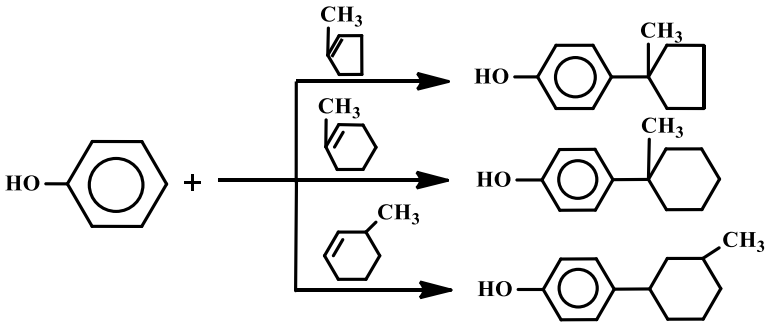

The schematic illustration of the continuous-flow pilot plant used for the cycloalkylation process is presented below.

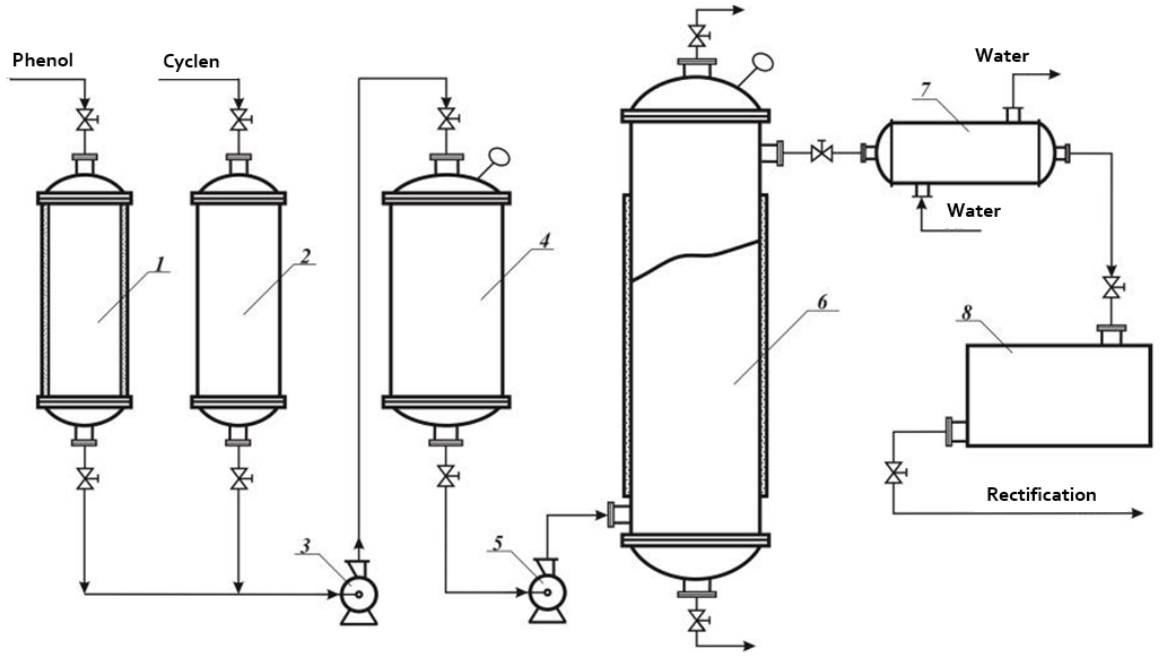

Fig. 1 Schematic representation of the technological process for the catalytic cycloalkylation of phenol with 1(3)-methylcycloalkenes

1 – Tank for phenol, 2 – Tank for cyclene, 3, 5 – Pumps, 4 – Mixer, 6 – Reactor, 7 -Condenser, 8 –Collection tank for alkylate

The phenol from tank (1) and the cyclene from tank (2) are fed into the mixer (4) at a predetermined ratio. The temperature in the phenol tank (1) is maintained at 40-45°C. The resulting mixture of phenol and cyclene is then directed from the mixer to the lower section of the reactor (6). The mixture of components passes over the catalyst and, after cooling in the condenser (7), is collected in the alkylate tank (8), from which it is directed to the rectification unit. During the rectification process, unreacted methylcyclohexene is first separated, followed by phenol and the target products under vacuum conditions (10 mm Hg). Once the experiment is completed, the raw material feed is halted, and the remaining product in the reactor is transferred to the receiving tank. After 500 hours of operation, the reactor is then switched to the regeneration mode.

The continuous operation of the phenol alkylation process in a pilot-scale plant provides a significant foundation for its potential industrial application. Conducting the process in such systems not only helps reduce production costs but also facilitates the development of a simpler and more practical technological scheme.

As an example, Figure 2 presents the results of the cycloalkylation reaction of phenol with 1-methylcyclohexene.

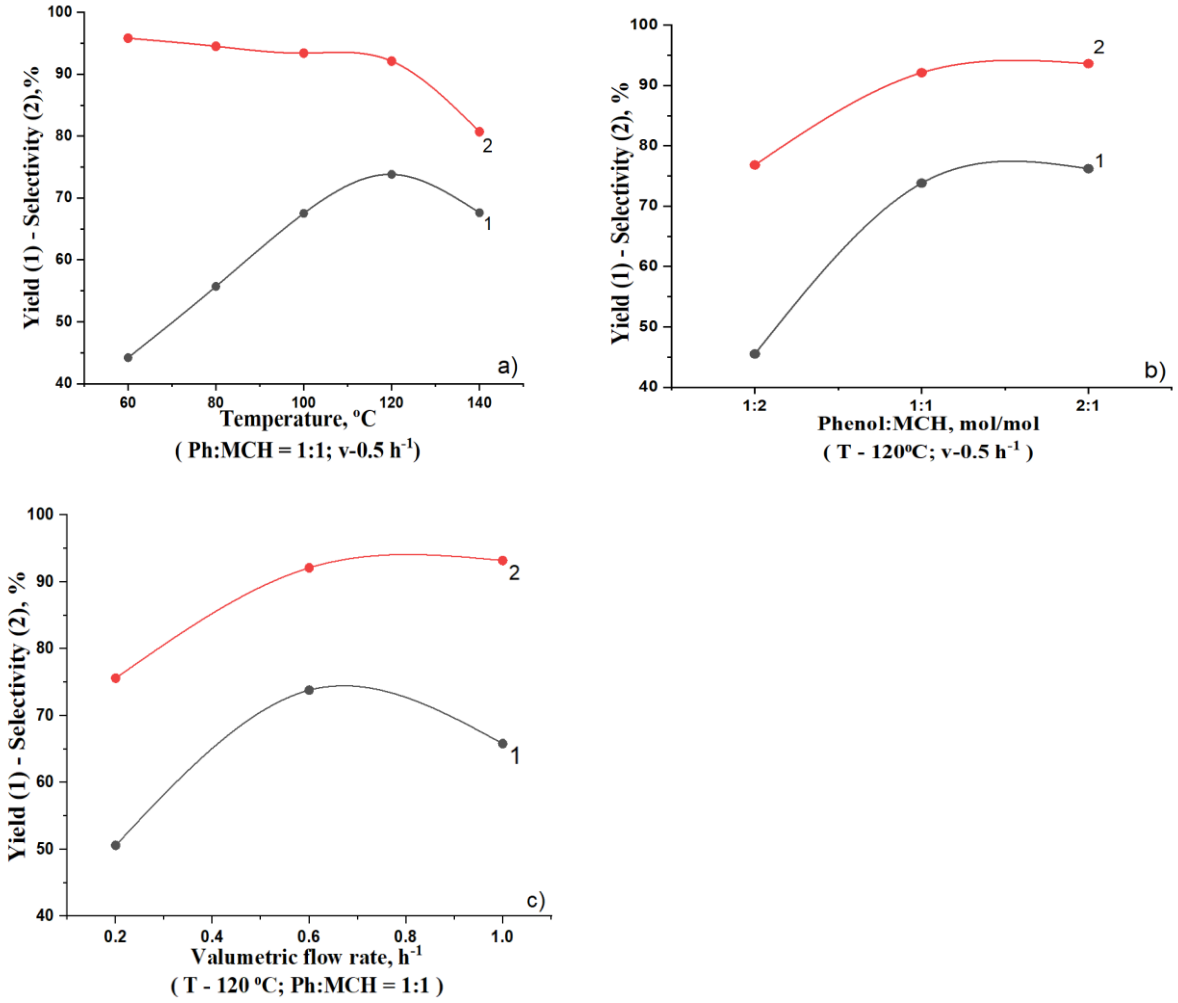

Fig. 2 Dependence curves of the yield (1) and selectivity (2) of *para*-(1-methylcyclohexyl)phenol on temperature (a), molar ratios of phenol to 1-MCH (b), and volumetric flow rate (c)

The study on the synthesis of *para*-(1-methylcyclohexyl)phenols examined the effects of temperature, the molar ratio of phenol to 1-MCH, and volumetric flow rate on the yield and selectivity of the target product. The reaction temperature for *para*-(1-methylcycloalkyl)phenols was investigated within the range of 60–140°C, the phenol-to-MCH molar ratio varied from 1:2 to 2:1 (mol/mol), and the volumetric flow rate was studied between 0.2 and 1.0 h^{-1}.

As shown in Figure 2, increasing the temperature from 60 to 120°C results in an increase in the yield of the target product from 44.2 to 73.8% (calculated based on phenol conversion). Within this temperature range, selectivity remains nearly constant, varying between 93.4 and 96.2%. However, when the temperature reaches 140°C, the yield decreases to 67.6%, and selectivity drops to 80.7%. This decline is attributed to the formation of undesirable isomers at elevated temperatures.

The amount of MCH in the reaction mixture also plays a crucial role. Under conditions of excess MCH, the yield of the target product decreases to 45.5%. This is attributed to the formation of di- and tri-substituted methylcyclohexylphenols.

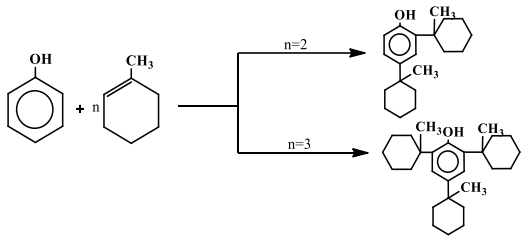

When the molar ratio of phenol to methylcyclohexene (MCH) is 1:1, the yield of *para*-(1-methylcyclohexyl)phenol reaches 73.8 with a selectivity of 92.1%. Increasing the amount of phenol in the reaction mixture results in a slight improvement in yield and selectivity, reaching 76.2 and 93.6%, respectively. However, this marginal increase is not considered economically significant, as the additional consumption of phenol does not lead to a substantial advantage in productivity or selectivity.

When the volumetric flow rate was investigated within the range of 0.6–1.0 h^{-1}, it was found that at a flow rate of 0.6 h^{-1}, the yield of the target product and the selectivity of the process were satisfactory (Fig. 2).

Thus, the optimal conditions for the continuous cycloalkylation of phenol with 1-methylcyclohexene over the KN-30 catalyst in a pilot-scale setup were established as follows: temperature of 120°C, phenol-to-1-MCH molar ratio of 1:1, and a volumetric flow rate of 0.6 h^{-1}. Under these optimal conditions, the yield of *para*-(1-methylcyclohexyl)phenol (based on phenol conversion) reached 73.8%, with a selectivity (based on the target product) of 92.1%.

Similarly, the continuous cycloalkylation reactions of phenol with 1-methylcyclopentene and 3-methylcyclohexene were investigated over the KN-30 catalyst. The cycloalkylation process was carried out under the optimal conditions previously established for the reactions of phenol with 1-MTP and 1-MCH**.** Under these conditions, the yield of *para*-(1-methylcyclopentyl)phenol based on phenol conversion reached 68.5%, with a selectivity of 89.2% relative to the target product. The yield and selectivity of *para*-(3-methylcyclohexyl)phenol were 69.4 and 89.7%, respectively.

3. Results and discussion

The figures below present the analysis results of *para*-(1-methylcyclopentyl)- and *para*-(1-methylcyclohexyl)phenols obtained by IR, ^{1}H and ^{13}C NMR, differential thermal analysis (DTA), and thermogravimetric (TG) methods.

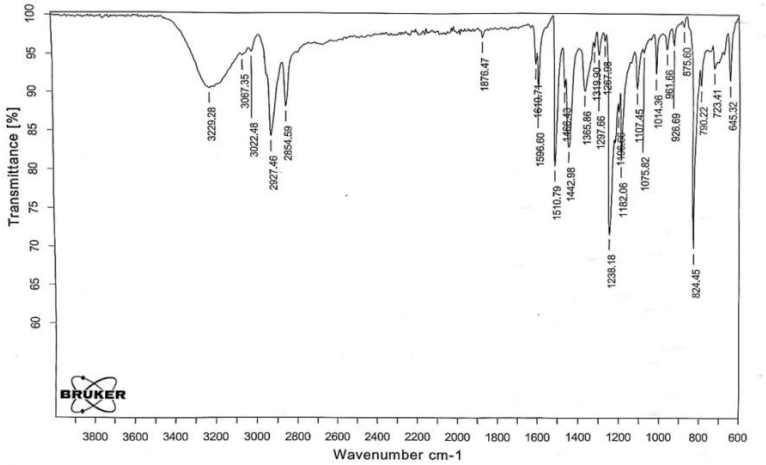

Fig. 3 IR Spectrum of *para*-(1-methylcyclopentyl)phenol

The IR spectrum of *para*-(1-methylcyclopentyl)phenol exhibited the following absorption bands:

- 824 cm^{-1} – *para*-substituted benzene ring;
- 926, 961 cm^{-1} – C–H bonds of the cyclic ring;
- 1014, 1075, 1107, 1182, 1238 cm^{-1} – stretching vibrations of the phenol C–O bond in the C–OH group;
- 1365, 1442, 1466 cm^{-1} – deformation vibrations of C–H bonds in CH_3 and CH_2 groups;
- 1510, 1596, 1610 cm^{-1} – stretching vibrations of the C=C bonds in the HC=C group;
- 2854, 2927 cm^{-1} – C–H stretching vibrations in CH_3 and CH_2 groups;
- 3022, 3067 cm^{-1} – stretching vibrations of the O–H bond in the CH=C group;
- 3229 cm^{-1} – stretching vibration of the O–H bond in the COH group.

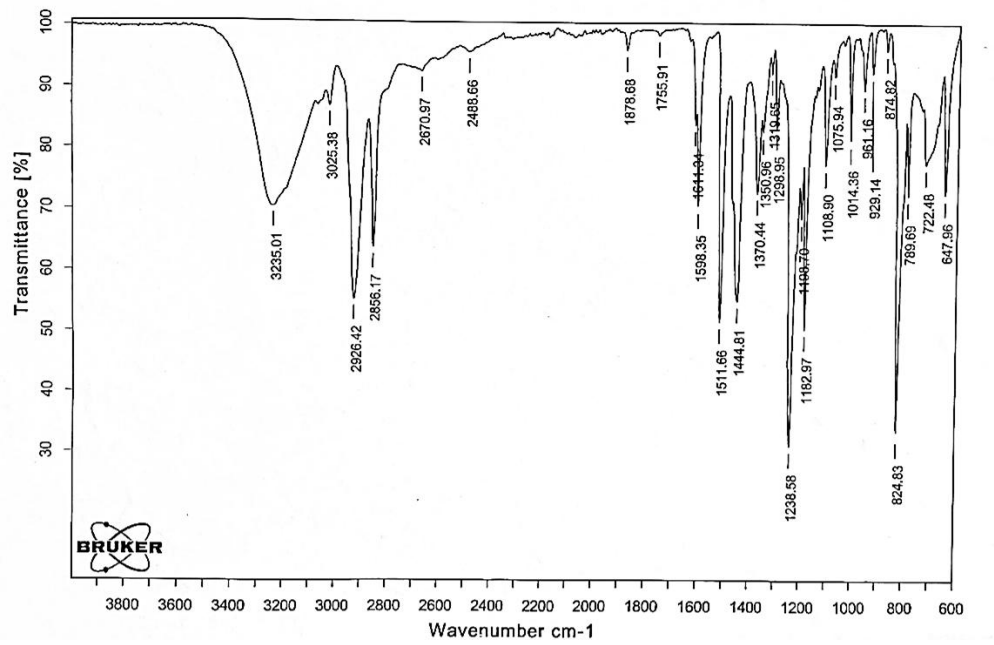

Fig 4. IR Spectrum of *para*-(1-methylcyclohexyl)phenol

In the IR spectrum of *para*-(1-methylcyclohexyl)phenol, the following characteristic absorption bands were observed: 824 cm^{-1} – indicative of a *para*-substituted benzene ring; 647, 722, 789 cm^{-1} – out-of-plane and in-plane deformation vibrations of C–H bonds; 929, 961 cm^{-1} – deformation vibrations of the cyclohexyl ring; 1014, 1075, 1182, 1196, 1238 cm^{-1} – stretching vibrations of the C–O bond; 1365, 1442, 1466 cm^{-1} – deformation vibrations of C–H bonds in CH_3 and CH_2 groups; 2854, 2927 cm^{-1} – stretching vibrations of C–H bonds in CH_3 and CH_2 groups; 1510, 1596, 1610 cm^{-1} – stretching vibrations of C=C bonds in the aromatic ring (–HC=CH– group); 3022, 3067 cm^{-1} – stretching vibrations of aromatic C–H bonds; 3229 cm^{-1} – stretching vibration of the O–H bond in the phenolic group.

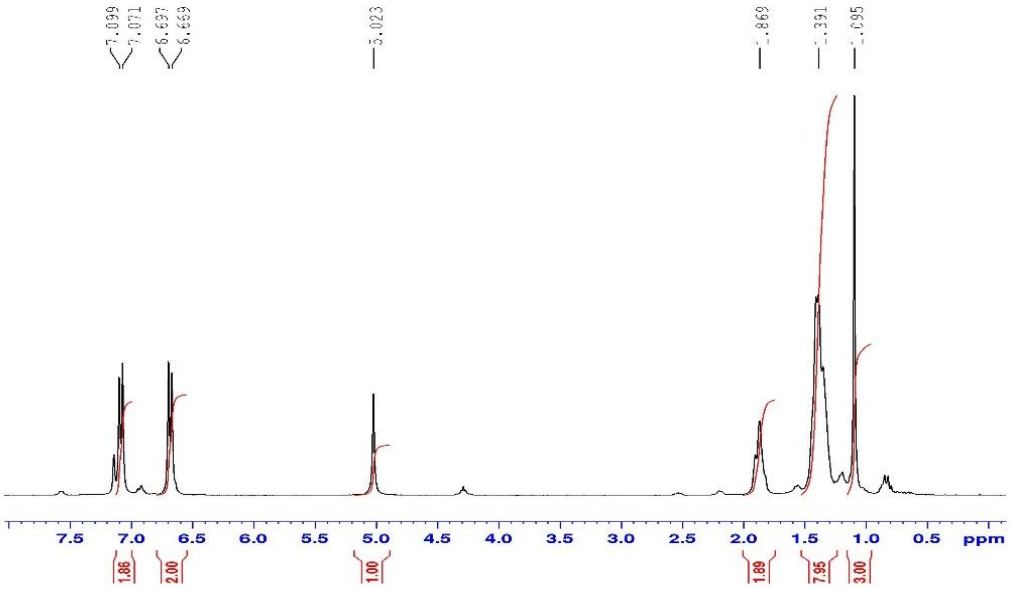

Fig 5. ^{1}H NMR spectra of *para*-(1-methylcyclopentyl)phenol

The results of the ^{1}H NMR spectroscopic analysis of *para*-(1-methylcyclopentyl)phenol ($CDCl_3$, δ, ppm) are as follows:

- 1.09–1.85 (multiplet, 8H, 4 CH_2 groups of the cyclopentyl ring);
- 1.37 (singlet, 3H, CH_3 methyl group on the cyclopentyl ring);
- 4.70 (singlet, 1H, OH group);
- 6.64 (doublet, 1H, aromatic proton);
- 7.08 (doublet, 1H, aromatic proton);
- 7.13 (singlet, 1H, aromatic proton).

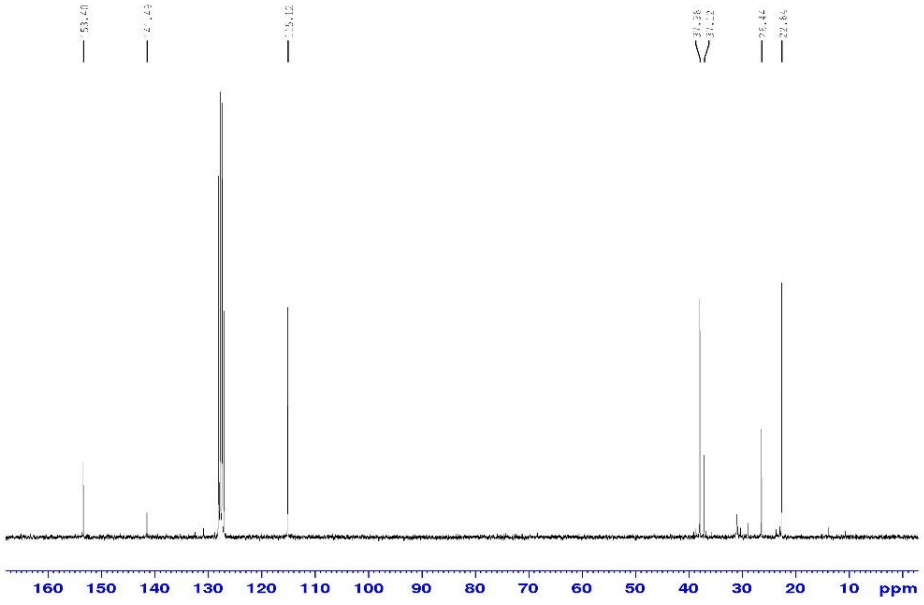

Fig 6. ^{13}C NMR spectra of *para*-(1-methylcyclopentyl)phenol

The results of the ^{13}C NMR spectroscopic analysis of *para*-(1-methylcyclopentyl)phenol ($CDCl_3$, δ, ppm) are as follows:

- 22.6 (CH_3, methyl group on the cyclopentyl ring);
- 26.8, 28.3, 34.5 (CH_2 groups, cyclopentyl ring);
- 43.1 (CH, quaternary carbon connected to the methyl group on the cyclopentyl ring);
- 115.2, 124.4, 129.6 (aromatic carbons);
- 138.9 (C–C, substituted carbon in the aromatic ring);
- 152.2 (C–OH, carbon bonded to the hydroxyl group in the phenol ring).

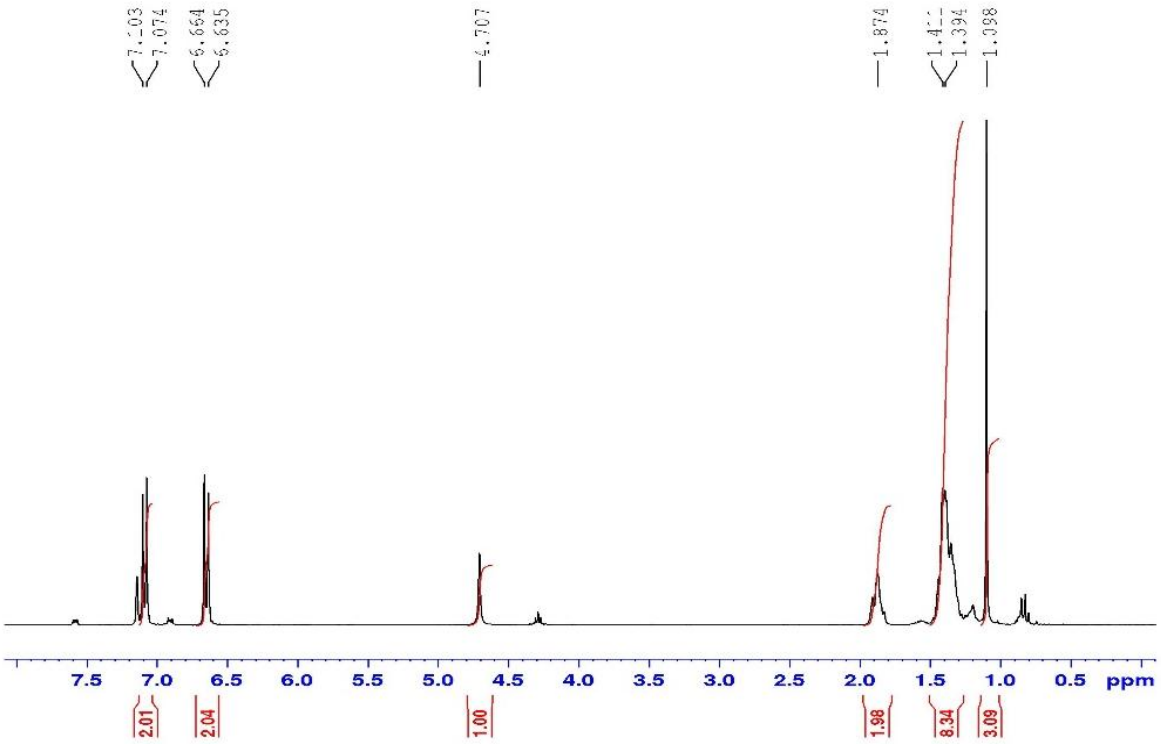

Fig. 7 ^{1}H NMR spectra of *para*-(1-methylcyclohexyl)phenol

The results of the ^{1}H NMR spectroscopic analysis for *para*-(1-methylcyclohexyl)phenol (in $CDCl_3$, δ, ppm) are as follows: 1.09–1.87 ppm (multiplet, 10H): corresponding to five CH_2 groups in the cyclohexyl ring; 1.39 ppm (singlet, 3H): methyl group attached to the cyclohexyl ring; 4.70 ppm (singlet, 1H): phenolic OH group; 6.63–6.67 ppm (doublet, 1H): aromatic proton; 7.07–7.10 ppm (doublet, 1H): aromatic proton; 7.10 ppm (singlet, 1H): aromatic proton

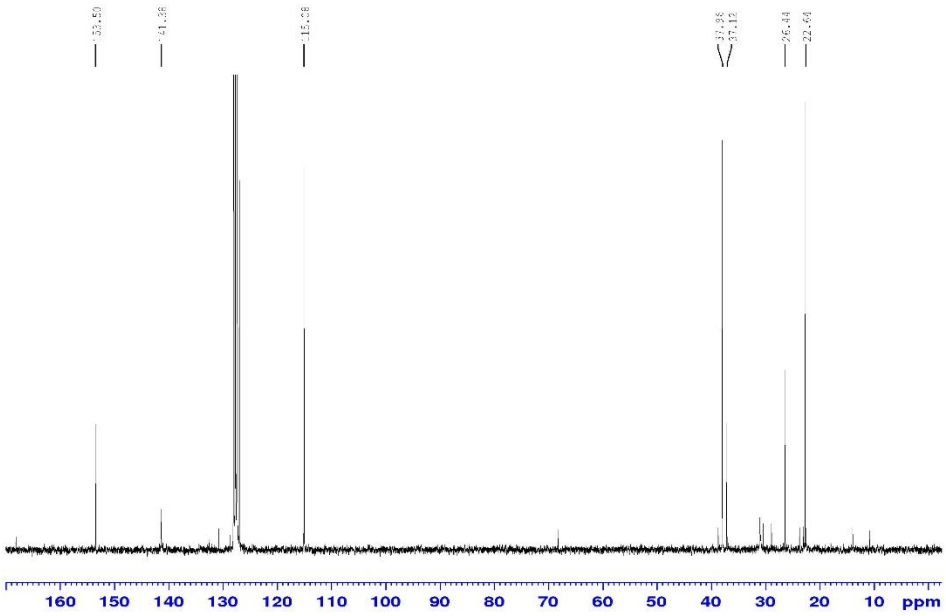

Fig 8. ^{13}C NMR spectra of *para*-(1-methylcyclohexyl)phenol

The results of the ^{13}C NMR spectroscopic analysis for *para*-(1-methylcyclohexyl)phenol: Aromatic carbons:153.5, 141.4, 139.5, 131.4, 129.3, 115.0 ppm; cyclohexyl ring carbons: 37.9, 37.1 ppm – quaternary carbons of the cyclohexyl ring; 26.4 ppm – CH_2 groups in the cyclohexyl ring; 22.6 ppm – CH group in the cyclohexyl ring; 31.0 ppm – methyl group attached to the cyclohexyl ring

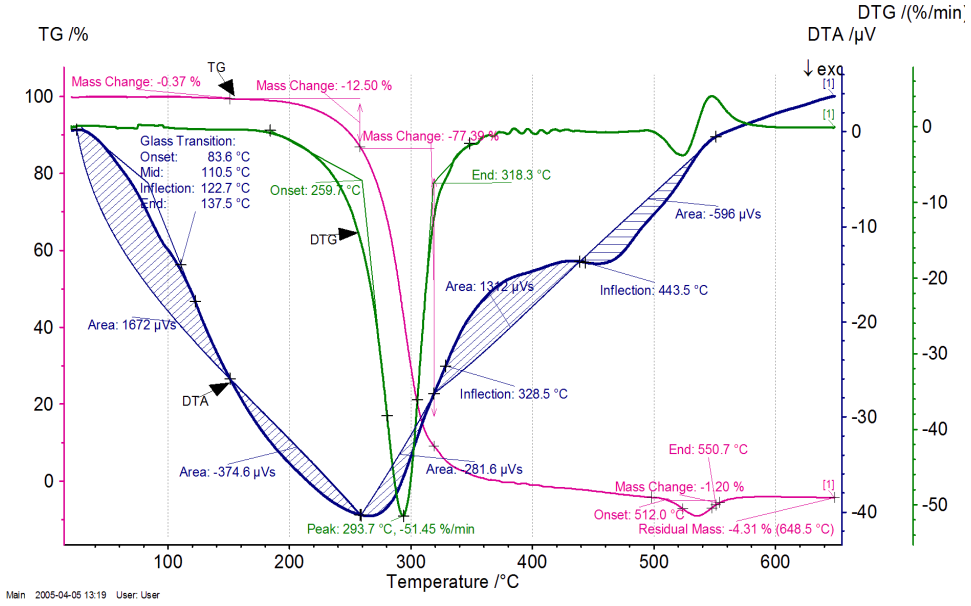

Fig. 9 TG/DTA thermogram of *para*-(1-methylcyclopentyl)phenol

Thermal analysis results of *para*-(1-methylcyclopentyl)phenol indicate that the compound undergoes a glass transition phase between 83.6°C and 137.5°C, characterized by increased molecular mobility within its amorphous structure without any observed mass loss. The main degradation occurs within the temperature range of 259.0°C to 318.3°C, during which a mass loss of 12.50% is recorded. The maximum decomposition rate is observed at 293.7°C, reaching -51.45%/min. Subsequently, a second major degradation takes place between 318.3°C and

550.7°C, with a mass loss of 77.39%. An exothermic process is observed in the final stage, leaving a residual mass of 4.31% at the end of the analysis. Overall, the compound can be considered thermally stable up to 250°C.

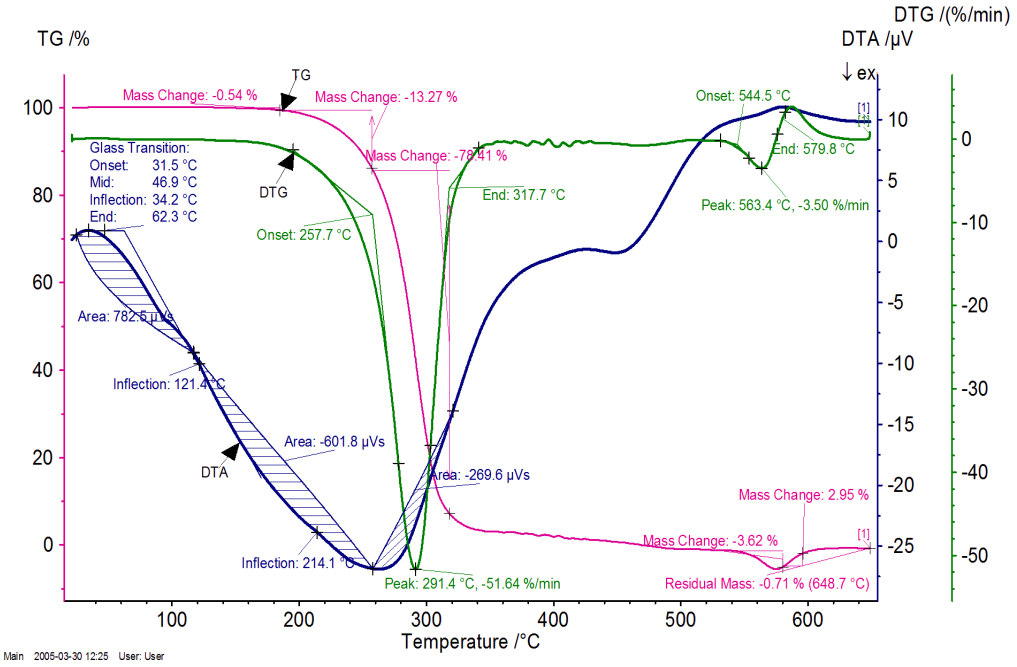

Fig. 10 TG/DTA thermogram of *para*-(1-methylcyclohexyl)phenol

According to the thermogravimetric analysis results, *para*-(1-methylcyclohexyl)phenol experiences an initial mass loss of approximately 0.54% within the temperature range of 31.5°C to 62.3°C. This loss is primarily attributed to the evaporation of adsorbed water and other volatile components on the compound's surface. The main thermal degradation occurs between 257.7°C and 317.7°C, with a recorded mass loss of 78.41%, which corresponds to the breakdown of the compound's primary carbon skeleton. The maximum decomposition rate is observed at 291.4°C, reaching -51.64%/min, indicating rapid degradation at this temperature. Based on these findings, *para*-(1-methylcyclohexyl)phenol can be considered thermally stable up to approximately 250°C, making it suitable for applications under conditions below this temperature.

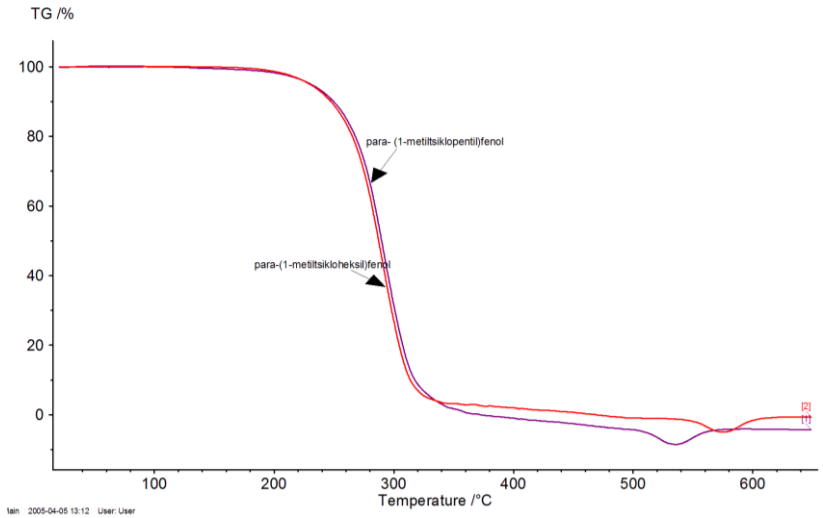

Fig. 11 Combined TG curve of *para*-(1-methylcyclopentyl)phenol and *para*-(1-methylcyclohexyl)phenol

Table 2. The table presents the physicochemical characteristics and elemental composition of *para*-(1-methylcycloalkyl)-phenols

Structural formula	Temp., °C/10 mm Hg	Temp., °C	Mol. Mass	Elemental composition, % $\frac{calculated}{found}$	
				C	H
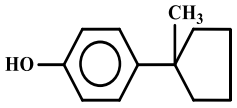	145-148	90	176	$\frac{81.8}{81.3}$	$\frac{9.1}{8.3}$
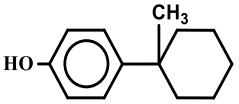	161-164	96	190	$\frac{82.1}{81.5}$	$\frac{9.5}{8.6}$
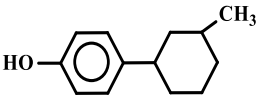	158-169	91	190	$\frac{82.1}{81.2}$	$\frac{9.5}{8.4}$

In the next stage, the obtained *para*-(1-methylcyclopentyl)- and *para*-[1(3)-methylcyclohexyl]phenols were subjected to acylation reactions in the presence of a dispersed $ZnCl_2$-supported γ-Al_2O_3 catalyst. The acylation was carried out at temperatures ranging from 120 to 160°C for durations of 20 to 60 minutes, with molar ratios of cycloalkylphenol to acetyl chloride varying from 1:0.5 to 1:3. The reactions were conducted using 20 wt% $ZnCl_2$/γ-Al_2O_3 catalyst.

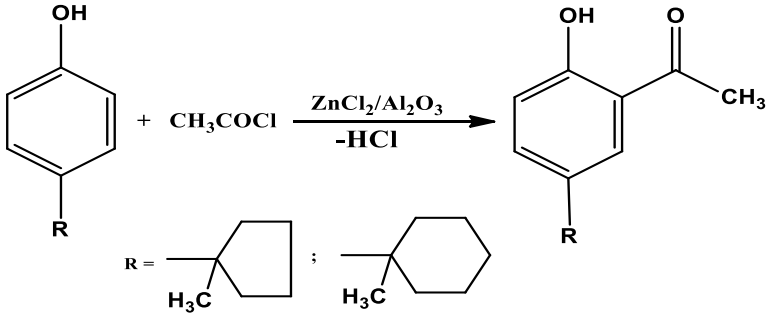

The acylation reaction of *para*-methylcycloalkylphenols with acetyl chloride was performed in a three-necked laboratory flask equipped with a thermometer, stirrer, and dropping funnel, using a $ZnCl_2$/γ-Al_2O_3 catalyst. The study investigated the effects of various factors such as temperature, reaction time, and molar ratio of reagents on the yield and selectivity of the target products. Optimal reaction conditions were determined as follows: at 140°C, for 30 minutes, with a molar ratio of cycloalkylphenol to acetyl chloride of 1:2 (mol/mol), the yields of the desired products ranged from 63.5% to 67.4%. The obtained 2-hydroxy-5-(1-methylcyclopentyl)- and 2-hydroxy-5-[1(3)-methylcyclohexyl]acetophenones were evaluated as photostabilizers for polystyrene, antioxidants in M-8 motor oil, and antirad additives in polypropylene. The results were positive.

para-[1(3)-Methylcycloalkyl]phenols obtained from the alkylation of phenol are widely used as intermediates in the petrochemical industry. Methylcyclohexylphenols undergo aminomethylation reactions with amines to form Mannich bases, which are utilized in various applications including as photo- and thermostabilizers in polymer materials, surfactants in lubricants, additives in rubber products, and pesticides widely used in agriculture — for example, as fungicides against powdery mildew in viticulture, insecticides against the Colorado potato beetle

in potato farming, as well as bactericides and disinfectants for diseases affecting both large and small livestock. These compounds have extensive applications in various other fields as well.

4. Conclusion

1. Cycloalkylation reactions of phenol with 1-methylcyclopentene and 1(3)-methylcyclohexenes were investigated in a continuous-flow laboratory setup using the industrial zeolite-based KN-30 catalyst. The optimal reaction conditions were established as follows: temperature of 120°C, molar ratio of phenol to 1(3)-methylcyclohexene of 1:1, and a volumetric flow rate of 0.6 h^{-1}. Under these conditions, the yields of *para*-[1(3)-methylcyclohexyl]phenols ranged from 69.4 to 73.8% with selectivities between 89.7 and 92.1%. The yield and selectivity of *para*-(1-methylcyclopentyl)phenol were 68.5 and 89.2%, respectively.

2. For the acylation of *para*-[1(3)-methylcycloalkyl]phenols using dispersed $ZnCl_2$-supported γ-Al_2O_3 catalyst, optimal reaction conditions were determined as follows: temperature of 140°C, reaction time of 30 minutes, and a cycloalkylphenol to acetyl chloride molar ratio of 1:2. The yields of the synthesized target products ranged from 63.5 to 67.4%.

REFERENCE LIST

1. Abbasov V., Rasulov Ch., Askerova P., İsmailov S. (2024). Cyclic and Nencyclic organic compounds, Cambridge Scholars Publishing, Newcastle, 242 p.
2. Weizhen S., Weizhong Zh., Ling Zh., Jinzhu L., Huanxin G. (2025). Chapter 1 - Introduction of aliphatic alkylation*:* Aliphatic Alkylation in Petroleum Refining (pp. 1-14). Elsevier. https://doi.org/10.1016/B978-0-443-21984-9.00002-7
3. Arifur R., Dr. Samantha L., Shuaijun P., Joseph J., Frank C. (2018). Phenolic Building Blocks for the Assembly of Functional Materials. Angewandte Chemie International Edition. 58(7), 1904-1927. https://doi.org/10.1002/anie.201807804
4. Lindner T. Stabilizers and additives for the polymer and lubricant industry. Journal of Industrial Chemistry. (2019). 62(1), 12–22
5. Kevin A., Philip B., Jon T. (2022).Phenols in Pharmaceuticals: Analysis of a Recurring Motif *J. Med. Chem.* 65(10), 7044–7072. https://doi.org/10.1021/acs.jmedchem.2c00223
6. Abbasov, V.M., Rasulov, Ch.K., Aliyeva, S.Q., Naghiyeva, M.V. [et al.]. Alkyl esters of 4[4-hydroxy-3-(2,6-diisopropylphenylamino-benzyl)]cyclohexane- and 4′-methylcyclohexanecarboxylic acids as antioxidants for diesel fuel. (2021). Republic of Azerbaijan, Invention I 2021 0029
7. Abbasov, V.M., Rasulov, Ch.K., Aghamaliyev, Z.Z., Naghiyeva, M.V. [et al.]. Tris[4-(cyclohexane- and 4-methylcyclohexanecarboxylic acid methyl esters)oxyphenyl] phosphites as antioxidants for T-46 turbine oil. (2020). Republic of Azerbaijan. Invention I 2020 0086
8. Naghiyeva E., Gadirov A., Farzaliyev V., Mammadova R., Nasirova S. (2023). Multifunctional alkylphenolate additives to motor oil. Processes of Petrochemistry and Oil Refining. Vol. 24, №3, 554-562. DOI: https://doi.org/10.36719/1726-4685/95/554-562
9. Rasulov Ch., Hasanov A. , Hasanova G., Heydarli G., Rustemov S. (2024). Polyphenols: general concepts and biological activity. Processes of Petrochemistry and Oil Refining. Vol. 25, № 4, 1090-1107. https://doi.org/10.62972/1726-4685.2024.4.1090
10. Hajiyeva G., Hasanov A., Rasulov Ch. (2023). Receiving ethyl tri-butyl ether. Azerbaijan Journal of Chemical News. Vol .5, № 2, 52-58.DOI:10.32010/AJCN040
11. Gurbanova U., Rasulov Ch. (2024). Catalytic alkylation of *para*-cresol with isoprene cyclodimers. XVI International Scientific and Practical Conference «Current questions of modern science». Tallinn, Estonia. World of Conferences. Tallinn, Estonia. pp.5-7. DOI:10.5281/zenodo.14003554
12. Gasimova F., Aghamalïyev, Z., Gasanova G., Rasulov, Ch. (2021). Some Features of Cycloalkylation Reactions of Phenol with 1-Methylcyclopentene. In Key Engineering Materials. Vol. 899. pp. 726–732. DOI:10.4028/www.scientific.net/KEM.899.726

13. Nasirov F., Djahangirov M., Agazade U., Hasanova G., Gurbanova U., Movsumova A., Rasulov Ch. (2025). Synthesis of nickel and cobalt catalytic dithiosystems based on chlorophenols for the polymerization of butadiene into low and high molecular weight polybutadienes. Processes of Petrochemistry and Oil Refining. Vol. 26, №2. pp. 580-587. DOI:10.62972/1726-4685.2025.2.580
14. Hongwei Zh., Ismail B., Stephan J., Gaik-Khuan Ch. (2022). Zeolites in catalysis: sustainable synthesis and its impact on properties and applications. Catalysis Science & Technology Vol. 12, pp. 6024-6039. DOI:10.1039/D2CY01325H
15. Kamlesh S. (2024). Studies on the synthesis and characterization of zeolites and their application as a catalyst. International Journal for Research Publication and Seminar. Vol. 15, №3, pp.357–364. DOI:10.36676/jrps.v15.i3.1518
16. Bai R., Song Y., Li Y., Yu J.(2019). Creating Hierarchical Pores in Zeolite Catalysts. Trends in Chemistry. Vol 1, №6, pp.601-611. DOI:10.1016/j.trechm.2019.05.010
17. Tan S. (2020). Comparative analysis of homogeneous and heterogeneous catalysts in industrial processes .Journal of Chemical Engineering. Vol. 7, pp. 387-400.
18. Rasulov Ch., Naghiyeva M., Gurbanova U., A. Pashayeva K., Abbasova A., Hajiyeva G., Salmanova Ch. (2025). İnteraction of phenol with methyl esters of cyclohexenecarboxylic acid in the presence of a modified zeolite-containing catalyst. Processes of Petrochemistry and Oil Refining. Vol .26, № 3. pp.657-666. DOI:10.62972/1726-4685.2025.2.580
19. Rasulov Ch., Aliyeva N., Aghamaliyev Z., Gasimova F., Hamzayeva G. (2024). The study of zeolite-based catalysts used in the process of preparatıon of *para*-cyclopenthenylphenols. Processes of Petrochemistry and Oil Refining. Vol. 25, №2, pp. 610-621. https://doi.org/10.62972/1726-4685.2024.2.610
20. Naghiyeva, M., Rasulov, Ch. (2025). Sterically hindered alkylphenols: methods of synthesis and fields of application. Baku: Savad, 192 p.

UDC: 66.094.522.8
DOI: https://doi.org/10.30546/2521-6317.2025.01.407

COMPREHENSIVE STUDY OF KINETIC AND TECHNOLOGICAL ASPECTS OF OXIDATIVE DESULFURIZATION AND THERMAL CONVERSIONS OF VACUUM GAS OIL

Khamis ABIYEV[1*], Elvira GUSEINOVA[1]

[1]*Azerbaijan State Oil and industry University, Baku, Azerbaijan*

ARTICLE INFO

Article history:
Received:2025-11-30
Received in revised form:2025-12-16
Accepted:2025-12-18
Available online

Keywords:
vacuum gas oil;
oxidative desulfurization;
sulfur-containing aromatics;
petroleum refining technology;
eco-friendly fuels

ABSTRACT

This article presents a study on the oxidative desulfurization of vacuum gas oil and its subsequent thermal conversions. One of the most critical challenges in modern petroleum refining is the improvement of fuel quality and ensuring their environmental safety. In particular, the reduction of sulfur content in fuels is a decisive factor in producing products that meet "Euro-5" and higher ecological standards.

Conventional hydrotreating processes require high temperatures, pressures, and significant hydrogen consumption, which makes them economically and technologically disadvantageous. Therefore, oxidative desulfurization (ODS) has attracted special interest as an alternative or complementary process.

The research focused on the preliminary oxidation of vacuum gas oil using peroxide systems, followed by thermal cracking. As a result, the kinetics of the decomposition of dibenzothiophene, benzonaphthothiophene, and their alkylated derivatives were investigated, and the rates of transformation of their stable and unstable forms were determined.

Various analytical methods (XRF, IR spectroscopy, GC–MS, etc.) were applied to monitor the structural changes of sulfur-containing compounds. The findings demonstrate that oxidative modification facilitates the decomposition of high-molecular-weight sulfur compounds during subsequent cracking and increases the yield of more valuable distillate fractions.

The scientific novelty lies in the fact that, for the first time, the kinetic parameters of sulfur-aromatic components of vacuum gas oil under combined oxidative desulfurization and thermal conversion were determined. The practical significance of the study is that such combined processes enable the more rational utilization of heavy petroleum feedstock and the production of fuels meeting modern environmental requirements.

**Corresponding author.*

E-mail address: xamisabiyev123@gmail.com (Khamis Abiyev Chingiz).

1. Introduction

In the 21st century, the development directions of the oil refining industry are determined by two main factors: resource limitations and environmental safety requirements. In recent years, the rate of depletion of oil reserves in major oil-producing countries has increased, and the

quality of the extracted raw materials has deteriorated. In these conditions, the main task facing oil refineries is to produce the maximum amount of valuable products from raw materials with a deeper degree of processing.

The presence of sulfur-containing compounds in fuel has a negative impact on both human health and the durability of equipment. Sulfur-containing gases such as SO_2 and H_2S, generated during fuel combustion, pose serious risks to human health, particularly to the respiratory system. In addition, these sulfur compounds contribute significantly to acid rain formation and play a key role in accelerating the corrosion of metallic equipment. In addition, sulfur compounds lead to the deactivation of catalysts [1].

Although the application of traditional hydrotreating - hydrotreating and hydrocracking - reduces sulfur to a certain extent, it does not achieve complete removal of highly stable molecules such as dibenzothiophene and benzonaphthothiophene. Also, the fact that these processes require high capital investment is a limiting factor in their economic aspect. Therefore, in scientific research, oxidative desulfurization has been the focus of attention as an alternative method. The advantages of this process are related to its mild conditions, simple apparatus design, and the absence of additional hydrogen consumption [3-5,8,10].

The main idea investigated in the research work is to combine oxidative modification with thermal conversion. As a result of oxidation, the sulfur atom is converted into a sulfone or sulfide form, which weakens the C–S bond. Thus, the decomposition of these compounds during subsequent thermal cracking occurs more readily, resulting in a reduction in sulfur content and an increase in the yield of distillate products. This approach opens up new opportunities for the rational processing of heavy high-sulfur feedstocks and the production of fuels that meet modern environmental standards.

2. Objective

The main objective of this research work is to study the behavioral patterns of sulfur aromatic compounds during oxidative modification and subsequent thermal conversion processes of vacuum gas oil. More precisely, the goal is to determine the decomposition kinetics of dibenzothiophene, benzonaphthothiophene and their alkylated derivatives under the influence of various oxidative conditions, to monitor changes in their thermal stability and, as a result, to increase the efficiency of desulfurization.

Within the framework of this goal, the following tasks were set:

- selection of optimal conditions (type of oxidizing system, temperature, time and reagent ratios) for oxidative processing of vacuum gas oil;
- separation of oxidized vacuum gas oil into polar and non-polar components and study of their individual behavior;
- study of the effect of oxidation on the structure and reactivity of sulfur-containing aromatic components;
- comparative analysis of the product composition of both the initial and oxidized gas oil in the cracking process;
- calculation of kinetic parameters (rate constants and activation energies) of decomposition and formation of sulfur aromatic compounds.

3. Materials and Components

The object of the research was a typical vacuum gas oil obtained from oil refineries. This raw material is characterized by its high average molecular weight and high sulfur content. The main characteristics of vacuum gas oil are as follows: its density varies in the range of 873–953 kg/m^3, kinematic viscosity is approximately 7.1 cSt at 40°C, initial boiling point is about 360 °C, and final boiling point is 500 °C. Gas oil mainly consists of a mixture of paraffin, naphthene and aromatic hydrocarbons. Its most problematic component is sulfur-containing aromatics, particularly, dibenzothiophene, benzonaphthothiophene and their derivatives. Since these compounds show high thermal stability and low reactivity, they are not completely decomposed in traditional hydrogenation processes.

A mixture of hydrogen peroxide (H_2O_2) and formic acid (HCOOH) was used as an oxidizing system. This system is distinguished by its efficiency, commercial availability and relative environmental safety. Hydrogen peroxide is an oxidizing agent with a high active oxygen content, while formic acid is a component that facilitates interphase mass transfer and plays a catalytic role [2].

In addition, adsorption methods were applied to select polar and non-polar fractions in the products obtained after oxidation. For this, sorbents with a high surface area were used, which allowed for the effective separation of oxidized derivatives of sulfur (sulfones and sulfoxides).

The reagents used in the study were of high purity, and the studies were conducted in certified laboratory conditions. The main chemical components and materials used are:

- hydrogen peroxide (30% aqueous solution);
- formic acid (analytical grade);
- methanol and other organic solvents (for extraction and chromatographic analysis);
- standard samples (dibenzothiophene, benzonaphthothiophene, etc.) for comparative analysis.

4. Apparatus and analyzing methods

The following analysis tools were used to monitor changes in the chemical composition of vacuum gas oil and its oxidized products:

- X-ray fluorescence spectroscopy (XRF): It was used to quantitatively determine the total sulfur content of vacuum gas oil and the products obtained after the experiment. This method provides high accuracy and repeatability.
- Infrared (IR) spectroscopy: It was applied to monitor changes in the functional groups of sulfur-containing compounds during the oxidation process. A comparative analysis was carried out with the intensity of characteristic vibration bands during the conversion of sulfides to sulfones and sulfoxides.
- Gas chromatography (GC): This technique was employed to analyze both liquid and gaseous products obtained from the oxidation and cracking processes. GC enabled the qualitative and quantitative identification of aromatic and sulfur-containing compounds in the oxidized and cracked samples, as well as the determination of the composition and relative proportions of low-molecular-weight gas products, including methane, ethane, propane, and related hydrocarbons.

- High-performance liquid chromatography: Used for the separation of polar and non-polar fractions, as well as for the assessment of the amount of main aromatic compounds in their composition.
- Thermal analysis methods like Thermogravimetric (TG) and Derivative Thermogravimetric (DTG): Used for the comparative analysis of the thermal stability of vacuum gas oil and its oxidized forms.

All devices used in the studies are calibrated, certified equipment that meets international standards. This ensured the reliability of the results and compliance with modern scientific requirements.

5. Methods

The research process consisted of several stages, and a specific methodology was applied at each stage:

1. **Oxidative treatment.** Vacuum gas oil was first treated with a mixture of hydrogen peroxide and formic acid. The main purpose of this process was to functionally modify sulfur-containing aromatics and facilitate their separation. The reaction was carried out at atmospheric pressure, in the temperature range of 50–70 °C, and in different time regimes.
2. **Separation by adsorption method.** Activated adsorbents were used to separate the oxidized gas oil into polar and non-polar fractions. This stage was based on the molecular properties of sulfur compounds: sulfones and sulfoxides, being polar in nature, bind more strongly to the adsorbent surface, while non-polar hydrocarbons are separated.
3. **Thermal cracking.** Samples taken before and after oxidation were subjected to thermal cracking at a certain temperature regime. As a result of this process, the decomposition of high-molecular compounds and the formation of distillate fractions were studied. Cracking was carried out at different temperatures and the kinetic parameters of the process were calculated.
4. **Kinetic analysis.** The conversion rates of dibenzothiophene, benzonaphthothiophene and their derivatives in the cracking process were compared. Based on the results obtained, the rate constants and activation energies of the reactions were determined.
5. **Comparative analysis.** The research results were compared between the initial (unoxidized) and oxidized gas oil. This approach made it possible to reveal the effect of oxidative processing on the degree of desulfurization and the yield of distillate products.

This sequence of the methodology was considered optimal both from a theoretical and practical point of view and increased the reliability of the results obtained.

6. Conducting research and its discussion

The first stage of the experiment was oxidative treatment of vacuum gas oil as specified above. As a result of the oxidation process, the functional groups of sulfur-containing aromatic compounds - mainly dibenzothiophene and benzonaphthothiophene derivatives - changed, and they were converted into sulfone and sulfoxide forms. The weakening of the C–S bond within the molecule during oxidation is of particular importance [6,7]. Because as the energy of this bond decreases, the decomposition process during subsequent thermal processing (cracking) becomes easier. Analytical results show that the total amount of sulfur in the oxidized samples

has significantly decreased, and vibration bands corresponding to the S=O bond were observed in IR spectroscopy. This confirms that sulfur compounds are converted into the oxide form.

At the next stage, the oxidized gas oil was separated into polar and non-polar components. For this purpose, adsorption methods were used. As a result, sulfones and sulfoxides entered the polar fraction, and aliphatic and aromatic hydrocarbons entered the non-polar fraction. The separation process was necessary both for the subsequent analytical study of the products and for the study of differences in behavior by fractions. An interesting point is that after oxidation, the share of sulfur in the polar fraction was significantly higher. This confirms that oxidative treatment leads to functional modification of sulfur-containing molecules and facilitates their separation.

The main studies were conducted on the thermal cracking of unoxidized and oxidized gas oil. It was found that during the cracking of unoxidized samples, high-molecular aromatic sulfur compounds retain their stability and remain largely undecomposed. This results in fewer distillate fractions in the output and more residue. On the contrary, during the cracking of oxidized samples, the decomposition of sulfur aromatics occurs more easily. At this time, the amount of distillate fractions increases, and the residual part decreases. The gas products contain more low-molecular compounds such as methane, ethane and propane. This proves that oxidation has an activating effect on thermal conversion [9].

The reaction kinetics of conversion of sulfur aromatic compounds were studied based on the experimental findings of this work. The reaction rate constants and activation energies were calculated for dibenzothiophene, benzonaphthothiophene and their derivatives. The results showed that:

- in non-oxidized samples, the conversion rate of these compounds is low, and the activation energy is high;
- in oxidized samples, the conversion rate increases significantly, and the activation energy decreases.

This fact once again confirms that oxidative modification weakens the chemical stability of sulfur compounds and creates conditions for their easier decomposition.

Based on the analysis, it was determined that during the cracking of oxidized gas oil, molecular structures of polyaromatic sulfur compounds gradually simplify. In particular, dibenzothiophene derivatives are converted to the sulfone form and then subjected to decomposition. As a result, the sulfur content in the distillate fractions is significantly reduced [11]. It was also found that the content of tar and asphaltenes in the products obtained as a result of cracking of oxidized samples decreased. This is an important result from a technological point of view, since such substances cause contamination of equipment and deactivation of catalysts during the processing process.

Table 1 shows the results of thermal cracking of unoxidized and oxidized samples of vacuum gas oil.

Table 1. Thermal cracking results of unoxidized and oxidized vacuum gas oil samples

Sample type	Yield of distillate fractions, %	Residual yield, %	Total sulfur content, ppm	Activation energy, kC/mol
Unoxidized VGO	42–45	55–58	7800–8200	185–190
Oxidized VGO	58–62	38–42	900–1200	120–130

As can be seen from the table, the yield of distillate fractions in the cracking of unoxidized vacuum gas oil was relatively low (42–45%), while the residual product was high (55–58%). The total sulfur content remained very high, and the activation energy was at the level of 185–190 kC/mol, which indicates that the decomposition process was difficult. In oxidized samples, the yield of distillate fractions increased to 58–62%, and the share of the residual product decreased. The total sulfur content decreased by 7–8 times, and the activation energy also decreased, which confirms that the decomposition was easier.

The results of the conducted studies show that combining oxidative modification with thermal conversion is a promising approach for the oil refining industry. This approach provides the following advantages:

- significantly reducing the sulfur content in fuels;
- increasing the yield of distillate products and improving their quality;
- not requiring additional hydrogen consumption, thus increasing economic efficiency;
- reducing the risk of equipment contamination and corrosion.

These findings are consistent with earlier studies on ozone-assisted oxidative desulfurization of vacuum gas oil [12–15]. The industrial application of such combined processes can allow for a more rational and environmentally safe use of heavy high-sulfur feedstock.

7. Results

The main findings of this work can be summarized as follows:

1. As a result of the oxidative processing of vacuum gas oil, the functional groups of sulfur aromatic compounds change, they pass into the sulfone and sulfoxide forms, which facilitates decomposition in the subsequent thermal cracking process.
2. As a result of the application of oxidative processing, the sulfur content in fuels is significantly reduced, which ensures the production of products that meet environmental standards (in particular, “Euro-5”).
3. The yield of distillate fractions increases with oxidative modification and the quality of the product improves, while the share of heavy residue decreases.
4. The decomposition kinetics of dibenzothiophene, benzonaphthothiophene and their derivatives have shown that after oxidative processing, the conversion rate increases, and the activation energy decreases.
5. As a result of the cracking process, the amount of tar and asphaltenes decreases, which significantly reduces the risk of equipment contamination and catalyst deactivation.
6. The applied method does not require additional hydrogen consumption, which improves the economic performance of the technological process.
7. The combination of oxidative desulfurization and thermal conversion can be considered a promising technological solution for a more rational and environmentally safe use of high-sulfur heavy fractions in oil refineries.

REFERENCE LIST

1. Pawelec, B., Navarro, R. M., Campos-Martín, J. M., & Fierro, J. L. G. (2011). Towards near zero-sulfur liquid fuels: A perspective review. *Catalysis Science & Technology*, 1(1), 23–42.
2. Rastegar, S. O., Yuzir, A., & Abdullah, A. Z. (2017). Catalytic oxidative desulfurization of model fuel using hydrogen peroxide and acetic acid. *Journal of Cleaner Production*, 142, 2345–2353.
3. Wan, J., Zhang, J., Wang, Y., & Li, C. (2016). Oxidative desulfurization of real diesel using polyoxometalate-based catalysts: A review. *Fuel Processing Technology*, 142, 264–278.
4. Nandiwale, K. Y., Bokade, V. V., & Joshi, P. N. (2018). Catalytic oxidative desulfurization using ionic liquids and their composites. *Renewable and Sustainable Energy Reviews*, 82, 3449–3462.
5. Li, Y., Jiang, Y., & Tang, X. (2019). Recent advances in oxidative desulfurization using deep eutectic solvents. *Chemosphere*, 237, 124460.
6. Xie, C., Wang, Z., Zhu, W., et al. (2021). Ozonation-assisted oxidative desulfurization of diesel fuel: Mechanisms and optimization. *Fuel*, 286, 119386.
7. Zhang, Q., Liu, X., & Wang, G. (2020). Kinetics and mechanism of ozone oxidation of sulfur compounds in petroleum fractions. *Energy & Fuels*, 34(6), 7102–7109.
8. Ali, M. F., & Al-Malki, A. L. (2018). Advances in diesel fuel desulfurization technologies. *Fuel*, 227, 390–408.
9. Tang, Z., Zhang, H., & Lu, J. (2022). Catalytic oxidative desulfurization of gas oil using ozone and transition metal catalysts. *Industrial & Engineering Chemistry Research*, 61(15), 5437–5445.
10. Yoon, H., & Lee, J. S. (2021). A review on ozone-based oxidative processes for petroleum desulfurization. *Journal of Environmental Chemical Engineering*, 9(6), 106364.
11. Gao, Q., Xu, G., & Li, S. (2020). Deep oxidative desulfurization of vacuum gas oil using ozone and extraction techniques. *Fuel Processing Technology*, 202, 106349.
12. Abiyev, Kh. Ch., & Guseinova, E. A. (2023). Oxidative desulfurization of vacuum gas oil with the participation of ozone. *Modern Approaches in Chemistry and Chemical Technology* (pp. 59–61). Republic Scientific Conference.
13. Abiyev, Kh. Ch., & Guseinova, E. A. (2025). Oxidative desulfurisation of vacuum gas oil in the presence of ozone. *International UFAZ Conference – CPM's 2025 Edition: Chemistry, Process, Materials* (pp. 32–33).
14. Guseinova, E. A., Mursalova, L. A., & Abiyev, Kh. Ch. (2023). Physicochemical properties of ozonized vacuum gas oil. *Science. Technology. Production* – 2023 (pp. 227–229) (In Russian).
15. Abiyev, Kh. Ch., Guseinova, E. A., & Serra, C. A. (2025). Sustainable desulfurization of VGO using ozone: Experimental insights. *Proceedings of the RISK 2025 Conference*.

UDC: 543.2
DOI: https://doi.org/10.30546/2521-6317.2025.01.402

ANALYSIS OF A MIXTURE OF HYDROXIDE CATIONS INSOLUBLE IN NAOH AND KOH SOLUTIONS (FIFTH ANALYTICAL GROUP OF CATIONS)

Damen NURGALIEVA*, Ainur KENZHEBAEVA[1], Akzhan KABYLKANOVA[2], Amadey MOISSEYENKO[3], Akulpa SATYBALDY[4]

[*] *Astana International University, Kazakhstan*
[1] *Astana International University, Kazakhstan*
[2] *Astana International University, Kazakhstan*
[3] *Astana International University, Kazakhstan*
[4] *Astana International University, Kazakhstan*

ARTICLE INFO

Article history:
Received: 2025-11-13
Received in revised form:2025-11-24
Accepted:2025-12-15
Available online

Keywords:
cations;
mixture analysis;
group reagent;
systematic run;
fractional course.

ABSTRACT

The article provides a detailed review of methods for the qualitative analysis of cations of the 5th analytical group, including iron (II) (Fe^{2+}), iron (III) (Fe^{3+}), magnesium (Mg^{+}) and manganese (Mn^{2+}). Their individual chemical properties, behaviour in various reaction environments and the importance of specific analytical techniques for their accurate identification are analysed. The authors paid considerable attention to fractional analysis, including the step-by-step separation and identification of cations in complex mixtures. Approaches to sequential analysis with minimisation of cross-reactions are described, which ensures the reliability of the results. Recommendations are given for the practical implementation of analytical procedures in laboratory conditions, and the main errors and their prevention are indicated. The aim of the study is to ensure high accuracy and reproducibility of the analysis of group 5 cations.

1. Introduction

Group reagents for cations of the fifth analytical group are alkalis (e.g., NaOH or KOH) and ammonium hydroxide (NH_4OH). When interacting with these reagents, cations form metal hydroxides that do not dissolve in excess alkali. These hydroxides precipitate as solids, allowing the corresponding metals to be isolated. The cations of the fifth group include magnesium (Mg^{2+}), iron (II) (Fe^{2+}), iron (III) (Fe^{3+}) and other elements, whose precipitation from solution serves as the basis for their further separation and identification.

According to N. Ya. Loginov's description [1, pp. 16–17], two types of analysis are used in analytical chemistry: systematic and fractional. The systematic course of analysis is largely associated with the precipitation of cations by a group reagent and the subsequent step-by-step detection of cations. It involves dividing the mixture into groups and subgroups using group reagents, and then detecting individual ions within these groups using specific reactions. This process allows for a complete analysis of the sample, detecting each ion after all interfering ions have been removed, but this type of work requires a huge amount of time and effort, which is not always possible. Therefore, we will consider the option of fractional analysis of the mixture of the fifth analytical group of cations.

As already mentioned, fractional analysis differs from systematic analysis in the speed of reactions and the detection of ions regardless of the presence of others.

2. Practical part

Fractional analysis of the mixture of the fifth analytical group of cations

Fractional analysis of ions is carried out with separate portions of the solution or dry sample in the presence of all sample components. For fractional analysis, characteristic or specific reactions are used that are unique to a given ion or substance.

Reagents: potassium hexacyanoferrate (III) ($K_3[Fe(CN)_6]$, potassium hexacyanoferrate (II) ($K_4[Fe(CN)_6]$, distilled water (dH_2 O), hydrochloric acid (HCl), sodium hydrophosphate ($NaHPO_4$), ammonium hydroxide (NH_4OH), ammonium chloride (NH_4Cl), nitric acid (HNO_3), lead minium (Pb_3O_4) .

Chemical glassware and equipment: test tube rack, conical flat-bottom flask, spirit burner, light microscope, pipette, microscope slide, test tube holder, porcelain dish, water bath.

Procedure:

Discovery of the Fe^{2+}cation.

Experiment conditions:

1) The reaction must be carried out at pH = 12-13.

2) The presence of ammonium salts prevents the formation of a precipitate.

3) Oxygen in the air causes colour changes due to partial oxidation of Fe^{2+}ions.

When opening the cation, several steps are performed. First, we took 3 drops of the control task and 3 drops of distilled water, 2 drops of potassium hexacyanoferrate (III) - $K_3[Fe (CN)_6]$ into a test tube. The presence of Fe^{2+}cations in the solution of group 5 cations we were studying was indicated by the formation of a blue precipitate, shown in Figure 1.

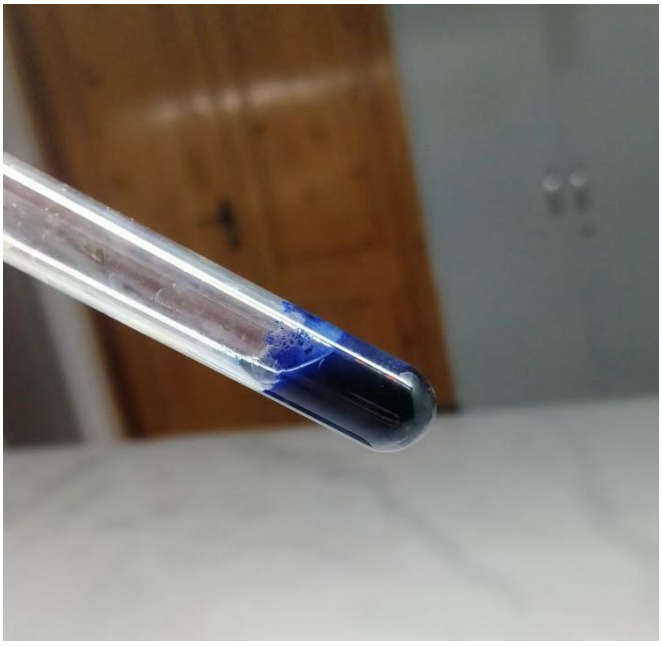

Figure 1 - Turnbull's blue

$3FeSO_4 + 2K_3[Fe(CN)_6] \rightarrow Fe_3[Fe(CN)_6]_2 + 3K_2SO_4$.

$3Fe^{2+} + 3SO_4^{2-} + 6K^+ + 2[Fe(CN)_6]^{3-} \rightarrow Fe_3[Fe(CN)_6]_2 + 6K^+ + 3SO_4^{2-}$

$3Fe^{2+} + 2[Fe(CN)_6]^{3-} \rightarrow Fe_3[Fe(CN)_6]_2$

Discovery of the Fe^{3+}cation.

Experiment conditions:

1) The reaction is carried out at pH < 3.

2) Free alkalis decompose Prussian blue.

3) Iron (II) and other cations do not interfere with the discovery of Fe^{3+}cations.

4) An excess of $K_4[Fe(CN)_6]$ is undesirable, as it can cause the formation of a soluble form of Prussian blue.

In one test tube, we took 3 drops of k/z, 3 drops of distilled water, 2 drops of 2n hydrochloric acid solution - HCI, and added 2 drops of potassium hexacyanoferrate (II) solution - $K_4[Fe(CN)_6]$. The presence of Fe^{3+}cations in the test solution was indicated by the appearance of a blue colour - Prussian blue, shown in Figure 2. To distinguish Turnbull's blue from Prussian blue, simply hold the test tubes up to the light. Then the colour in the test tube with the Fe^{2+}cation will be dark blue, and in the test tube with the Fe^{3+}cation the colour will be a lighter shade of blue, and sometimes even greener. It is also possible to distinguish between them by the physical properties of the solution. In our opinion, the solution of Turnbull's blue is denser than that of Prussian blue, which is confirmed by the research of Glushchenko V.A. [2, p. 8].

Figure 2 - Prussian blue

$2Fe_2(SO_4)_3 + 3K_4[Fe(CN)_6] \rightarrow Fe_4[Fe(CN)_6]_3 + 6K_2SO_4$.

$4Fe^{2+} + 6SO_4^{2-} + 12K^+ + 3[Fe(CN)_6]^{3-} \rightarrow Fe_4[Fe(CN)_6]_3 + 12K^+ + 6SO_4^{2-}$

$4Fe^{2+} + 3[Fe(CN)_6]^{3-} \rightarrow Fe_4[Fe(CN)_6]_3$

Discovery of the Mg^{2+}cation.

Experimental conditions:

1) The reaction is carried out in an ammoniacal environment at pH=8.

2) An excess of NH_4Cl prevents the precipitation of $MgNH_4PO_4$, so an excess of hydrochloric acid should not be used.

3) Cations of all analytical groups, except for the first one, may interfere with the reaction.

We took a microscope slide and placed one drop of k/z on it. Next, we placed two NH_4Cl crystals and one drop of Na_2HPO_4solution on this drop. Then, we held the microscope slide over ammonia vapours, which had been poured into a porcelain cup beforehand, for about one minute. After that, the microscope slide was held over the burner flame until it was completely dry. We examined the resulting crystals under a microscope and observed the characteristic shape shown in Figure 3.

$MgSO_4 + Na_2HPO_4 + NH_4OH \rightarrow MgNH_4PO_4 + Na_2SO_4 + H_2O$

$Mg^{2+} + SO_4^{2-} + 2Na^+ + HPO_4^{2-} + NH_4OH \rightarrow MgNH_4PO_4 + 2Na^+ + SO_4^{2-} + H_2O$

$Mg^{2+} + HPO_4^{2-} + NH_4OH \rightarrow MgNH_4PO_4 + H_2O$

Figure 3 - $MgNH_4PO_4$crystals

Discovery of the Mn^{2+}cation.

We took 3 drops of c/t, 6 drops of distilled water and 5 drops of concentrated nitric acid - $HNO_{3(conc.)}$ into a test test tube and added a small amount of lead minium - Pb_3O_4. Then we heated the test tube in a water bath until it boiled. In the presence of Mn^{2+}cations in the solution manganic acid is formed, which decomposes when heated or settled, forming MnO_4^- as indicated by the appearance of a crimson colour in the solution we obtained (Figure 4).

Figure 4 - Manganic acid ($HMnO_4$)

$2Mn(NO_3)_2 + 5PbO + 6HNO_3 \rightarrow 2HMnO_4 + 5Pb(NO_3)_2 + 2H_2O$

$Mn^{2+} + 6H^+ + 5PbO + 6NO_3^- \rightarrow 2MnO_4^- + 5Pb^{2+} + 10NO_3^- + 2H_2O$

$Mn^{2+} + 6H^+ + 5PbO \rightarrow 2MnO_4^- + 5Pb^{2+} + 2H_2O$

For more details on all qualitative reactions to fifth group cations, see the table below

Table. Qualitative reactions to fifth group cations

Cation	Reagent	Analytical effect
Mg^{2+}	Sodium hydrogen phosphate Na_2HPO_4 in the presence of NH_3 and NH_4Cl	White crystalline precipitate $MgNH_4PO_4$
	8-hydroxyquinoline $C_9H_6N(OH)$ in NH_3 (aq)	Yellow-green crystalline precipitate of magnesium oxyquinolinate
Mn^{2+}	Oxalic acid $H_2C_2O_4 \cdot 2H_2O$ in an alkaline environment	Pink solution of $Na_3[Mn(C_2O_4)_3]$
	Bismuthate sodium $NaBiO_3$ in HNO_3 (diluted)	Raspberry-purple solution of $HMnO_4$
Fe^{2+}	Potassium hexacyanoferrate (III) $K_3[Fe(CN)_6]$	Formation of a dark blue precipitate ("Turnbull's blue")
	Dimethylglyoxime $C_4H_6N_2(OH)_2$ in NH_3 (aqueous) medium	Alo-red solution $[Fe(C_4H_6N_2O_2)_2] \cdot xNH_3$
Fe^{3+}	Potassium hexacyanoferrate (II) $K_4[Fe(CN)_6]$	Formation of a dark blue precipitate ("Berlin blue")
	Potassium thiocyanate KSCN	Red solution of thiocyanates $[Fe(SCN)]^{2+}$, etc.
	Salicylic acid $HCO_2C_6H_4OH$ in NH_3 (aqueous)	Red-purple solution of iron(III) salicylate

3. Conclusion

In conclusion, we can conclude that in fractional analysis of fifth group cations, each cation can be determined by a specific reaction regardless of the presence of other cations in the mixture. This confirms the speed and accessibility of fractional analysis.

Fractional analysis, a method of qualitative chemical analysis that allows the detection of individual ions in a solution without their preliminary sequential separation, is based on the use of highly sensitive selective reagents, with the help of which the desired ion can be detected in the presence of others.

The advantage of this method is that it uses small amounts of solution and the analysis time is short. The method is highly sensitive: the minimum detectable concentration of the ions of interest can reach 0.05–0.001 μg.

REFERENCE LIST

1. N. Ya. Loginov, A. G. Voskresensky, I. S. Solodkin. Analytical Chemistry: A Textbook for Students of Pedagogical Institutes Specialising in Chemistry and Biology / 2nd edition, revised. Moscow: Prosveshchenie, 1979.
2. Glushchenko V.A. - "Berlin Blue and Turnbull Blue" Synthesis of $KFe^{III}[Fe^{II}(CN)6] \cdot H2O$ crystallohydrate by two methods and comparison of external differences. Moscow 2021
3. D.A. Nurgaliyeva – Analytical Chemistry: Qualitative Analysis – Nur-Sultan, 2021

UDC: 544.72
DOI: https://doi.org/10.30546/2521-6317.2025.01.459

SYNTHESIS OF SURFACTANTS BASED ON OCTYLAMINE, PROPYLENE OXIDE, AND DICARBOXYLIC ACIDS AND INVESTIGATION OF THEIR ANTIBACTERIAL PROPERTIES

Gulnara AHMADOVA*, Nizami MURSALOV, Nigar YAGUBOVA, Khuraman MAMMADOVA, Tarana GULIYEVA

Academician Y.H. Mammadaliyev Institute of Petrochemical Processes of the Ministry of Science and Education of the Republic of Azerbaijan,

Baku, Azerbaijan

ARTICLE INFO

Article history:
Received:2025-12-08
Received in revised form:2025-12-08
Accepted:2025-12-18
Available online

Keywords:
gemini surfactant, propylene oxide, dicarboxylic acids, surface tension, specific electrical conductivity, antibacterial

ABSTRACT

Using a twofold molar excess of propylene oxide at 25 °C, octylbis(2-hydroxypropyl) amine was synthesized. A series of gemini surfactants was obtained by reacting this product with dicarboxylic acids (oxalic, succinic, adipic, and sebacic) in a 2:1 molar ratio at 53–55 °C. The structures of the synthesized products were confirmed using IR spectroscopy. Tensiometric measurements of surface tension over a wide concentration range at the air–water interface revealed that the obtained compounds exhibit high surface activity. For example, the product based on oxalic acid reduces the surface tension from 70.33 mN/m at 0.0001% to 29.51 mN/m at 0.1%. It was also shown that their specific electrical conductivity significantly exceeds that of deionized water, confirming the ionic nature of the synthesized compounds. Furthermore, disk diffusion tests demonstrated that the antibacterial activity of these products depends not only on the length of the spacer group but also on the type of bacterial strain.

*Corresponding author.

E-mail: ahmadovagulnara@mail.ru (Gulnara Ahmadova).

5. INTRODUCTION

The current stage of scientific development is marked by growing interest in surfactants, which is driven by their wide application in various fields, including industry, agriculture, medicine, and everyday life. In recent years, researchers have increasingly focused on the synthesis of surfactants with novel structural architectures [1-3]. Among these, gemini surfactants deserve special attention. The distinctive feature of their structure is the presence of two hydrophobic moieties and two headgroups (typically charged), linked by spacer fragments of varying length and composition [4-9]. Compared to their monomeric analogues, gemini surfactants exhibit a combination of high positive surface charge, conformational flexibility, and the ability to adapt spatially during association. They are also characterized by low critical micelle concentration values, allowing their use in significantly lower dosages [10]. These attributes impart enhanced performance properties [11–13]. Due to their high efficiency, gemini surfactants represent a more

environmentally friendly and economically advantageous alternative to conventional surfactants.

The present study focuses on the synthesis of new gemini surfactants based on octylamine, propylene oxide, and dicarboxylic acids, as well as on investigating how the structure of the spacer group influences their surface-active and antibacterial properties.

6. MATERIALS AND EXPERIMENTAL METHODS

Octylamine (99% purity; Alfa Aesar, Shore Road, Heysham), propylene oxide (99.9%; Alfa Aesar, Great Britain), oxalic acid dihydrate (99%), succinic acid (99%), adipic acid (99%), and sebacic acid (98%) were all supplied by Alfa Aesar. The chemical structures of the prepared compounds were confirmed by ALPHA FT-IR analysis. The surface tension values of the aqueous solutions of the synthesized gemini surfactants were measured at the air–water interface using a du Nouy tensiometer (KSV Sigma 702, Finland) with the ring method. The specific electrical conductivity was determined using an ANION-410 ionometer (Russia). The antibacterial activity of the synthesized substances was assessed by the disk diffusion method in accordance with standard microbiological procedures [14]. The antibacterial activity was evaluated against the following microorganisms: *Staphylococcus aureus* (MRSA and MSSA) and *Escherichia coli*.

7. RESULTS AND DISCUSSION

In the first stage, octylamine and propylene oxide were synthesized at a molar ratio of 1:2 at room temperature (20–25 °C) for 15–35 hours. The obtained compound, octylbis(2-hydroxypropyl) amine, is a transparent, viscous substance. It is partially soluble in water and highly soluble in ethanol, acetone, hexane, kerosene, CCl_4, and isopropanol. The reaction scheme can be described as follows:

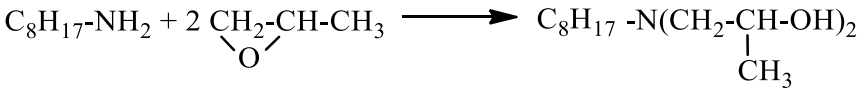

In the IR spectrum of octylbis(2-hydroxypropyl)amine (cm^{-1}), the following absorption bands were identified: 3391 ν (OH), 2959, 2824 and 2854 ν (CH), 1458, 1373 and 1332 δ (CH), 1279 ν (C–N), 1132 ν (C–O), and 722 δ $(CH_2)_x$.

In the second stage, gemini surfactants were obtained from the interaction of octylbis(2-hydroxypropyl)amine with dicarboxylic acids (oxalic, succinic, adipic, and sebacic). The reactions were carried out in a flask equipped with a magnetic stirrer at 70–80 °C at a molar ratio of 2:1. The main components obtained are illustrated in the reaction scheme below:

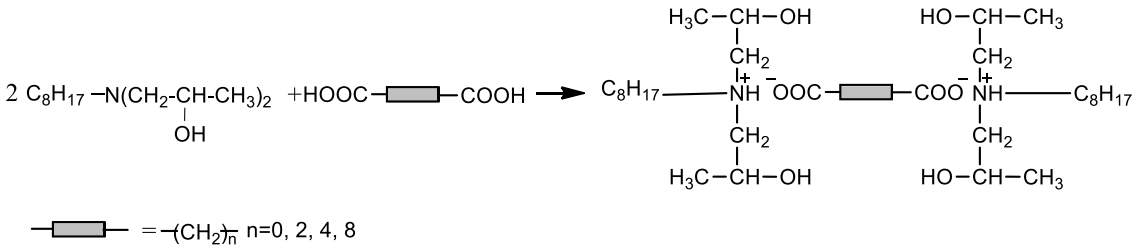

The gemini surfactants obtained as a result of the synthesis can be designated as follows: $C_8C_0C_8$ (based on oxalic acid) – a yellow liquid; $C_8C_2C_8$ (based on succinic acid) and $C_8C_4C_8$ (based on adipic acid) – viscous, light brown substances; $C_8C_8C_8$ (based on sebacic acid) – a viscous brown liquid.

The structures of the synthesized products were confirmed using IR spectroscopy. The IR spectrum of the compound obtained from octylbis(2-hydroxypropyl)amine and sebacic acid is shown in Fig. 1. In the IR spectrum,cm^{-1}: 3311 ν (OH and NH), 2953, 2924 and 2854 ν (CH), 2540 and 2387 (NH^+), 1561 ν_{as} (COO^-), 1376 ν_s (COO^-), 1457 δ (CH), 1135 ν (C-N), 1079 (C-O), 722 δ $(CH_2)_x$.

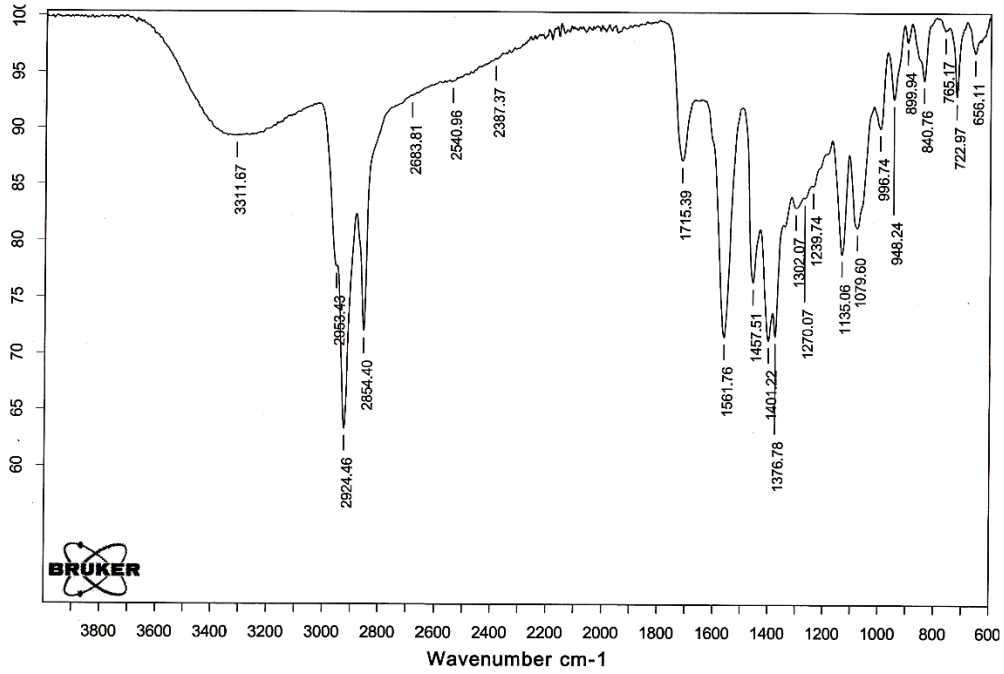

Fig. 1. IR spectrum of the gemini surfactant obtained from **octylbis(2-hydroxypropyl)amine** and sebacic acid

Table 1 presents the surface tension values of aqueous solutions of the synthesized gemini surfactants with spacer groups of different lengths over a wide concentration range. The results show that all investigated compounds reduce the surface tension depending on their concentration; however, the extent of this reduction varies significantly with the structure of the spacer group.

For $C_8C_0C_8$, the most pronounced and consistent decrease in surface tension is observed: from 70.33 mN/m at 0.0001% to 29.51 mN/m at 0.1%. This behavior indicates high surface activity and effective adsorption of the molecules at the air–water interface even at low concentrations.

Table 1. Interfacial tension at the air–water interface of aqueous solutions of gemini surfactants at various concentrations

Gemini surfactants	Concentration of substances in water (by weight), %												
	0.0001	0.00025	0.0005	0.00075	0.001	0.0025	0.005	0.0075	0.01	0.025	0.05	0.075	0.1
	Surface tension at the water-air interface, mN/m (20 °C)												
$C_8C_0C_8$	70.33	67.43	62.39	60.75	59.43	56.22	52.95	48.27	44.57	40.32	35.52	30.72	29.51
$C_8C_2C_8$	70.97	70.56	70.69	69.08	67.02	67.62	67.42	63.53	62.05	56.09	49.49	46.67	44.47
$C_8C_4C_8$	71.58	67.78	61.53	62.70	66.63	62.29	49.35	56.42	58.32	49.18	48.17	48.28	46.00
$C_8C_8C_8$	70.78	69.15	62.41	62.53	50.52	52.93	52.65	52.53	52.07	54.97	39.12	39.30	38.41

The compound $C_8C_2C_8$ shows a less intensive decrease in surface tension at low concentrations. The values remain relatively high up to 0.005–0.01%, but at higher concentrations the surface tension decreases to 44.47 mN/m. This suggests lower efficiency compared to $C_8C_0C_8$, which may be attributed to reduced packing density at the interface due to the longer spacer.

For $C_8C_4C_8$, an irregular pattern of surface tension changes is observed. Along with notable decreases (e.g., 49.35 mN/m at 0.005%), local increases are also present. Such behavior is likely associated with structural rearrangements and conformational changes of the monomers and aggregates in solution, leading to unstable adsorption at the interface.

The compound $C_8C_8C_8$ exhibits particularly interesting behavior. Despite having the longest spacer group, it shows a noticeable reduction in surface tension at intermediate concentrations (~50–52 mN/m at 0.001–0.01%). As the concentration increases further, very low surface tension values (38.41 mN/m at 0.1%) are achieved, comparable to the most efficient compound, $C_8C_0C_8$. This indicates the possibility of a more compact intermolecular organization at higher concentrations, compensating for the effect of the long spacer.

Overall, the results demonstrate a strong influence of spacer length on the surface-active properties of the gemini surfactants. The most stable and efficient compound in reducing surface tension across the entire concentration range is $C_8C_0C_8$. Increasing the spacer length generally leads to lower efficiency; however, $C_8C_8C_8$ shows a distinct improvement in performance at higher concentrations, which may be attributed to specific features of its aggregation behavior.

Table 2 presents the data on the specific electrical conductivity of the new gemini surfactants synthesized on the basis of octyldiisopropylolamine and various dicarboxylic acids. The measurements were carried out in aqueous solutions at 22 °C within the mass concentration range of 0.00625% to 0.1%.

Table 2. Specific electrical conductivity of new gemini surfactants obtained on the basis of octyldiisopropylolamine and dicarboxylic acids

Gemini surfactants	Concentration of gemini surfactants in water (by weight), %				
	0.00625	0.0125	0.025	0.05	0.1
	Specific electrical conductivity, μS/cm (22 °C)				
$C_8C_0C_8$	10.6	22.9	39.0	85.5	226.1
$C_8C_2C_8$	10.8	20.7	37.7	82.5	146.3
$C_8C_4C_8$	12.0	25.0	45.0	96.0	170.1
$C_8C_8C_8$	10.8	19.7	35.5	83.9	150.2

As seen from the table, an increase in the concentration of all studied surfactants leads to a rise in specific electrical conductivity, which is associated with an increased number of ions in the solution. The highest conductivity values at the maximum concentration (0.1%) are observed for the compound $C_8C_0C_8$, while $C_8C_2C_8$, $C_8C_4C_8$, and $C_8C_8C_8$ exhibit slightly lower but comparable values. The differences in conductivity among the series members are attributed to the length of the spacer group and its influence on the degree of ionization and the micellar structure in solution.

The antimicrobial activity of the synthesized gemini surfactants was evaluated using the disk diffusion method, and the results are presented in Table 3. The data show varying degrees of inhibitory activity depending on the structure of the spacer group and the type of microorganism tested.

Table 3. Antimicrobial activity of gemini surfactants

Microbes	Inhibition zone diameter (mm)			
	$C_8C_0C_8$	$C_8C_2C_8$	$C_8C_4C_8$	$C_8C_8C_8$
Gram-positive bacteria				
Escherichia coli	15	8	7	-
Gram-negative bacteria				
Staphylococcus aureus MRSA	8	-	7	8
Staphylococcus aureus MSSA	9	-	13	8

For the gram-positive bacterium *Escherichia coli*, the highest activity is observed for $C_8C_0C_8$, which forms an inhibition zone of 15 mm. The compounds $C_8C_2C_8$ and $C_8C_4C_8$ exhibit significantly weaker activity (8 and 7 mm, respectively), while $C_8C_8C_8$ shows no activity. This indicates high sensitivity of *E. coli* to structures with a short spacer and a gradual decrease in activity as the spacer length increases.

In the case of *Staphylococcus aureus* MRSA, a different trend is observed. The compounds $C_8C_0C_8$ and $C_8C_8C_8$ inhibit bacterial growth with equal efficiency (8 mm), whereas $C_8C_4C_8$ shows moderate activity (7 mm). The compound $C_8C_2C_8$ is ineffective against MRSA. These findings suggest that spacer length influences the interaction of gemini surfactants with resistant *S. aureus* strains in a different manner compared to other microorganisms.

For *Staphylococcus aureus* MSSA, the largest inhibition zone (13 mm) is observed for $C_8C_4C_8$, which differs from its behavior in other tests. The compounds $C_8C_0C_8$ and $C_8C_8C_8$ show moderate activity (9 and 8 mm, respectively), while $C_8C_2C_8$ remains inactive.

Overall, the data demonstrate that the antimicrobial activity of gemini surfactants depends not only on the length of the spacer group but also on the specific bacterial strain. The compound $C_8C_0C_8$ is the most universal, exhibiting consistent activity against all tested microorganisms, whereas $C_8C_2C_8$ is the least effective in most cases. These differences may be related to how the surfactant molecules interact with bacterial cell walls and their aggregation behavior in aqueous media.

8. Conclusion

New gemini surfactants based on octyldiisopropylolamine and a series of dicarboxylic acids (oxalic, succinic, adipic, and sebacic) were synthesized. The structures of the obtained compounds were confirmed by IR spectroscopy. The surface tension values of their aqueous solutions were determined using a tensiometric method. It was established that the length of the spacer group significantly influences the surface-active properties of the gemini surfactants. The most stable and efficient compound in terms of reducing surface tension across the entire investigated concentration range is $C_8C_0C_8$. An increase in spacer length generally leads to a decrease in efficiency; however, for $C_8C_8C_8$, a pronounced improvement in properties is observed at higher concentrations, which may indicate specific features of its aggregation behavior. The antibacterial activity of the synthesized gemini surfactants was evaluated using the disk diffusion method. Analysis of the obtained data shows that the antibacterial effect is determined not only by the length of the spacer group but also by the type of bacterial strain. The compound $C_8C_0C_8$ exhibits the most universal properties, demonstrating consistent activity against all tested microorganisms.

This research was supported by the Azerbaijan Science Foundation Grant № AEF-MGC-2025-1(54)-20/15/4-M-15

REFERENCE LIST

1. Pal, D. (2020). Gemini surfactants – A short overview. *Journal of the Indian Chemical Society*, 97(11a), 2242–2247.
2. Rahimov, R. A., Ahmadova, G. A., Isayeva, A. M., Rustamova, I. V., Agamaliyeva, D. B., & Zubkov, F. I. (2023). Anionic cocogem surfactants containing propyl-2-ol groups: Synthesis, surface properties and antibacterial activity against SRB bacteria. *Egyptian Journal of Petroleum*, 32, 15–21.
3. Gawali, I., & Usmani, G. (2020). Synthesis, surface active properties and applications of cationic gemini surfactants from triethylenetetramine. *Journal of Dispersion Science and Technology*, 41, 450–460.
4. Fan, Y.-X., Han, Y.-C., & Wang, Y.-L. (2016). Effects of molecular structures on aggregation behavior of gemini surfactants in aqueous solutions. *Acta Physico-Chimica Sinica*, 32(1), 214–226.
5. Wang, P., Pei, S., Wang, M., Yan, Y., Sun, X., & Zhang, J. (2017). Coarse-grained molecular dynamics study on the self-assembly of gemini surfactants: The effect of spacer length. *Physical Chemistry Chemical Physics*, 19(6), 4462–4468.
6. Menger, F. M., & Keiper, J. S. (2000). *Gemini surfactants*. Angewandte Chemie International Edition, 39, 1906–1920.
7. Shaheen, A., Mir, A. W., Arif, R., & Wani, A. L. (2020). Synthesis, micellization behavior and cytotoxic properties of imidazolium-based gemini surfactants. *Colloids and Interface Science Communications*, 36, 100257.
8. Pinazo, A., Pons, R., Bustelo, M., Manresa, M. Á., Morán, C., Raluy, M., & Perez, L. (2019). Gemini histidine-based surfactants: Characterization, surface properties and biological activity. *Journal of Molecular Liquids*, 289, 111156.
9. Mondal, M. H., Roy, A., Malik, S., Ghosh, A., & Saha, B. (2016). Review on chemically bonded geminis with cationic heads: Second-generation interfactants. *Journal of Research in Chemistry Intermediates*, 42, 1913–1928.
10. Mirgorodskaya, A. B., Zakharova, L. Y., Khairutdinova, E. I., Lukashenko, S. S., & Sinyashin, O. G. (2016). Supramolecular systems based on gemini surfactants for enhancing solubility of spectral probes and drugs in aqueous solution. *Colloids and Surfaces A: Physicochemical and Engineering Aspects*, 510, 33–42.
11. Brycki, B. E., Szulc, A., Kowalczyk, I., Koziróg, A., & Sobolewska, E. (2021). Antimicrobial activity of gemini surfactants with ether group in the spacer part. *Molecules*, 26, 5759.
12. Kamal, M. S. (2016). Review of gemini surfactants: Potential application in enhanced oil recovery. *Journal of Surfactants and Detergents*, 19, 223–236.
13. Wang, Y. X., Cao, Y. Q., Zhang, Q., & Meng, Q. (2016). Novel cationic gemini surfactants based on piperazine: Synthesis, surface activity, and foam ability. *Journal of Dispersion Science and Technology*, 37, 465–471.
14. Hasanov, E. E., Rahimov, R. A., Ahmadova, G. A., Muradova, S. A., & Gurbanov, A. V. (2024). Dissipative particle dynamics simulation and experimental studies of pseudo-gemini surfactants with different hydrophobic chain lengths. *Journal of Molecular Liquids*, 411, 125766.

2025. Volume 9, Number 1 Pages 52-72

UDC: 547.625
DOI: https://doi.org/10.30546/2521-6317.2025.01.485

SYNTHESIS, CHARACTERIZATION, AND APPLICATIONS OF POLYMERS, BASED ON AROMATIC AMINES: A BRIEF REVIEW

Ramil RZAYEV[*1,2,3], Bakhtiyar A. MAMMADOV[3], Fliur Z. MACAEV[1]

[1] *Laboratory of Organic Synthesis, Institute of Chemistry of the Moldova State University, str. Academiei 3, MD-2028, Chisinau, Republic of Moldova*

[2] *Department of Chemical Engineering, Baku Engineering University, Hasan Aliyev str. 120, Baku, Absheron, AZ0101, Azerbaijan Republic*

[3] *Institute of Polymer Materials, Azerbaijan National Academy of Sciences, Vurgun Str., 124, Sumgait, AZ5004, Azerbaijan Republic*

ARTICLE INFO

Article history
Received:2025-12-14
Received in revised form:2025-12-16
Accepted:2025-12-19
Available online

Keywords:
ortho-phenylenediamine;
meta-phenylenediamine;
para-phenylenediamine;
aniline;
oxidative polymerization;

ABSTRACT

Aromatic amines represent one of the most extensively studied classes of organic compounds due to the valuable polymeric products they form and their exceptional properties. This review provides an overview of their synthesis, principal properties, a broad range of applications and some limitations.

Aniline and its derivatives are regarded as promising candidates for intrinsically conductive polymers (CPs), which can be employed as electroactive materials in electronics, energy storage, sensors, smart textiles, and biomedical technologies. Owing to their conjugated structures, tunable redox chemistry, and excellent environmental stability, aromatic-amine-based polymers-particularly polyaniline and its derivatives-remain among the most versatile materials in the field of synthetic metals. Their lightweight nature, chemical robustness, processability, and mechanical flexibility, combined with the ability to modulate electrical conductivity through protonic or oxidative doping, enable these materials to serve as potential alternatives to conventional metals, and semiconductors.

This review highlights recent advances in the synthesis, doping mechanisms, and structure–property relationships of aromatic-amine-based conductive aromatic polymers. Special attention is given to established synthetic routes, including chemical and electrochemical oxidative polymerization, interfacial and template-assisted methods, plasma and photochemical techniques, and emerging green synthesis strategies. This article aims to support the continued development of next-generation functional materials for advanced technological applications.

* *Corresponding author:*
E-mail: ramilrzayev81@gmail.com

1. Introduction

Aromatic amines are a structurally important class of organic molecules in which an amine group is conjugated with an aromatic ring, imparting distinctive electronic and reactivity profiles. Since their discovery, conducting polymers (CPs) have attracted considerable attention due to their unique combination of electronic conductivity and polymeric properties, prompting numerous comprehensive reviews of their synthesis, structure, and applications. The pioneering

work in this field was recognized with the 2000 Nobel Prize in Chemistry, awarded to MacDiarmid, Shirakawa, and Heeger for demonstrating that organic polymers can exhibit metallic conductivity under suitable conditions [1–6] This breakthrough sparked widespread interest in a variety of conducting polymers, including polythiophene, poly-pyrrole, and polyaniline. These materials are characterized by an extended π-conjugated system, in which a large number of π-electrons are delocalized across the polymer backbone [7, 8]. The delocalized π-electron system in conducting polymers underpins their intrinsic electrical conductivity, while the presence of a finite energy gap between the valence and conduction bands imparts semiconducting behavior, allowing charge transport under appropriate conditions [9, 10].

Among conducting polymers aniline and its derivatives have been particularly notable, as their oxidative polymerization produces materials with tunable redox states, good environmental stability, and versatile processability. Furthermore, aromatic diamines such as o-, m-, and p-phenylenediamines provide extra functionality, enabling the formation of ladder-type or phenazine-like structures with enhanced electronic and physicochemical properties, broadening their potential applications in sensing, energy storage, optoelectronics, and biomedical technologies [11].

This review provides a comprehensive overview of the development of aromatic conducting polymers derived from key monomers, including aniline, o-toluidine, and o-, m-, and p-phenylenediamines. It examines their classification (Figure 1), synthetic methodologies, structural and physicochemical characterization, and diverse potential applications. In addition, the review critically addresses the current limitations and challenges associated with these polymers, highlighting areas where further research is required to enhance their performance and broaden their practical applicability.

2. Classification of aromatic amines

Aromatic amines are a fundamental class of organic compounds characterized by the presence of one or more amino groups (-NH_2, -NHR, or -NR_2) directly attached to an aromatic ring. The simplest example is aniline ($C_6H_5NH_2$)[12–14]. Their unique structural features combine the nucleophilicity of the amino group with the stability and electronic properties of the aromatic system, making them highly versatile in chemical synthesis and industrial applications. These compounds serve as key intermediates in the production of dyes, pharmaceuticals, agrochemicals, and high-performance polymers. The classification of aromatic amines-based on the number of amino groups, substitution patterns, and type of aromatic ring-not only provides a systematic understanding of their structural diversity but also plays a critical role in predicting their chemical reactivity and suitability for specific applications. Given their broad utility, aromatic amines continue to be a focus of research in material science, medicinal chemistry, and polymer chemistry, particularly in the development of conductive polymers, functional materials, and biologically active molecules.

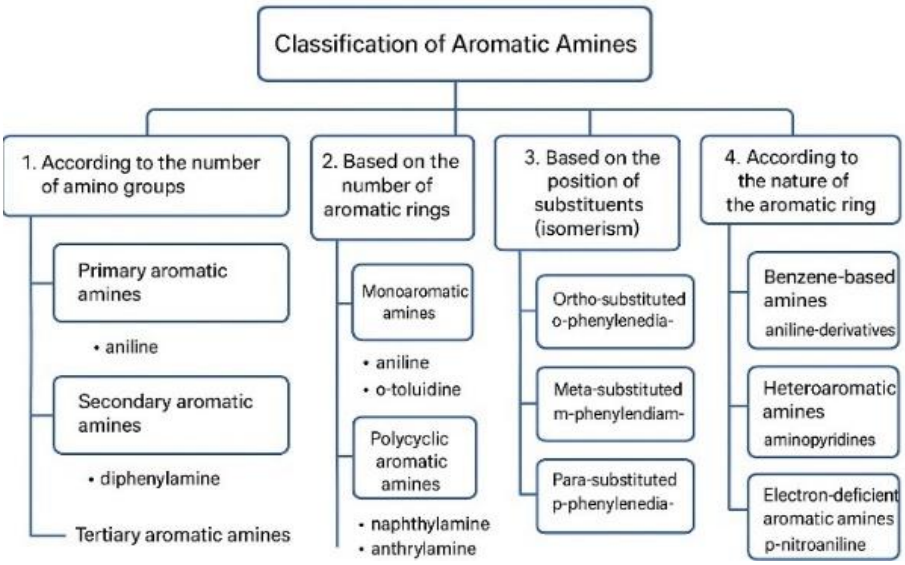

Figure 1. Classification of aromatic amines

2.1. Methods of polymer synthesis

Conductive polymers obtained from aromatic amines - such as aniline, toluidine isomers, and *o*-/*m*-/*p*-phenylenediamine - have attracted significant attention due to their unique redox activity, tunable conductivity, environmental stability, and broad applicability in electronics, sensors, catalysis, and energy storage systems. The method of synthesis plays a central role in defining the polymer's molecular structure, oxidation state, doping level, morphology, and resulting electronic properties. Accordingly, numerous synthetic approaches have been developed to manipulate polymer growth, control nanostructure formation, and tailor physicochemical characteristics to meet specific functional requirements. This section provides a comprehensive review of the principal synthesis routes employed for conductive polymers derived from aromatic amines, emphasizing mechanistic features, processing variables, structural outcomes, and application-relevant characteristics.

2.1.1. Chemical Oxidative Polymerization

Chemical oxidative polymerization (COP) remains the most extensively used method for synthesizing conductive polymers from aromatic amines. In this approach, polymerization is initiated by the oxidation of the monomer in the presence of strong oxidants such as ammonium or potassium persulfate, ferric chloride, or ceric ammonium nitrate. When dissolved in acidic media, aromatic amines become protonated, facilitating the generation of radical cations upon oxidation. These reactive intermediates undergo head–tail or para–para coupling to form dimers, oligomers, and ultimately high-molecular-weight polymer chains. For aniline and *phenylenediamine* derivatives, COP typically yields polymers in mixed oxidation states, including leucoemeraldine, emeraldine, and pernigraniline forms. The final oxidation state strongly influences conductivity and is largely dictated by oxidant concentration, reaction temperature, and acidity of the medium. The method is versatile, allowing production of powders, colloidal dispersions, nanofibers, nanotubes, and composite structures depending on the choice of surfactants, templates, co-monomers, and dopants. Its simplicity, scalability, and compatibility with various functional additives make COP the dominant route for industrial-scale production [15–17].

2.1.2 Electrochemical Polymerization

Electrochemical polymerization provides a highly controlled method to deposit conductive polymer films directly onto electrode surfaces. In this technique, the aromatic amine undergoes anodic oxidation under a precisely controlled potential or current. The resulting radical cations couple at the electrode interface, leading to the sequential formation of oligomers and polymer chains tightly adhering to the substrate. This method offers several key advantages: it eliminates the need for chemical oxidants, produces highly pure materials, and enables precise tuning of film thickness, morphology, redox state, and doping level. Electrochemical polymerization of aniline and various phenylenediamines often results in smooth, uniform, and strongly adherent films with excellent electroactivity. Cyclic voltammetry, chronoamperometry, and chronopotentiometry are typically employed to control polymer growth. This approach is widely used in the fabrication of electrochemical sensors, anticorrosive coatings, redox-active thin films, and energy-storage electrodes [18–22].

2.1.3. Enzymatic Polymerization

Enzymatic polymerization has emerged as an environmentally benign alternative to traditional oxidative methods. Enzymes such as laccase and horseradish peroxidase catalyze the oxidation of aromatic amines under mild aqueous conditions, generating radical species with high selectivity. This form of biocatalytic oxidation typically produces oligomers and polymers with fewer structural defects and narrower molecular-weight distributions compared to chemical oxidative routes.

In the case of aniline and phenylenediamines, enzymatic approaches often yield materials with enhanced biocompatibility and improved environmental sustainability. Because the reaction occurs without harsh oxidants or extreme acidity, the resulting polymers are suitable for biomedical applications, biosensing, and environmentally friendly coatings. Control over pH, hydrogen peroxide concentration, enzyme loading, and reaction temperature is essential for determining polymer architecture and oxidation state [23–28].

2.1.4 Photochemical Polymerization

Photochemical polymerization relies on the use of ultraviolet irradiation or photo-initiators to drive oxidative coupling of aromatic amines. Upon exposure to light, photosensitizers and electron-transfer agents generate radical species from the monomer, initiating polymer growth. This method enables spatial control over polymerization and is particularly valuable for producing micro-patterned or lithographically structured films.

For aniline and substituted amines, photopolymerization can be conducted in solution or directly on surfaces, yielding thin, uniform films with tunable properties. The ability to restrict polymerization to illuminated regions facilitates fabrication of microelectrodes, photonic structures, and patterned conductive coatings. The structural features and conductivity of the resulting polymers depend on light intensity, exposure time, wavelength, and the presence of photosensitizing additives.

2.1.5. Plasma Polymerization

Plasma polymerization involves subjecting volatile monomers to a plasma discharge within a low-pressure environment. The energetic species present in the plasma partially fragment and activate the aromatic amine molecules, allowing them to recombine on a surface to form highly

crosslinked polymeric films. The resulting materials are typically ultra-thin, pinhole-free, and highly adherent. Although plasma polymerization often leads to partially disordered structures with limited conjugation, optimizing plasma power, pressure, and monomer flow can preserve aromatic functionality and allow useful levels of conductivity. Plasma-deposited films of aniline and phenylenediamines offer exceptional conformality and chemical robustness, making them attractive for protective coatings, biomedical interfaces, and electronic insulation layers [29].

2.1.6. Vapor-Phase Polymerization

Vapor-phase polymerization (VPP) has become an important method for fabricating high-quality conductive polymer films. The technique involves depositing an oxidant layer-commonly ferric chloride, iron (III) tosylate, or ammonium persulfate - onto a substrate, followed by exposure to monomer vapor. The monomer diffuses into the oxidant-rich layer, initiating polymerization at a controlled rate. VPP is especially effective for deriving thin, uniform films of polyaniline and its derivatives with high crystallinity and excellent electrical conductivity. The absence of bulk solution enables more ordered chain growth and minimizes aggregation and impurity incorporation. Process parameters such as oxidant loading, humidity, temperature, and additives profoundly influence polymer morphology, nanostructure, and film conductivity. VPP has become a key technique in flexible electronics, antistatic coatings, and transparent conductive layers.

2.1.7 Solid-State Polymerization

Solid-state polymerization represents a solvent-free approach in which aromatic amine crystals undergo polymerization under elevated temperature, pressure, or irradiation. The constrained mobility of monomers in the solid state can promote highly ordered polymer structures and unique packing arrangements. Although this method is less commonly applied to aniline and phenylenediamines, several studies have demonstrated its utility for producing crystalline oligomers, nanostructured materials, and hybrid frameworks. Solid-state methods are attractive from a sustainability standpoint, offering minimal solvent use and low environmental impact. They also enable the formation of materials that may be difficult to access through traditional solution-phase polymerization [30–33].

2.1.8. Template-Assisted Polymerization

Template-assisted synthesis is a powerful means of directing the growth of conductive polymers into well-defined nanostructures. Hard templates such as anodic alumina, silica, or polycarbonate membranes are widely used to produce nanowires, nanotubes, and nanorods. Soft templates-such as surfactant micelles, microemulsions, or liquid-crystalline phases-guide the formation of nanospheres, nanofibers, and other self-assembled morphologies. When aromatic amines undergo oxidative or electrochemical polymerization within these templates, the resulting nanostructures exhibit enhanced surface area, improved ion transport, and increased electrochemical performance. Template-assisted polymerization is particularly advantageous for fabricating nanostructured polyaniline and phenylenediamine derivatives for sensing, catalysis, and energy-storage applications [34–37].

2.1.9. Interfacial Polymerization

Interfacial polymerization exploits the boundary between two immiscible phases - typically an aqueous solution containing the aromatic amine and an organic phase containing an oxidant or

co-reactant. Polymerization occurs exclusively at the interface, yielding thin films, membranes, shells, or hollow nanostructures. For aromatic amines, this approach provides exceptional control over film thickness and enables the fabrication of ultrathin polyaniline membranes with uniform morphology. The confined nature of the interfacial region produces materials with reduced structural disorder and improved electronic properties. These films find applications in separation technologies, coating materials, and controlled-release systems [38–42].

2.1.10 Hydrothermal and Solvothermal Polymerization

Hydrothermal and solvothermal methods involve conducting polymerization reactions in sealed autoclaves at elevated temperatures and pressures. Under these conditions, aromatic amines exhibit enhanced solubility, reactivity, and diffusivity, promoting the formation of crystalline or hierarchically organized polymer structures.

Hydrothermal polymerization of aniline and phenylenediamines often results in nanorods, nanosheets, hollow spheres, or flower-like architectures with high structural coherence. These materials are promising for applications in catalysis, electrochemical devices, and advanced functional composites. The solvent type, reaction temperature, pressure, and duration critically determine the resulting morphology and polymer chain structure [43].

2.1.11. Emulsion and Miniemulsion Polymerization

Emulsion and miniemulsion techniques utilize surfactant-stabilized droplets to disperse aromatic amines in an aqueous medium. Oxidative polymerization proceeds within individual micelles or droplets, yielding polymer nanoparticles with well-controlled sizes and narrow distributions. Miniemulsion systems, with smaller and more stable droplets, provide superior control over particle uniformity. Polyaniline and substituted amine nanoparticles produced through these techniques possess high dispersibility, making them suitable for inks, coatings, and composite formulations. The method is compatible with large-scale industrial processing and allows incorporation of dopants, stabilizers, or functional particles into the polymer matrix [44, 45].

2.1.12. Sol–Gel Assisted Polymerization

Sol–gel assisted polymerization integrates conductive polymers with inorganic networks such as silica or metal oxides. During the solgel process, polymerization of the aromatic amine occurs simultaneously with the formation of a growing inorganic matrix, resulting in hybrid materials that combine the conductivity of organic polymers with the structural stability of inorganic hosts. These organic-inorganic hybrids exhibit enhanced thermal stability, mechanical strength, and environmental resistance. Incorporation of aniline or phenylenediamine derivatives within sol–gel networks enables precise control over morphology, porosity, and interfacial interactions. Such materials are widely used in sensors, catalysis, corrosion protection, and multifunctional coatings [46, 47].

Conclusion

The synthesis method profoundly influences the structural, electronic, and functional properties of conductive polymers derived from aromatic amines. Chemical oxidative polymerization and electrochemical deposition remain the most widely used techniques due to their simplicity and versatility, while emerging methods such as enzymatic, photochemical, and vapor-phase polymerization offer new opportunities for achieving highly controlled architectures and

environmentally sustainable processing. Template-based, hydrothermal, and sol-gel-assisted approaches further expand the morphological diversity of these materials, enabling precise manipulation of nanoscale features critical for advanced applications. Collectively, these methods form a robust toolbox for tailoring the properties of aromatic-amine-based conductive polymers for next-generation electronic, electrochemical, sensing, and catalytic systems.

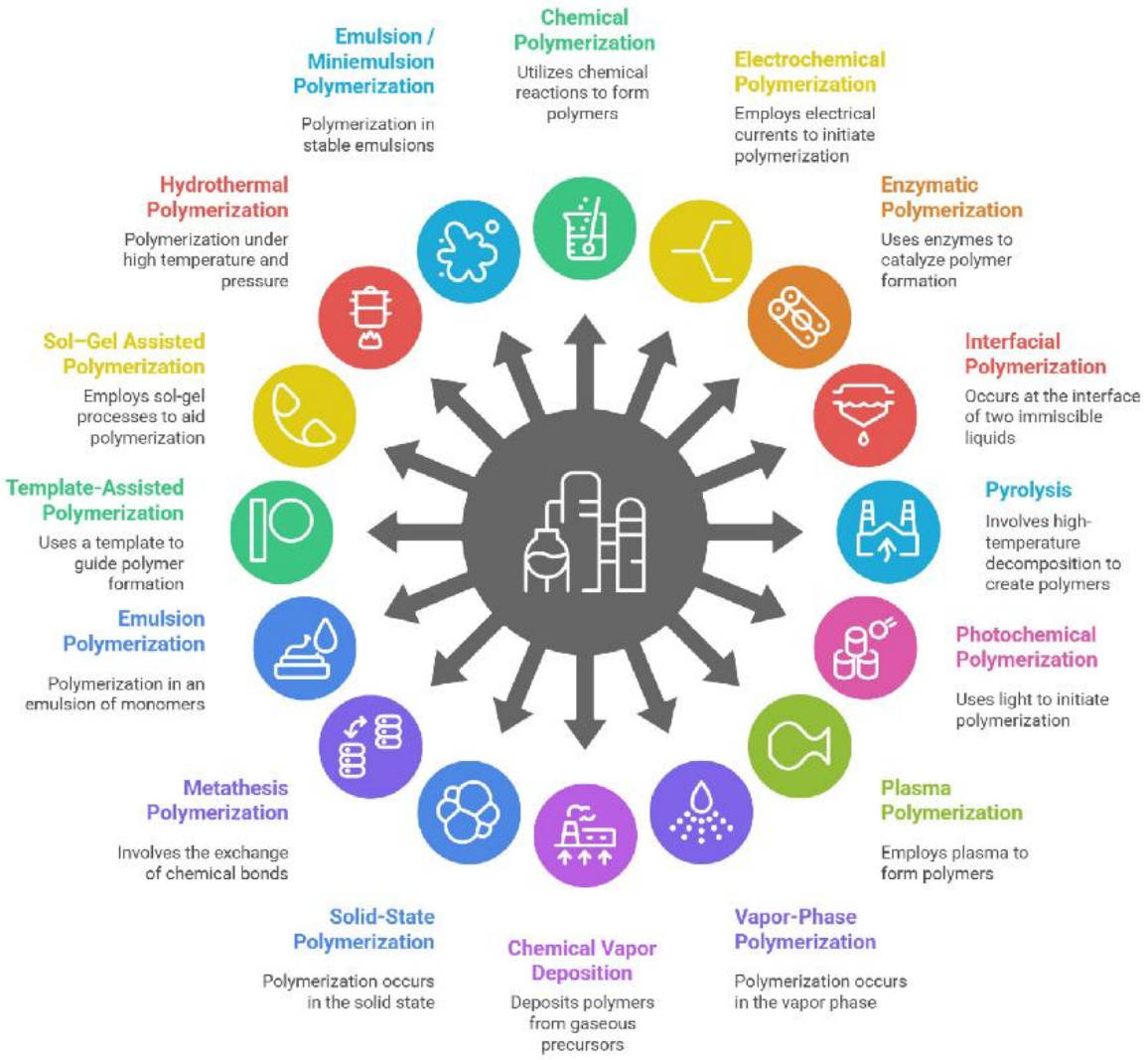

Figure 2. The synthesis methods of aromatic polymers

2.2 Characterization of Polymers

Polymer characterization is the process of determining the physical, chemical, thermal, mechanical, and structural properties of polymers. This is essential to understand their behavior, performance, and suitability for various applications, including conductive polymers, coatings, biomedical devices, and composites. Proper characterization ensures reproducibility, quality control, and guides further chemical modifications. In Figure 3, some essential characterization techniques of polymers are given [15, 48–51].

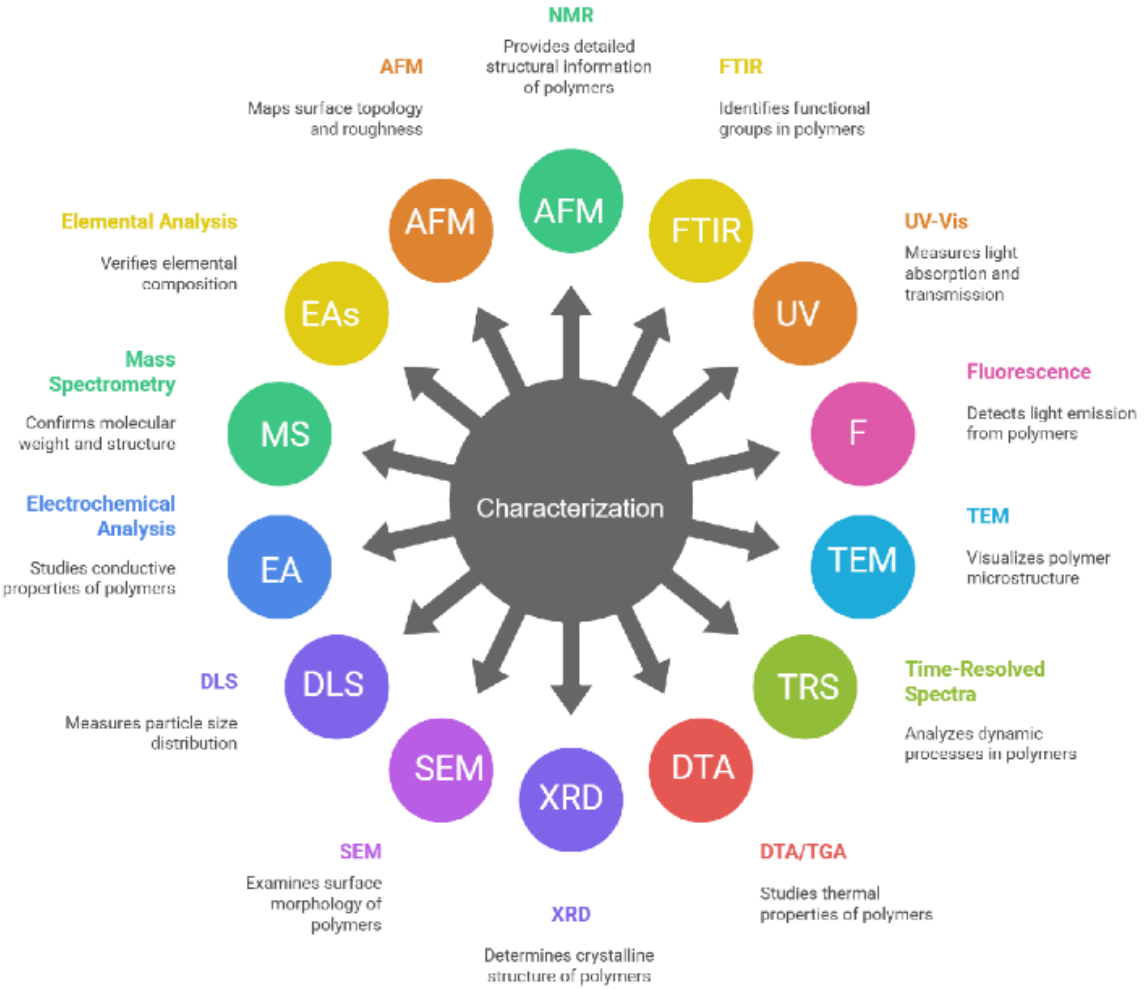

Figure 3. Characterization techniques of polymers.

3. Members of aromatic amines

Polymers and oligomers with extended π-conjugated systems are commonly called "conjugated polymers" or "conjugated oligomers." These materials are made of regularly repeating units with alternating single and double bonds. Often, heteroatoms such as nitrogen, oxygen, and sulfur, which have lone electron pairs, participate in conjugation by interacting with neighboring π-orbitals, helping form an extended poly-conjugated system [7, 8]. The high level of electron delocalization along the polymer backbone results in a variety of unique physicochemical properties. As a consequence, conjugated polymers show electronic and optical activity, resistance to radiation, semiconducting behavior, paramagnetism, and catalytic functions, making them essential for developing sensors and detectors [52–54], polymer batteries [55–57], semiconductor diodes [10, 58], solar cells [59], and various biomedical devices [60–62].

Polyaromatic amines, specifically, are high-molecular-weight compounds with a conjugated bond system and a nitrogen atom with a lone electron pair incorporated into the aromatic ring. The synthesis of these polymers and oligomers-widely used across various technological fields due to their distinctive properties-along with understanding their composition, structure, and functional features, is a complex yet fascinating area of research.

3.1 Historical background of Aniline

The history of the oxidative polycondensation of aniline - the first and most fundamental aromatic amine - begins in the early 19th century. Aniline is an organic compound originally derived from coal tar. The German chemist Otto Unverdorben first isolated it from indigo dye in 1826 and named it "crystallin" [63], although its chemical structure was unknown at the time. In 1835, Friedlieb Ferdinand Runge isolated another coal-tar substance called "kyanol" (or "cyanol"), which turned a vivid blue when treated with calcium hypochlorite. The word "kyanol," rooted in the Greek kuanos (blue) and Latin oleum (oil), actually referred to aniline [4]. The first person to officially name the substance "aniline" (from anil, the Spanish name for indigo) was Karl Julius Fritzsche, who obtained it by treating indigo with caustic potash in 1840 [5]. During his studies of coal-tar distillation, Runge also discovered pyrrole and quinoline. Notably, he observed that aniline formed insoluble, variably colored solids when exposed to different oxidizing agents. In one experiment, he added hydrochloric acid to a porcelain cup containing gold oxide and a few drops of aniline, then heated the mixture to 100 °C. This produced a violet material that turned blue-gray upon drying. Two years later, in 1842, Nikolai Nikolaevich Zinin synthesized the same substance by reducing nitrobenzene and called it "benzydam" [64]. In 1843, August Wilhelm von Hofmann (1818–1892) demonstrated that Unverdorben's "crystallin," Runge's "kyanol," Fritzsche's "aniline," and Zinin's "benzydam" were actually identical compounds, confirming the true identity of aniline, later known as phenylamine or simply aniline [13, 64, 65]. Fritzsche also reported that aniline first turns yellow, then brown, upon exposure to air. Under certain conditions, reacting with nitrous acid (HNO_2) produces blue or green products. Treating aniline salts with chromic acid (H_2CrO_4) results in a dark green precipitate that later turns blue-black. In 1853, Beissenhirz showed that aniline produces a blue color when exposed to concentrated sulfuric acid and potassium dichromate. However, none of these early scientists managed to turn their discoveries into commercial applications.

In the mid-19th century, chemists began exploring the potential of aniline as a dye for textiles. Their investigations demonstrated that aniline and its derivatives could generate a wide spectrum of colors. In 1860, Crace-Calvert, Samuel Clift, and their assistant Charles Lowe obtained green and blue cotton dyes by oxidizing aniline, for which they received a joint patent the same year [66, 67]. A prolonged, 12-hour reaction of aniline salts with potassium chlorate yielded a green product known as "emeraldine," a name that later became widely associated with aniline derivatives. When this material was boiled in an alkaline or soapy medium, it converted into a blue substance referred to as "azurine"[68].

Lightfoot [67] demonstrated that only a small amount of potassium chlorate was required to oxidize aniline salts; however, achieving an intense coloration required an additional oxidizing agent, such as copper [66]. The use of copper salts caused corrosion, leaving marks on printed fabrics. This problem was resolved by Charles Louth in 1864, who introduced copper sulfide as an alternative. Because copper sulfide is insoluble, it remained inactive during the printing process, and only after aniline black was formed did the chlorate convert it into copper sulfate, significantly reducing damage to printing cylinders [68, 69].

Around the same period, in 1860, Heinrich Caro synthesized the second black aniline dye. Caro later supervised the production of numerous new dyes, including artificial alizarin, eosin, methylene blue, and several azo dyes. He also contributed to early studies on indigo synthesis

and helped elucidate the structures of triphenylmethane dyes [69, 70]. In 1863, Charles Louth and August Wilhelm von Hofmann oxidized aniline hydrochloride with potassium dichromate, producing a deep black pigment known as aniline black - one of the first synthetic black dyes. Its intense coloration, washfastness, and ease of application led to its rapid adoption in the textile industry.

The discovery of aniline black marked a major milestone in the transition from natural to synthetic dyes and stimulated extensive research into aniline-based pigments. This work laid the foundation for synthetic dye chemistry and enabled the development of a broad palette of artificial colors still used today. Following this breakthrough, a significant contribution was made by the physician and chemist Henry Letheby [15], who, while investigating nitrobenzene poisoning, discovered that nitrobenzene is metabolically reduced to aniline. This finding prompted the development of early chemical tests for detecting aniline [71].

Subsequent studies established that the highest-quality aniline black is obtained by oxidizing aniline salts-typically using HCl or H_2SO_4 as the reaction medium, in the presence of strong inorganic oxidants such as dichromates or chlorates and catalysts including $CuSO_4$ or $Fe(CH_3COO)_2$ at temperatures of 333–373 K [72].

In the 1870s and 1880s, Adolf Baeyer and several other chemists made significant scientific advances in collaboration with Caro and leading industrial researchers. Baeyer contributed to the understanding of tautomerism and proposed the modern structural formula for indigo. Although technical challenges-particularly those related to synthesizing indigo from inexpensive starting materials-remained unresolved for many years, major progress toward artificial indigo production resulted from Baeyer's research, initiated in 1865 at the Berlin Institute of Chemistry and supported by Caro during the mid-1870s [12].

Following these discoveries, a distinct group of electroactive materials known as intrinsically conductive polymers (ICPs) emerged. Achieving high conductivity in these polymers typically requires doping, which increases the density of mobile charge carriers. Among the various ICPs, polyaniline (PANI) is one of the most intensively studied. PANI stands out due to its straightforward synthesis, low cost, versatile redox behavior, and the ability to undergo reversible doping and dedoping through simple acid–base reactions. It also offers greater chemical and environmental stability than many other conductive polymers. Nevertheless, PANI still encounters persistent challenges related to poor solubility and limited processability, largely resulting from the rigidity of its conjugated backbone. These issues have constrained its widespread technological deployment, prompting continued research aimed at improving its solubility and processability.

A major advancement in this field was the introduction of copolymerization strategies involving aniline and structurally compatible monomers. Self-doped polyaniline derivatives produced through these approaches exhibit substantial improvements, including enhanced solubility, greater flexibility, and more stable redox and conductivity behavior across a wide pH range. Numerous comonomers containing functional groups such as –OH, $–NH_2$, $–SO_3H$, and –COOH etc., have been incorporated to achieve intrinsic doping, increase processability, and tailor the electronic properties of the resulting materials. In recent years, considerable research attention has been devoted to the synthesis and physicochemical characterization of aniline-based copolymers and their derivatives using a variety of polymerization techniques.

As a result, a series of soluble, thermally stable, flexible, and multifunctional copolymers/co-oligomers have been successfully synthesized from aniline and a range of versatile monomers. These materials exhibit improved processability, enhanced mechanical integrity, and tunable physicochemical properties owing to the incorporation of functional groups introduced through copolymerization. Owing to their conjugated structures and adjustable electronic behavior, such polymers find broad application in Optoelectronic Devices, including use in coating technologies, chemical and electrochemical sensors, rechargeable battery components, supercapacitors, flexible electronics, and other advanced functional devices.

3.2 Methyl aniline (o-Toluidine)

O-Toluidine (2-aminotoluene or *o*-methylaniline), a methyl-substituted derivative of aniline, has been an important compound in the evolution of synthetic organic chemistry and the early dye industry. Its history extends over nearly two centuries and reflects the rapid industrial and scientific developments of the 19th century. The compound was first conclusively identified in 1845, when James Sheridan Muspratt and August Wilhelm von Hofmann characterized *o*-toluidine alongside its *m*- and *p*-isomeric forms. Their work built upon earlier studies of coal-tar–derived aniline derivatives, which were becoming significant industrial raw materials at the time.

The commercial relevance of *o*-toluidine became apparent with the emergence of the first synthetic organic dyes. Landmark colorants such as mauveine and fuchsine marked the beginning of the synthetic dye industry, and *o*-toluidine soon became a key precursor in the manufacture of these early "aniline dyes." Its chemical reactivity and propensity to form intensely colored oxidation products made it a valuable intermediate for large-scale dye production.

By 1880, the increasing demand for toluidine-based dyes led to the establishment of commercial *o*-toluidine production in the United Kingdom. This development positioned *o*-toluidine as an important industrial building block in the synthesis of dyes, pigments, pharmaceuticals, and various polymeric materials, while also facilitating the broader adoption of coal-tar chemistry in industrial practice.

Following the discovery of intrinsically conductive polymers (ICPs), interest in aniline and its derivatives grew significantly. These compounds have been extensively studied because of their ability to polymerize in various media and copolymerize with a wide range of monomers. O-Toluidine, in particular, has frequently been used in copolymerization reactions to create materials with customized structural and electronic properties. The resulting homopolymers, copolymers, and their oligomeric counterparts have applications in sensors, energy storage devices, electronic components, and protective coatings.

3.3 Ortho-phenylenediamine

The story of phenylenediamine polymers has to be started with polyaniline. Phenylenediamine is the common name for diaminobenzene, which exists as three isomers: 1,2-, 1,3-, and 1,4-diaminobenzene. The 1,2-isomer is commonly called o-phenylenediamine; the 1,3-isomer is m-phenylenediamine; and the 1,4-isomer is p-phenylenediamine. O-phenylenediamine (o-PDA or 1,2-benzenediol), containing two amino groups in the 1st and 2nd positions, has been used as a precursor for heterocycles, dyes, and pharmacologically active molecules since the late 19th century. Initially, these compounds were obtained by reducing substances such as o-

dinitrobenzene and o-nitroaniline [73]. Its importance increased in the 20th century with the development of benzimidazole chemistry and the subsequent development of POPD by oxidation-polycondensation, which allowed the production of redox-active films for electronic and electroanalytical applications [74, 75]. Poly-ortho-phenylenediamine (p-OPD) has been synthesized mostly chemical and electrochemical methods [76, 77].

In chemical synthesis, OPD is typically polymerized by exposing its solution to an appropriate oxidant, reductant, or initiator, leading to the formation of polymeric materials in either powder or thin-film form. Common oxidizing agents employed in OPD polymerization include $K_2Cr_2O_7$, $FeCl_3$, $K_2S_2O_8$, $(NH_4)_2S_2O_8$, and H_2O_2. Extensive studies have utilized this chemical oxidative polymerization approach to produce and characterize poly(o-phenylenediamine) and its derivatives [78].

In electrochemical polymerization, redox-active units may be incorporated directly into the growing polymer backbone, added as pendant substituents through pre-functionalized monomers, or introduced in a separate post-functionalization step after film deposition. Poly(o-phenylenediamine) (POPD) was first obtained as a robust and adherent coating on electrode surfaces by electropolymerizing OPD in acidic media [19]. Since the mid-1980s, extensive studies have explored the electro-polymerization behavior of aromatic diamines. Importantly, POPD films generated via cyclic voltammetry display IR absorption patterns distinct from those produced under potentiostatic conditions [79, 80]. Moreover, polymers synthesized electrochemically exhibit NMR characteristics that differ noticeably from POPD obtained through conventional chemical oxidative methods. Copolymerization offers an effective route to functionalize OPD and tailor its photo-physical, optical, and structural characteristics [75, 76, 81]. Numerous studies have demonstrated that combining OPD with other conducting or semiconducting monomers-acting as donor or acceptor units-can significantly modify and improve the resulting material's properties. The wide range of possible co-monomers and the freedom to adjust their ratios provide a versatile platform for designing OPD-based nanomaterials with enhanced physical, optical, and performance attributes. The composition of the monomer feed, along with reaction parameters such as temperature, catalyst, and medium pH, plays a decisive role in determining the structural and functional characteristics of the resulting co-polymer [75, 77].

POPD and its copolymers have been applied in a broad range of fields, including electrode materials[82], optoelectronic and solar cells [83], anode materials for lithium-ion batteries [84], sensors [85], supercapacitors [86, 87], anticorrosion coatings [88], and the removal of Cd(II) from aqueous solutions [89], etc.

Despite its broad range of applications, OPD and its polymers exhibit several limitations. The monomer is intrinsically toxic and therefore requires careful handling. Poly(o-phenylenediamine) also suffers from low solubility and only moderate conductivity relative to polyaniline. Furthermore, oxidative polymerization often produces heterogeneous structures and variations in color, and some formulations show limited mechanical flexibility. Ongoing research aims to address and overcome these drawbacks.

3.4 Metha-phenylenediamine

Metha-Phenylenediamine (m-PDA or 1,3-diaminobenzene), one of the three phenylenediamine isomers, has been recognized as an important intermediate in dye chemistry and early polymer science since the late 19th century. Historically, it served as a key precursor for azo dyes,

photographic developers, and rubber antioxidants. Industrially, m-PDA is produced by catalytic hydrogenation of 1,3-dinitrobenzene - the principal product obtained from the dinitration of benzene using sulfuric–nitric acid mixtures. This hydrogenation step is typically carried out in water or methanol over supported palladium catalysts or Raney nickel [90]. Over time, m-PDA is used in several industrially significant sectors:

a. High-performance polymers: – m-PDA is a critical monomer in the synthesis of aramids, such as poly(m-phenyleneterephthalamide), and in high-temperature polyimides, poly(amide-imide) s, and heteroaromatic frameworks [91, 92]. Examples are protective clothing and aircraft interiors. The polymer is made in the United States by Du Pont (Nomex), in Japan by Teijin, and in the former Soviet Union. The m-PDA is also used for curing epoxy resins to impart high-temperature strength and good resistance to chemical solvents. Such cured resins are used in filamentwound casings and adhesives. m-PDA is still used as the starting material for many dyes. Examples include Basic Brown 1 (Bismarck Brown), Basic Orange 2, Direct Black 38, and Developed Black BH [93, 94].

b. Conducting and electroactive materials : - m-PDA plays a significant role in the development of conducting and electroactive materials due to its bifunctional amine groups and rigid aromatic backbone, which facilitate electron delocalization and redox activity [95]. It is widely employed in the synthesis of aromatic poly(amine) frameworks, redox-active oligomers, and electrochemically responsive thin films. These materials often exhibit tunable conductivity, reversible redox behavior, and strong adhesion to various substrates, contributing to their utility in sensors, anticorrosion coatings, and electronic devices [96].

In addition, m-PDA readily participates in oxidative polymerization and metal-coordination reactions, enabling the formation of electrocatalytic films and metal - organic hybrid materials with enhanced electron-transfer properties[52]. Recent studies have emphasized its potential as a monomer for heat-resistant conductive polymers, organometallic complexes exhibiting high catalytic activity, and advanced composite materials that combine mechanical stability with improved electrical or electrochemical performance [95]. The structural versatility and redox behavior of m-PDA continue to support innovations in energy-storage materials, electrocatalysis, and functional protective coatings.

c. Dyes and pigments : - It serves as an intermediate for azo dyes, developer agents, and hair-color formulations [73].

d. Corrosion inhibitors : - m-PDA acts as a corrosion inhibitor through adsorption on metal surfaces and formation of protective films.

e. Pharmaceuticals and fine chemicals : - It is a precursor to numerous heterocycles and medicinal intermediates.

f. Nanomaterials and adsorbents : - m-PDA is used for synthesizing functional nanoparticles, carbon dots, and polymer-based adsorbents for water purification [97].

Limitations - Despite its wide utility, m-PDA presents several limitations. It is classified as harmful and a skin sensitizer, requiring regulated handling. The compound oxidizes readily in air, forming quinonoid species that change color and alter reactivity. Solubility limitations and undesirable color formation complicate its use in optical or transparent systems. Additionally, the highly reactive amine groups may lead to rapid crosslinking or uncontrolled branching in polymer synthesis.

Conclusion

m-Phenylenediamine is a versatile aromatic diamine with broad impact across polymer science, dye chemistry, and materials engineering. Its rigid aromatic core and reactive amine groups enable the formation of high-performance polymers, functional coatings, and advanced nanomaterials. Although challenges remain - including toxicity, oxidative instability, and processing difficulties - ongoing advances in green chemistry, controlled polymerization, and functional material design continue to expand the relevance of m-PDA in modern research and applications.

3.5 Para-phenylenediamine

Para-phenylenediamine (p-PDA), one of the three phenylenediamine isomers (in 1,4- postions), has been known since the late 19th century. The p-PDA is a crystalline solid that can appear in various colors, including pink, gray, yellow, or even colorless. Upon exposure to air, it undergoes oxidation, first turning red, then brown, and finally black. Many sources state that p-PDA was first synthesized by August Wilhelm von Hofmann in 1863, who was notably the chemistry professor of William Henry Perkin, the discoverer of the world's first synthetic dye, mauve (MOTM, January 1996) [98]. It was initially used as an intermediate for azo dyes and as a photographic developer, reducing silver halides to metallic silver under alkaline conditions, with its oxidation products exploited in dye formation. The industrial synthesis of p-PDA takes place in two steps: dinitration of benzene and catalytic hydrogenation of dinitrobenzene. Early applications also included rubber antioxidants and vulcanization accelerators. Its bifunctional amine groups and rigid para-substituted aromatic structure later made p-PDA a key monomer for wide range of polymers [99–101]. Over time, it has remained an important building block in organic synthesis, high-performance polymers such as aramids and poly-ureas, dyes and pigments, photographic and electronic applications, rubber, coatings, and other related fields [43, 73, 102–104].

Despite its broad range of applications, p-PDA also presents several limitations. It is a well-known skin sensitizer and allergen, and exposure through inhalation or ingestion poses health risks, leading to strict regulatory restrictions. Similar to other aromatic diamines, p-PDA readily oxidizes in air to form quinonoid species, which can affect its color, reactivity, and overall storage stability. Furthermore, its moderate solubility in organic solvents and highly reactive amine groups require careful handling to avoid unintended crosslinking during polymer processing.

4. Potential application of polymers

Aromatic amine-based polymers are an important class of conjugated and functional polymers with diverse technological applications (Figure 4). Their rich redox chemistry, environmental stability, tunable electronic structure, and ability to incorporate diverse substituents make them useful in a number of modern materials systems.

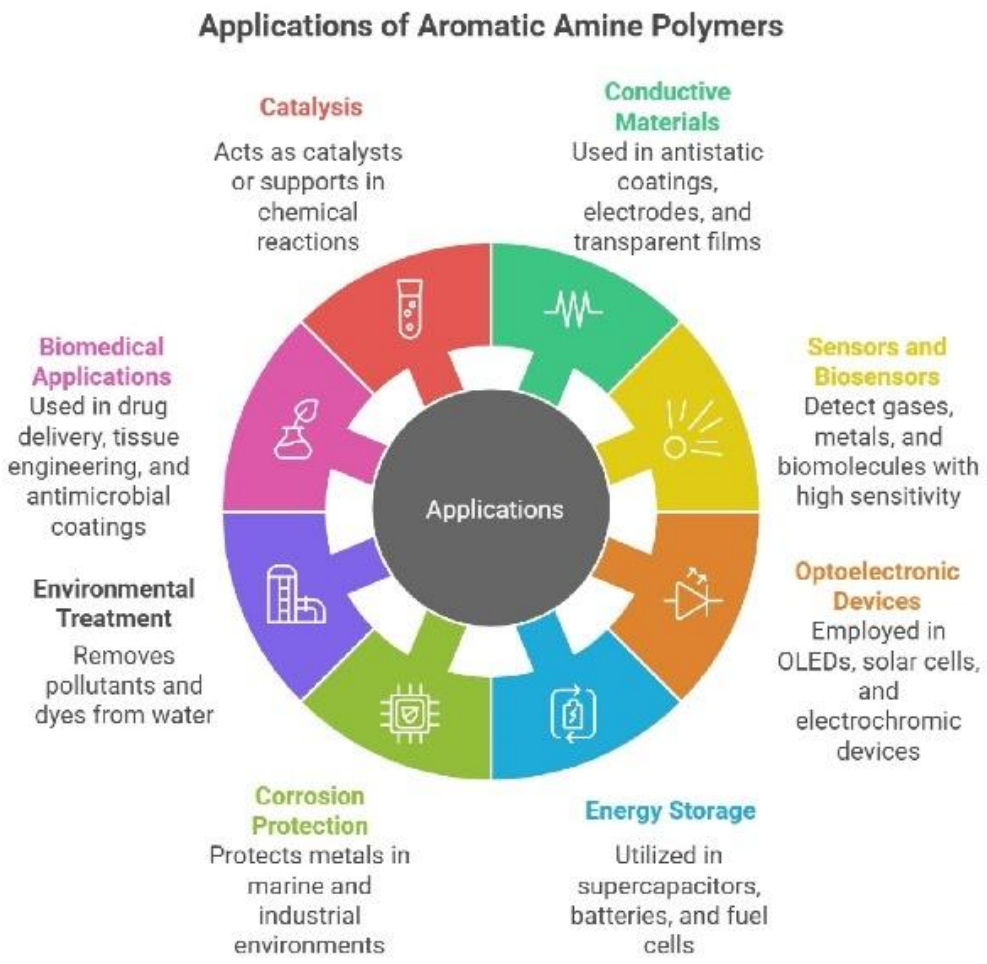

Figure 4. Applications of polymers based on aromatic amines monomers.

Conclusion

Although aromatic amines have been investigated for more than a century, compounds such as aniline and the diaminobenzenes continue to attract significant scientific attention. Polyaniline, for instance, was originally used as a dye but later emerged as one of the most extensively studied conducting polymers, finding applications in electronics, sensors, energy storage, anticorrosion coatings, and other advanced technologies. To enhance its physicochemical properties - including stability, solubility, and processability - researchers have widely explored the copolymerization of aniline with various monomers.

Compared with aniline, aromatic diamines (o-PDA, m-PDA, p-PDA) received scientific interest somewhat later, yet their importance has grown substantially over the past several decades. While their early use was largely limited to dye and pigment manufacture, the homo- and copolymers derived from these diamines are now employed across a broad range of modern technological fields, including optics, optoelectronics, sensing devices, smart and responsive materials, anticorrosion coating, semiconductor applications and etc. Their bifunctional amine groups, ability to form highly conjugated structures, and capacity for metal coordination further expand their utility in advanced materials.

Nevertheless, despite their valuable mechanical, electronic, and chemical characteristics, several intrinsic properties of aromatic amines - such as oxidative instability, toxicity, limited solubility, and high reactivity - continue to restrict their wider application and require careful management in both research and industrial setting.

Currently, researchers are pursuing various strategies to overcome these limitations and improve the performance of aromatic amine–based materials.

Acknowledgments

The authors R.R. and F.Z.M. are grateful for the project 25.80012.5007.72SE supported by the Moldovan National Agency for Research and Development (NARD).

Conflict of Interest

The authors declare no conflict of interest.

REFERENCES

1. Chiang, C. K., Fincher, C. R., Park, Y. W., Heeger, A. J., Shirakawa*, H., Louis, E. J., Gau, S. C., MacDiarmid, A. G. (1977). Electrical Conductivity in Doped Polyacetylene. *Phys. Rev. Lett,* 39(17), 1098–1101. DOI: **DOI.**org/10.1103/PhysRevLett.39.1098
2. Chiang, C. K., Fincher, C. R., Park, Y. W., Heeger, A. J., Shirakawa*, H., Louis, E. J., MacDiarmid, A. G.. (1978). Conducting polymers: Halogen doped polyacetylene. *J. Chem Phys, 69*(11), 5098–5104. **DOI.**org/10.1063/1.436503
3. MacDiarmid, A. G. (1997). Polyaniline and polypyrrole: Where are we headed? Synth Met, *84*(1-3), 27–34. **DOI.**org/10.1016/S0379-6779(97)80658-3
4. Macdiarmid, A. G., Heeger, A. J. (1979). Organic Metals and Semiconductors: The Chemistry of Polyacetylene, (CHX, And Its Derivatives. *Synthetic Metals, 1*(2), 101-118. **DOI**.org/10.1016/0379-6779(80)90002-8
5. Chiang, J. C., Macdiarmid, A. G. (1986). Polyaniline: Protonic Acid Doping of the Emeraldine form to the Metallic Regime. *Synthetic Metals, 13*(1-3), 195-205. **DOI.**org/10.1016/0379-6779(86)90070-6
6. Heeger, A. J. (2001). Semiconducting and metallic polymers: the fourth generation of polymeric materials. *J Phys Chem B, 105*(36), 8475–8491. **DOI.**org/10.1021/jp011611w
7. Gerhard Koßmehl. (1979). Semiconductive Conjugated Polymers. *Berichte der Bunsengesellschaft für physikalische Chemie,* 83(4), 417–426. **DOI.**org/10.1002/bbpc.19790830422
8. Brédas, J. L., Elsenbaumer, R. L., Chance, R. R., Silbey, R. (1983). Electronic properties of sulfur containing conjugated polymers. *J Chem Phys, 78*, 5656–5662. **DOI**.org/10.1063/1.445447
9. Reynolds JRTBCSTA (2019). Conjugated Polymers, 4th Edition. CRC Press, Boca Raton
10. Jadoun S, Riaz U (2020). Conjugated Polymer Light-Emitting Diodes. In: Polymers for Light-Emitting Devices and Displays. Wiley, pp 77–98. **DOI:**10.1002/9781119654643.ch4
11. Ganachari, S.V., Mogre, P., Tapaskar, R.P., Yaradoddi, J.S., Banapurmath, N. R. (2018). Polyaniline Synthesis and Its Wide-Range Sensor and Electronic Applications. Springer International Publishing 1267–1292. https://doi.org/10.1007/978-3-319-68255-6_186
12. Antony, S.T. (2009). Anilines: Historical Background. In: Patai's Chemistry of Functional Groups. Wiley, 1-73. **DOI.**org/10.1002/9780470682531.pat0383
13. Fritsche, J. (1840). Ueber das Anilin, ein neues Zersetzungsproduct des Indigo. *J. Fritzsche*, *36*(1), 84–90. **DOI:**10.1002/jlac.18400360108
14. M. Probst RH (1997). A systematic spectroelectrochemical investigation of alkyl substituted anilines and their polymers. *Macromol Chem Phys,* 198, 1499–1509.
15. Poddar, A., Patel, S.S., Patel, H.D. (2021). Synthesis, characterization and applications of conductive polymers: A brief review. *Polym Adv Technol,* 32(12), 4616–4641. **DOI**.org/10.1002/pat.5483

16. Rzayev, R.S., Mammadov, B.A., Abdullayev, Y.F., Ibadov, E. A. (2022). Synthesis and characterization of new nano-sized poly(p-phenylenediamine) in the presence of potassium persulfate. *Processes of Petrochemistry and oil Refining (PPOR),* 23(2),495–509.
17. Rzayev, R., Sucman, N., Geru, I., et al. (2025). Synthesis and Characterization of Nano-Sized Poly-(1,4-Diaminonaphthalene) in Potassium Persulfate. *Acta Chim Slov,* 72, 260–268. **DOI.**org/10.17344/acsi.2024.9032
18. Mortimer, R.J. (1995). Spectroelectrochemistry of electrochromicpoly(o-toluidine) and poly(m-toluidine) films. *J Mater Chem*, 5, 969–973. **DOI**.org/10.1039/JM9950500969
19. Maiyalagan, T. (2008). Electrochemical synthesis, characterization and electro-oxidation of methanol on platinum nanoparticles supported poly(o-phenylenediamine) nanotubes. *J Power Sources,* 179, 443–450. **DOI.**org/10.1016/j.jpowsour.2008.01.048
20. Geise, R. J. Adams, J. M., Barone, N, J., Yacynych, A. M. (1991). Electropolymerized films to prevent interferences and electrode fouling in biosensors. *Biosens Bioelectron, 6(*2),151–160. **DOI:**10.1016/0956-5663(91)87039-e
21. Sipahi, M., Parlak, A. E., Gul, A., Ekinci, E., Yard;m, M.F., Sarac, A.S. (2008). Electrochemical impedance study of polyaniline electrocoated porous carbon foam. *Prog Organic Coatings, 62,* 96–104. **DOI.**org/10.1016/j.porgcoat.2007.09.023
22. Buzarovska, A., Arsova, I., Larsov, L. (2001). Electrochemical synthesis of poly-(2-methyl aniline): electro-chemical and spectroscopic characterization. *Journal of the Serbian Chemical Society,* 66(1), 27–37. **DOI:**10.2298/JSC0101027B
23. Shan, J., Han, L., Bai, F,. Cao, Sh. (2003). Enzymatic polymerization of aniline and phenol derivatives catalyzed by horseradish peroxidase in dioxane (II). *Polym Adv Technol,* 14(3-5), 330–336. **DOI:**10.1002/pat.316
24. Kaya, İ., Yağmur, H. (2021). Synthesis of poly(4-aminosalicylic acid) through enzymatic and oxidative polycondensation by H_2O_2 oxidant. *Iranian Polymer Journal, 31,* 199–214. **DOI.**org/10.1007/s13726-021-00990-1
25. Alva, K. Shridhara., Kumar, Jayant., Marx, Kenneth A., Tripathy, S. K. (1997). Enzymatic synthesis and characterization of a novel water-soluble polyaniline: poly (2,5-diaminobenzenesulfonate). *Macromolecules,* 30, 4024–4029. **DOI.**org/10.1021/ma961544h
26. Cruz-silva, R., Escamilla, A., Nicho, M. E, et al. (2007). Enzymatic synthesis of pH-responsive polyaniline colloids by using chitosan as steric stabilizer. *European Polymer Journal,* 43(8), 3471–3479. **DOI**.org/10.1016/j.eurpolymj.2007.05.027
27. Kaya, I., Yağmur, H. K. (2020). Synthesis and characterization of poly-(3,5-diaminobenzoic acid) via enzymatic and oxidative polymerization and application in methylene blue adsorption. *J Mol Struct,* 1216, 128323. **DOI.**org/https://doi.org/10.1016/j.molstruc.2020.128323
28. Tonami, H., Uyama, H., Kobayashi, S., Reihmann, M. (2002). Enzymatic polymerization of m -substituted phenols in the presence of 2, 6-di-O-methyl-β-cyclodextrin in water. *e-Polymers,* 1–7. **DOI.**org/10.1515/epoly.2002.2.1.46
29. Cruz, G. J., Morales, J., Castillo-Ortega, M.M., Olayo, R. (1997). Synthesis of polyaniline films by plasma polymerization. *Synthetic Metals, 88(3),* 213-218. **DOI.**org/10.1016/S0379-6779(97)03853-8
30. Abdiryim, T., Jamal, R., Nurulla, I. (2007). Doping effect of organic sulphonic acids on the solid-state synthesized polyaniline. *J Appl Polym Sci,* 105, 576–584. **DOI.**org/10.1002/app.26070
31. Jamal, R., Abdiryim, T., Nurulla, I. (2008). Comparative studies of solid-state synthesized poly(o-methoxyaniline) and poly (o-toluidine). Polym Adv Technol, 19(11), 1461–1466. **DOI.**org/10.1002/pat.1139
32. Behzadi, M., Noroozian, E., Mirzaei, M. (2013). A novel coating based on carbon nanotubes/poly-ortho-phenylenediamine composite for headspace solid-phase microextraction of polycyclic aromatic hydrocarbons. *Talanta, 108,* 66–73. **DOI.**org/10.1016/j.talanta.2013.02.040
33. Kubota, M. M., Sacco, B. L., Bento, D.C., Santana, H. De. (2015). Spectrochimica Acta Part A: Molecular and Biomolecular Spectroscopy Synthesis and spectroscopic analysis of polydiphenylamine via oxidation with bentonite clay in the solid state. *Spectrochim Acta A Mol Biomol Spectrosc, 151,* 80–88. **DOI.**org/10.1016/j.saa.2015.06.092
34. Hongjin, Q., Wan, M., Matthews, B., Dai, L. (2001). Conducting Polyaniline Nanotubes by Template-Free Polymerization. *Macromolecules, 4,* 675–677. **DOI.**10.1021/ma001525e
35. Wu, J., Zhou, D., Looney, M. G., Too, C.O. (2009). A molecular template approach to integration of polyaniline into textiles. *Synthetic Metals, 159,* 1135–1140. **DOI.**org/10.1016/j.synthmet.2009.01.054
36. Jin, X., Yu, L., Zeng, X. (2008). Chemical Enhancing the sensitivity of ionic liquid sensors for methane detection with polyaniline template. *Sensors and Actuators B, 133,* 526–532. **DOI.**org/10.1016/j.snb.2008.03.022

37. Xian, Y., Liu, F., Feng, L., Wu, F., Wang, F., Jin, L. et al (2007) Nanoelectrode ensembles based on conductive polyaniline/poly (acrylic acid) using porous sol–gel films as template. *ScienceDirect,* 9, 773–780. **DOI.**org/10.1016/j.elecom.2006.11.017
38. Ferreira, A. A., Sanches, E. A. (2017). Multimorphologies of hydrochloride polyaniline synthesized by conventional and interfacial polymerization. *J Mol Struct, 1143,* 294–305. **DOI**.org/10.1016/j.molstruc.2017.04.104
39. Dallas, P., Stamopoulos, D., Boukos, N., Tzitzios, V., Niarchos, D., Petridis, D. (2007). Characterization, magnetic and transport properties of polyaniline synthesized through interfacial polymerization. *Polymer (Guildf),* 48, 3162–3169. https://doi.org/10.1016/j.polymer.2007.03.055
40. Kuo, C. W, Wen, T. C. (2008). Dispersible polyaniline nanoparticles in aqueous poly-(styrenesulfonic acid) via the interfacial polymerization route. *Eur Polym J,* 44, 3393–3401. **DOI.**org/10.1016/j.eurpolymj.2008.07.018
41. Dallas, P., Georgakilas, V. (2015). Interfacial polymerization of conductive polymers: Generation of polymeric nanostructures in a 2-D space. *Adv Colloid Interface Sci, 224*, 46–61. **DOI.**org/10.1016/j.cis.2015.07.008
42. Detsri, E., Dubas, S. T. (2009). Interfacial Polymerization of Water-Soluble Polyaniline and Its Assembly Using the Layer-By-Layer Technique. *J Metals, Materials and Minerals,19*, 39-44.
43. Soltane, L., Sediri, F. (2013). Hydrothermal synthesis, characterization and electrical investigation of poly (para-phenylenediamine) / vanadium oxide nanocomposite nanosheets. *Materials Science & Engineering B*, 178, 502–510. **DOI.**org/10.1016/j.mseb.2013.02.005
44. Lakouraj, M. M., Zare, E. N., Moghadam, P. N. (2014). Synthesis of novel conductive poly(p-phenylenediamine)/ Fe 3O4 nanocomposite via emulsion polymerization and investigation of antioxidant activity. *Advances in Polymer Technology* 33, 1-7. **DOI.**org/10.1002/adv.21385
45. Palaniappan, S., Jhon, A. (2008). Polyaniline materials by emulsion polymerization pathway. *Prog Polym Sci* 33, 732–758. **DOI.**org/10.1016/j.progpolymsci.2008.02.002
46. Jadoun, S., Verma, A., Ashraf, S. M., Riaz, U. (2017). A short review on the synthesis, characterization, and application studies of poly(1-naphthylamine): a seldom explored polyaniline derivative. *Colloid Polym Sci*, 295, 1443–1453. **DOI**.org/10.1007/s00396-017-4129-2
47. Jadoun, S., Riaz, U., Yáñez, J., Chauhan, N. P.S. (2021). Synthesis, characterization and potential applications of Poly(o-phenylenediamine) based copolymers and Nanocomposites: A comprehensive review. *Eur Polym J,* 156, 110600. **DOI.**org/10.1016/j.eurpolymj.2021.110600
48. Chauhan, R. P, Kumar, R., Chakarvarti, S.K. (2010). Synthesis of conducting polymers and their characterization. *Indian Journal of Pure and Applied Physics,* 48(7), 524–526.
49. Dumitrescu, I., Nicolae, C-A., Mocioiu, A.M., Gabor, R.A., Grigorescu, M., Mihailescu, M. (2009). Synthesis and characterization of conductive polymers with enhanced solubility. *UPB Sci Bull, Series A, 71,* 63–72.
50. Grigoras, M., Antonoaia, N-C. (2005). Synthesis and characterization of some carbazole-based imine polymers. *Eur Polym J,* 41,1079–1089. **DOI:**10.1016/j.eurpolymj.2004.11.019
51. Yağmur, H. K., Kaya, I. (2020). Synthesis and characterization of new polymers derived from 2-methyl-m-phenylenediamine as an effective adsorbent for cationic dye removal. *Arabian Journal of Chemistry,* 13, 8183–8199. **DOI.**org/10.1016/j.arabjc.2020.09.052
52. Dube, A., Malode, S. J., Alodhayb, A. N., et al. (2025). Conducting polymer-based electrochemical sensors: Progress, challenges, and future perspectives. *Talanta Open,* 11, 100395. **DOI.**org/10.1016/j.talo.2024.100395
53. Baranwal, J., Barse, B., Gatto, G., Broncova, G., Kumar, A. (2022). Electrochemical Sensors and Their Applications: A Review. *Chemosensor*, 10(9), 363. **DOI.**org/10.3390/chemosensors10090363
54. Bai, H., Shi, G. (2007). Gas sensors based on conducting polymers. *Sensors,* 7, 267–307. **DOI.**org/10.3390/s7030267
55. Chen, Ch., Gan, Z., Xu, Ch., Lu, L., Liu, Y., Gao, Y. (2017). Electrosynthesis of poly(aniline-co-azure B) for aqueous rechargeable zinc-conducting polymer batteries. *Electrochim Acta,* 252, 226–234.
56. Bahceci, S., Esat, B. (2013). A polyacetylene derivative with pendant TEMPO group as cathode material for rechargeable batteries. *J Power Sources,* 242, 33–40. **DOI**.org/10.1016/j.jpowsour.2013.05.051
57. Costa, C.M., Lizundia, E., Lanceros-Méndez, S. (2020). Polymers for advanced lithium-ion batteries: State of the art and future needs on polymers for the different battery components. *Prog Energy Combust Sci*, 79, 100846. **DOI.**org/10.1016/j.pecs.2020.100846

58. Karg, S., Scott, J.C., Salem, J.R., Angelopoulos, M. (1996). Increased brightness and lifetime of polymer light-emitting diodes with polyaniline anodes. *Synth Met,* 80, 111–117.
59. Get, R., Islam, Sk. M., Sing, S., Mahala, P. (2020). Organic Polymer Bilayer Structures for Applications in Flexible Solar Cell Devices. *Microelectron Eng*, 222, 111200. **DOI.**org/doi:10.1016/j.mee.2019.111200
60. Toktam Nezakati ASAT and AMSeifalian (2018). Conductive Polymers: Opportunities and Challenges in Biomedical Applications. *Chem Rev,* 118, 6766–6843. **DOI:**10.1021/acs.chemrev.6b00275
61. Du, A., Liu, Sh., Li, Y. (2025). Hollow Conductive Polymer Nanospheres with Metal–Polyphenol Interfaces for Tunable Hydrogen Peroxide Activation and Energy Conversion. *Polymers, 17*(24), 3305. **DOI.**org/10.3390/polym17243305
62. Zhang, H., Zhao, T., Newland, B., et al. (2018). Catechol functionalized hyperbranched polymers as biomedical materials. *Prog Polym Sci,* 78, 47–55. **DOI.**org/10.1016/j.progpolymsci.2017.09.002
63. Johnston, W. T. (2008). The discovery of aniline and the origin of the term "aniline dye." *Biotechnic and Histochemistry*, 83, 83–87. **DOI.**org/10.1080/10520290802136793
64. Rasmussen, S. C. (2017). The Early History of Polyaniline: Discovery and Origins. *Substantia*, *1*(2). **DOI.**org/10.13128/Substantia-30
65. Hofmann, A. W. (1843). Chemical investigation of organic bases in coal tar oil. *Ann Chem Pharm*, 47, 140.
66. Travis, A.S. (1994). From Manchester to Massachusetts via Mulhouse: The Transatlantic Voyage of Aniline Black. *Technology and Culture,* 35(1), 70-99. **DOI:**10.2307/3106749
67. Lightfoot, J. (1871). The Chemical History and Progress of Aniline Black. *Lower House, Lancashire.*
68. Noelting, E. (1889). Scientific and Industrial History of Aniline Black. *Wm. J. Matheson & Co., New York,* 1851-1922.
69. Travis, A. S. (1994). From Manchester to Massachusetts via Mulhouse: The Transatlantic Voyage of Aniline Black. *JSTOR*, 35(1), 70–99. **DOI.**10.1353/tech.1994.0118
70. Seymour, R.B. (1988). Polymers are everywhere. *J Chem Educ*, 65(4), 327-342.
71. H. Letheby (1862) XXIX. - On the production of a blue substance by the electrolysis of sulphate of aniline. *J Chem Soc,* 15, 161–163
72. Bibault, E. (1983). Les polymers conductrrs d'electricite: des "metaux syntetiques" riches en promesses. *Actualite chimique*, 7, 23–30.
73. Zollinger, H. (2004). Color Chemistry. Synthesis, Properties and Applications of Organic Dyes and Pigments. third revised. *Wiley*, 43(40), 5291-5292. **DOI.**org/10.1002/anie.200385122
74. Kang, E., Neoha, K., G, Tanh, K. L. (1998). Polyaniline: A Polymer with Many Interesting Intrinsic Redox States. *Progress in Polymer Science*, 23(2), 277-324. **DOI.**org/10.1016/S0079-6700(97)00030-0
75. Palaniappan, S. (2008). Electrochemical co-polymerization of aniline and o-phenylenediamine. *J Solid State Electrochem,* 12, 953–962.
76. Wang, Z., Liao, F., Yang, S., Guo, T. (2012). Synthesis of poly (o-phenylenediamine)/ ferric oxide composites with rose-like hierarchical microstructures. *Mater Lett*, 67, 121–123. **DOI:**10.1016/j.matlet.2011.09.032
77. Samanta, S., Kar, P. (2015). Influence of pH of the reaction medium on the structure and property of conducting poly (o-phenylenediamine). *Mater Today Proc,* 2, 1301–1308. **DOI:**10.1016/j.matpr.2015.07.046
78. Kannapiran, N., Muthusamy, A., Anand, S., Jayaprakash, R. (2018). Synthesis, Structural, Magnetic and Electrical Characterization of Poly(o-phenylenediamine)/CoFe2O4 Nanocomposites. *J Supercond Nov Magn*, 31, 1489–1497. **DOI.**org/10.1007/s10948-017-4343-7
79. Zhang, X., Li, G., Wang, J., Chu, J., Wang, F., Hu, Z., Song, Z. (2022). Revisiting the Structure and Electrochemical Performance of Poly(o-Phenylenediamine) as an Organic Cathode Material. *ACS. Appl Mater Interfaces,* 14, 27968-27978. **DOI:**10.1021/acsami.2c06208
80. Ariffin, A. A., O'Neill, D. R., Yahya, M.Z.A., Zain, Z.M. (2012). Electropolymerization of ortho-Phenylenediamine and its Use for Detection on Hydrogen Peroxide and Ascorbic Acid by Electrochemical Impedance Spectroscopy. *International Journal of Electrochemistry*, 7, 10154–10163. **DOI:**10.1016/S1452-3981(23)16266-3
81. Li, X.-G., Huang, M.-R., Yang Y-L. (2001). Synthesis and characterization of o-phenylenediamine and xylidine copolymers. *Polymer (Guildf),* 42, 4099–4107. **DOI:**10.1016/S0032-3861(00)00661-3
82. Lan, H., Muslim, A., Hojiahmat, M., et al. (2021). Morphology formation mechanism and electrochemical performance of poly(o-phenylenediamine) based electrode materials. *Synth Met,* 273, 116688.

DOI.org/10.1016/j.synthmet.2020.116688

83. Bourezgui, A., Al-Hossainy, A.F., El Azab, I.H., et al. (2021). Combined experimental and TDDFT computations for the structural and optical properties for poly (ortho phenylene diamine) thin film with different surfactants. *Journal of Materials Science: Materials in Electronics*, 32, 5489–5503. **DOI**.org/10.1007/s10854-021-05271-4
84. Su, C., Ma, J., Han, B., Xu, L. (2021). Preparation of graphene oxide/poly(o-phenylenediamine) hybrid composite via facile in situ assembly and post-polymerization technology for the anode material of lithium ion battery. *Journal of Solid State Electrochemistry,* 25, 535–544. **DOI.**org/10.1007/s10008-020-04827-4
85. Sousa, M.S.P., de Sá, A.C., de Oliveira, J.P.J., et al. (2020). Impedimetric Sensor for Pentoses Based on Electrodeposited Carbon Nanotubes and Molecularly Imprinted poly-o-phenylenediamine. *ECS Journal of Solid State Science and Technology*, 9(4), 041006. **DOI**.org/10.1149/2162-8777/ab85bd
86. Cheng, Y., LYX; YLY; YSG (2023). Poly-(o-Phenylenediamine)-Decorated V4C3Tx Mxene/Poly(o-Phenylenediamine) Blends as Electrode Materials to Boost Storage Capacity for Supercapacitors and Lithium-Ion Batteries. Cheng, Y., LYX; YLY; YSG (2023). Poly-(o-Phenylenediamine)-Decorated V4C3Tx Mxene/Poly(o-Phenylenediamine) Blends as Electrode Materials to Boost Storage Capacity for Supercapacitors and Lithium-Ion Batteries. *ACS Appl Nano Mater,* 6, 9186–9196. **DOI**.org/10.1021/acsanm.3c00624
87. Deng, W., Zhang, Y., Tan, Y., Ma, M. (2017). Three-dimensional nitrogen-doped graphene derived from poly-o-phenylenediamine for high-performance supercapacitors. *Journal of Electroanalytical Chemistry,* 787:103–109. **DOI.**org/10.1016/j.jelechem.2017.01.047
88. Chen, C., Qiu, S., Qin, S., et al. (2017). Anticorrosion performance of epoxy coating containing reactive poly (o-phenylenediamine) nanoparticles. *Int J Electrochem Sci*, 12, 3417–3431. **DOI.**org/10.20964/2017.04.47
89. Rahman, N., Nasir, M. (2018). Application of Box–Behnken design and desirability function in the optimization of Cd(II) removal from aqueous solution using poly(o-phenylenediamine)/hydrous zirconium oxide composite: equilibrium modeling, kinetic and thermodynamic studies. *Environmental Science and Pollution Research*, 25, 26114–26134. **DOI.**org/10.1007/s11356-018-2566-1
90. Smiley, R.A. (2000). Phenylene- and Toluenediamines. In: Ullmann's Encyclopedia of Industrial Chemistry. Wiley, **DOI.**org/10.1002/14356007.a19_405
91. Chan, .H.S.O., Ng, S.C., Hor, T.S.A., Sun, J., Tan,K.L., Tan, B.T.G. (1991). Poly(*m*-phenylenediamine): Synthesis and characterization by X-ray photoelectron spectroscopy. *European Polymer Journal,* 27(11), 1303-1308. **DOI.**org/10.1016/0014-3057(91)90069-Z
92. Kimura, Y., Tsucida A., Katsuraya, K. (2016). The Society of Fiber Science and Technology, Japan High-Performance and Specialty Fibers Concepts, Technology and Modern Applications of Man-Made Fibers for the Future. Springer, 1-451. ISBN 4431552030, 9784431552031.
93. Rebouillat, S., Steffenino, B. (2006). High performance fibres and the mechanical attributes of cut resistant structures made therewith. *In: WIT Transactions on the Built Environment. 86,* 279–299. **DOI:**10.2495/HPSM06028
94. Li, X.G., Huang, M. R., Duan, W., Yang, Y.L. (2002). Novel multifunctional polymers from aromatic diamines by oxidative polymerizations. *Chem Rev,* 102, 2925–3030. **DOI.**org/10.1021/cr010423z
95. Le, T. H., Kim, Y., Yoon, H. (2017). Electrical and electrochemical properties of conducting polymers. *Polymers, 9*(4), 150. **DOI.**org/10.3390/polym9040150
96. Ayankojo, A., Reut, G., Boroznjak, R., Öpik, A., Syritski, V. (2018). Sensors and Actuators B: Chemical Molecularly imprinted poly (meta-phenylenediamine) based QCM sensor for detecting Amoxicillin. *Sens Actuators B Chem,* 258, 766–774. **DOI:**10.1016/j.snb.2017.11.194
97. Amer I., Young, D.A., Vosloo, H.C.M. (2013). Chemical oxidative polymerization of m-phenylenediamine and its derivatives using aluminium triflate as a co-catalyst. *Eur. Polym. J,* 49, 3251–3260. **DOI.**org/10.1016/j.eurpolymj.2013.06.031
98. The colourful chemistry of artificial dyes. https://www.sciencehistory.org/education/scientific-biographies/william-henry-perkin/
99. Chatzi, E.G., Koenig, J.L. (1987). Morphology and Structure of Kevlar Fibers: A Review. *Polymer-Plastics Technology and Engineering*, *26*(3-4), 229-270.
100. Reashad, E., Kabir, B., Ferdous, E.N. (2012). Kevlar-The Super Tough Fiber. *International Journal of Textile Science,* 1(6), 78–83. **DOI.**org/10.5923/j.textile.20120106.04

101. Abdullayev, Y., Rzayev, R., Autschbach, J. (2022). Computational mechanistic studies on persulfate assisted p-phenylenediamine polymerization. *Journal of Computational chemistry Wiley Online Library, 43*,1313–1319. **DOI.**org/https://doi.org/10.1002/jcc.26943

102. Negi, A. (2025). Natural Dyes and Pigments: Sustainable Applications and Future Scope. *Sustain. Chem, 6*(3), 23. **DOI.**org/10.3390/suschem6030023

103. Meyer, A., Fischer, K. (2015). Oxidative transformation processes and products of para-phenylenediamine (PPD) and para-toluenediamine (PTD)—a review. *Environ Sci Eur*, 27(11). **DOI.**org/10.1186/s12302-015-0044-7

104. Xiong, S., Li, Z., Gong, M., et al. (2014). Covalently Bonded Polyaniline and para- phenylenediamine Functionalized Graphene Oxide: How the Conductive Two-dimensional Nanostructure Influences the Electrochromic Behaviors of Polyaniline. *Electrochim Acta*. *138*, 101–108. **DOI.**org/10.1016/j.electacta.2014.06.108

UDC: 544.72
DOI: https://doi.org/10.30546/2521-6317.2025.01.478

SYNTHESIS AND STUDY OF SURFACTANTS BASED ON TETRADECANOIC ACID, 1,2-DIAMINOETHANE AND N –(2-AMINOETHYL)-1,2-ETHANEDIAMINE

Amina N. ALIMOVA[1*], Ilhama A. ZARBALIYEVA[1,2,3]

[1]*Institute of Petrochemical Processes of the Ministry of Science and Education of the Republic of Azerbaijan, 30 Khojaly ave., AZ 1025, Baku, Azerbaijan*

[2]*Baku Higher Oil School, White City, 5 Khazar str., AZ 1025, Baku, Azerbaijan*

[3]*Azerbaijan State University of Economics (UNEC), 194 M.Mukhtarov str., AZ1065, Baku, Azerbaijan*

e-mail: alimova.amina91@gmail.com

ARTICLE INFO

Article history:
Received:2025-12-19
Received in revised form:2025-12-22
Accepted:2025-12-22
Available online

Keywords:
surface tension, surfactant, critical micelle concentration (CMC), thermodynamic parameters, oil-collecting

ABSTRACT

In this study, we synthesized and characterized the surface-active properties of products obtained from tetradeconoic acid, 1,2-diaminoethane and N –(2-amino-ethyl)-1,2-ethanediamine. The composition and structure of the synthesized compounds were confirmed by IR spectroscopy, and their physicochemical properties were determined. Aqueous solutions of the synthesized products were prepared over a wide range of concentrations, and their surface tension was measured using a tensiometer at the water-air interface. Based on the obtained data, isotherms were constructed for calculating key colloidal chemical parameters: critical micelle concentration, surface tension at CMC, maximum adsorption, (G_{max}), minimum surface area of the molecule at the air-water interface (A_{min}), surface pressure (π_{CMC}). Electrical conductivity properties were investigated using the conductometric method. Plots of specific electrical conductivity as a function of concentration were constructed, and the corresponding thermodynamic parameters, including the Gibbs free energy of micellization (ΔG_{mic}) and adsorption (ΔG_{ads}), were calculated. The oil-collecting capacity of the synthesized surfactant was studied under laboratory conditions against thin (<1 cm) films of Balakhany oil on the surface of waters with varying mineralization (seawater, freshwater, and distilled water). The effectiveness of the reagents was assessed both in their original form and in 5% aqueous solutions.

1. Introduction

Surfactants are amphiphilic molecules widely used in chemistry, biology, and pharmaceuticals [1]. They consist of a polar head group, which can be anionic, cationic, nonionic, or zwitterionic, and a hydrophobic tail, which can have varying lengths and structures. It is well known that surfactants form micelles at concentrations above the critical micelle concentration (CMC). Research into micellization processes has been conducted for many years, and thousands of papers on this topic are published annually [2-6]. The micellar behavior of anionic and cationic surfactants is influenced by the presence of nonelectrolytes in solution [7-9]. Much attention has also been paid to the effect of non-aqueous polar solvents on the micellization of cationic

surfactants [10-12]. Previously, Evans et al. [13] suggested that solvent hydrogen bonds are necessary for micelle formation. However, later studies showed that the structure of water and its hydrogen bonds are not always necessary for surfactant self-association [14-17].

2. Experimental part

Spectral analysis methods were employed to characterize the synthesized products. Infrared spectra were recorded using an ALPHA IR Fourier spectrometer (BRUKER, Germany) within the wavenumber range of 600–4000 cm^{-1}. UV–Vis spectra were obtained on a JENWAY UV/Vis 6850 dual-beam spectrophotometer operating in the 100–400 nm range with an optical resolution of 0.1 nm.

Surface tension measurements of aqueous surfactant solutions were conducted at 25 °C using a KSV Sigma 702 tensiometer (Attension Biolin Scientific, Finland) equipped with a Du Noy platinum ring. Specific electrical conductivity was measured with an ANION-402 conductometer (Russia).

Tetradecanoic acid (Aldrich, 98%), 1,2-diaminoethane (97%), N-(2-aminoethyl)-1,2-ethanediamine (97%), were used as starting materials. Thissalts were synthesized from tetradecanoic acid and each of the amine components. The obtained products exhibited a yellowish appearance. The salt synthesized from tetradecanoic acid and N-(2-aminoethyl)-1,2-ethanediamine in a 1:1 molar ratio formed at 70–85 °C over 10–11 h, producing a brownish solid, the salt synthesized from tetradecanoic acid and 1,2-diaminoethane in a 1:1 molar ratio formed at 70–80 °C over 10–11 h, producing a brownish solid. Surface tension values for distilled water (71.5 mN/m at 25 °C) aligned with standard reference values and were used to verify the measurement accuracy. Critical micelle concentration (CMC) values for the surfactants were determined from surface tension isotherms.

Electrical conductivity measurements were calibrated to 25 °C and showed a deviation of less than 1% from true values. Distilled water exhibited a conductivity of 2–2.8 μS/cm. After dissolving 0.025 g of each synthesized salt in 25 mL of distilled water, the conductivity of the solutions was measured, and CMC values were derived from conductivity–concentration plots.

Petrocollecting and petrodispersing properties of the synthesized surfactants were evaluated using established procedures. 40 mL of water with varying mineralization was placed in a Petri dish, followed by the addition of 1 mL of Balakhani crude oil forming a film of approximately 0.17 mm in thickness. A surfactant or its 5 wt.% solution was applied to the periphery of the oil film. The initial oil-film area and subsequent areas of dispersed oil patches were periodically measured. The surface-cleaning coefficient (K_d, %) was calculated as the ratio of the initial to the final oil-film area.

3. Results and discussion

The reaction schemes are presented below:

$C_{13}H_{27}COOH + H_2N\text{-}(CH_2)_2\text{-}NH_2 \rightarrow C_{13}H_{27}COOH^{\cdots} NH_2\text{-}(CH_2)_2\text{-} NH_2$

Salt of tetradecanoic acid with 1,2 diaminoethane (1)

$C_{13}H_{27}COOH + H_2N\text{-}(CH_2)_2\text{-}NH_2\text{-}(CH_2)_2\text{-}NH_2 \rightarrow C_{13}H_{27}COOH^{\cdots}NH_2\text{-}(CH_2)_2\text{-}NH_2\text{-}(CH_2)_2\text{-} NH_2$

Salt of tetradecanoic acid with N –(2-aminoethyl)-1,2-ethanediamine (2)

The structures of the synthesized salts were confirmed using Fourier-transform infrared spectroscopy (FTIR, BRUKER, Germany) in the wavenumber range of 600–4000 cm^{-1}, as well as UV–Vis spectroscopy. The corresponding spectra are presented below.

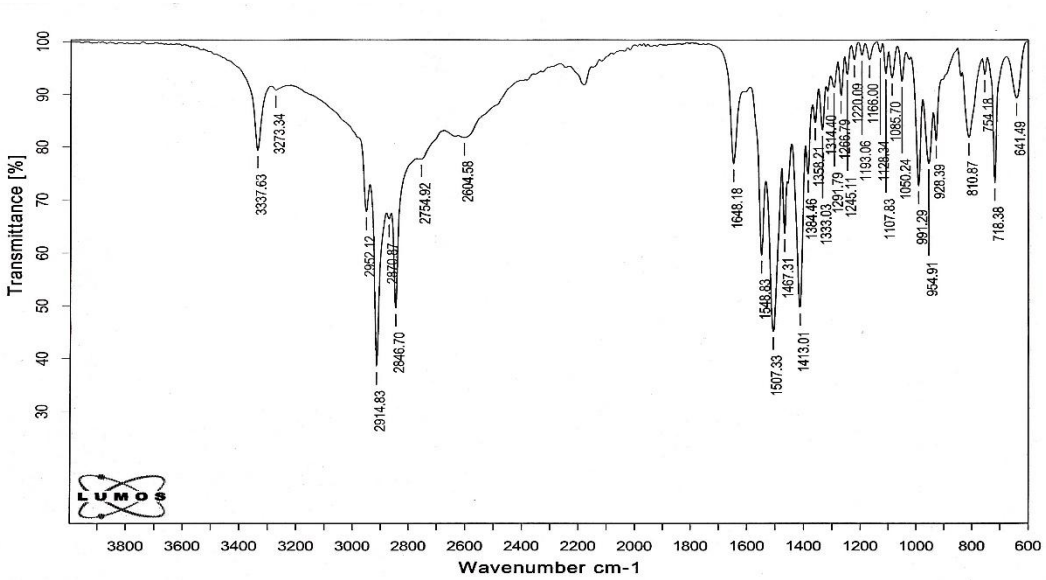

Fig. 1 IR spectrum of tetradecanoic acid salt with 1,2 diaminoethane

The IR spectrum of the sample (Fig. 1) contains the following absorption bands:

deformation (1467 cm^{-1}) and stretching (2846, 2870, 2914, 2957 cm^{-1}) vibrations of the C–H bond of the CH_3 and CH_2 groups; stretching (1050, 1085, 1107 cm^{-1}) vibrations of the C–O bond; stretching (1413, 1507 cm^{-1}) vibrations of the COO^- group; deformation (1548 cm^{-1}) and stretching (3273, 3337 cm^{-1}) vibrations of the H–N bond; ammonium band (2604, 2754 cm^{-1}).

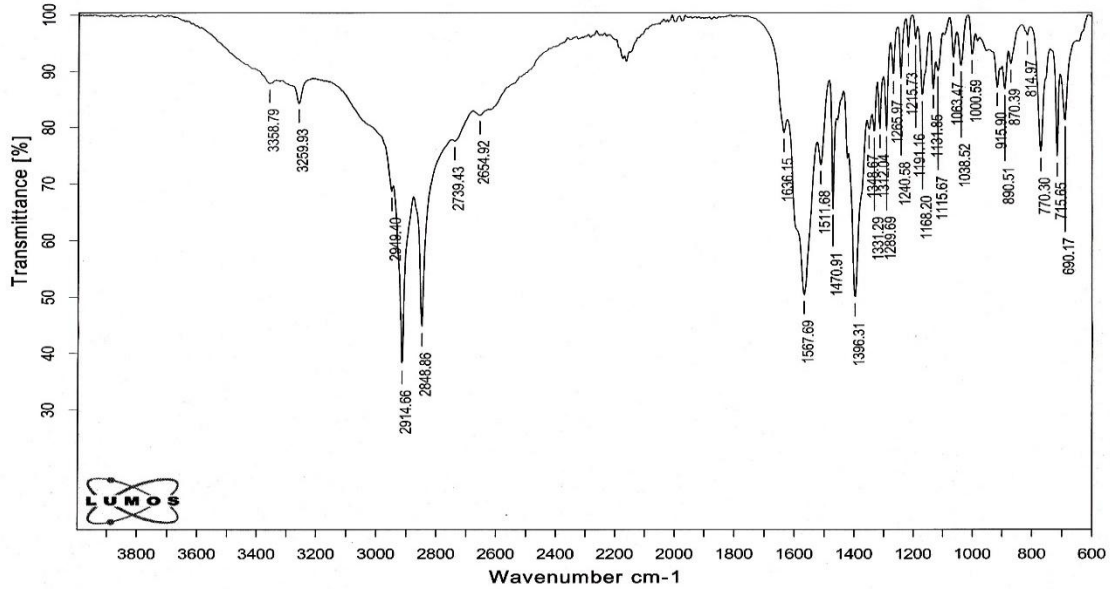

Fig.2 IR spectrum of tetradecanoic acid salt with N-(2-aminoethyl)-1,2-ethanediamine

The IR spectrum (Fig. 2) of a sample of the salt of tetradecanoic acid with N-(2 aminoethyl)-1,2-ethanediamine has the following absorption bands: deformation (1470 cm^{-1}) and stretching (2848, 2914, 2949 cm^{-1}) vibrations of the C–H bond of the CH_3 and CH_2 groups; stretching (1000, 1038,

1068 cm^{-1}) vibrations of the C–O bond; stretching (1396, 1567 cm^{-1}) vibrations of the COO^- group; deformation (1511 cm^{-1}) and stretching (3259, 3358 cm^{-1}) vibrations of the H–N bond; ammonium band (2654, 2739 cm^{-1}).

In Fig. 3, the absorption band n→σ*, belonging to the nitrogen atom, appears at 220 nm of the spectrum, in Fig. 4 - 230 nm.

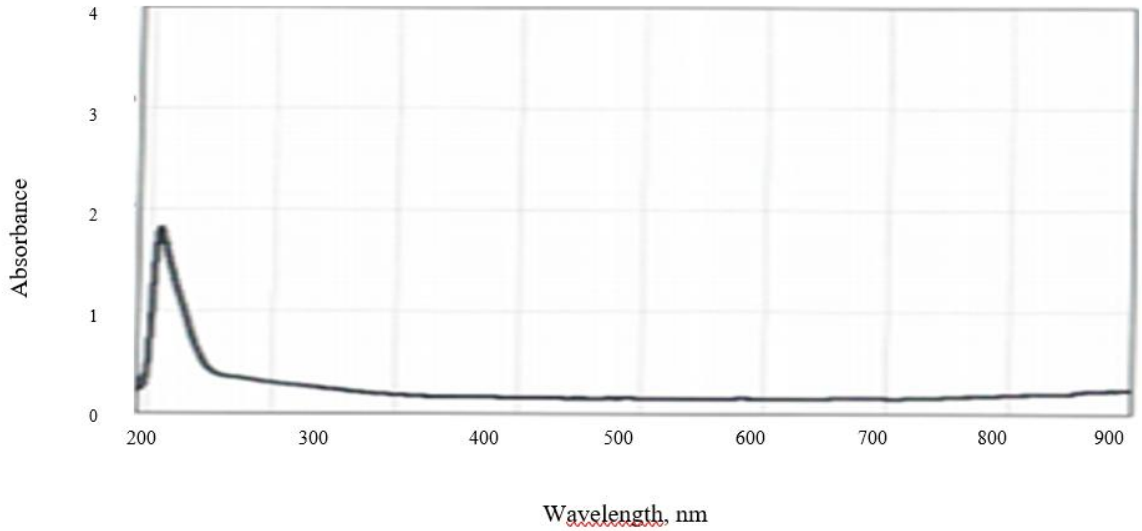

Fig 3 UV absorption spectrum of tetradecanoic acid salt with 1,2 diaminoethane

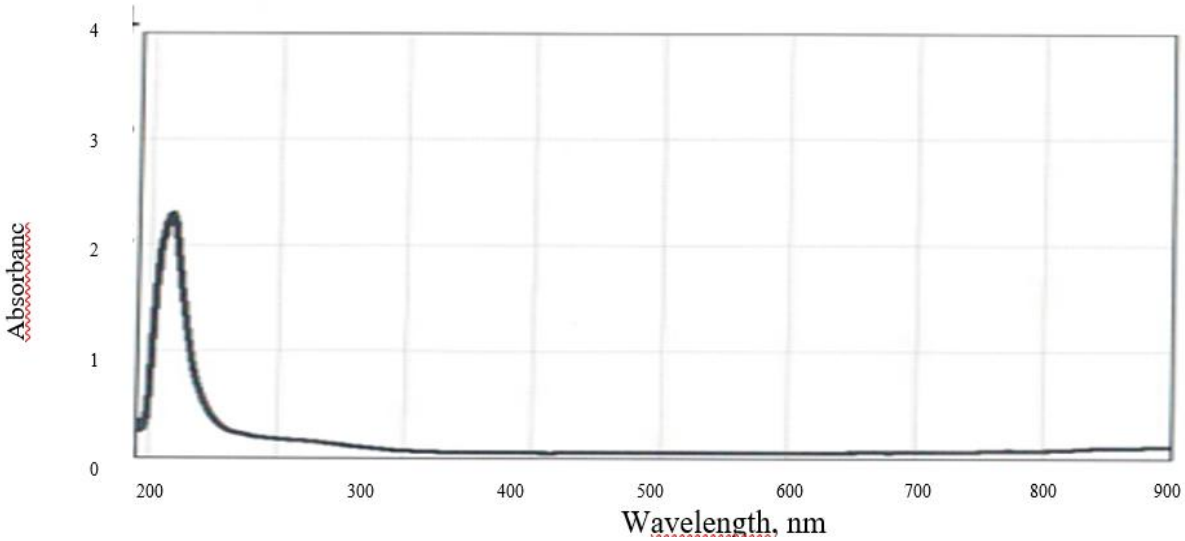

Fig. 4 UV absorption spectrum of tetradecanoic acid salt with N –(2-aminoethyl)-1,2- ethanediamine

Surface tension measurements of aqueous solutions of the synthesized surfactants were performed using a KSV Sigma 702 tensiometer (Attension Biolin Scientific, Finland) equipped with a Du Noy platinum ring at the air–water interface. This instrument was employed to evaluate the surface-active properties of this surfactants. The surface tension of the formed salts depending on various concentrations was determined from the graph in Fig. 5, the CMC (critical concentration of micelle formation) was determined.

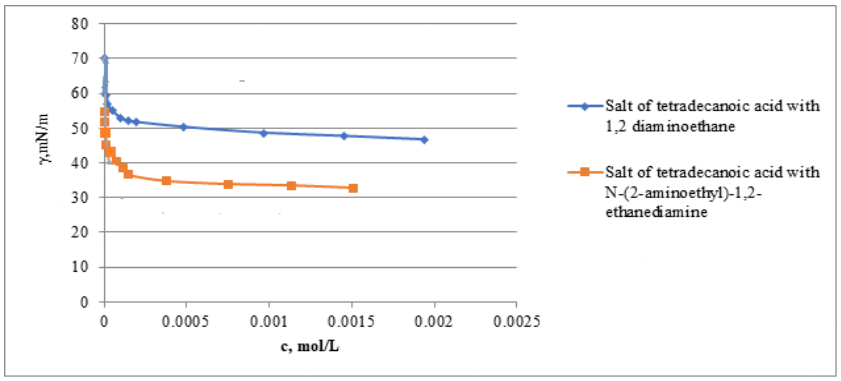

Fig.5 Surface tension diagram of surfactants at the water-air interface depending on the concentration

Table 1 summarizes the surface activity parameters of the synthesized surfactants, calculated from the data presented in Fig. 5. The critical micelle concentration (CMC) of the obtained salts was determined, along with the surface pressure at the CMC (π_{CMC}), $C_{(20)}$ (the concentration required to reduce the surface tension by 20 mN/m), adsorption efficiency

($pC_{20} = -\log C_{20}$), and the CMC/C_{20} ratio, which reflects the interfacial activity of the surface-active substances [18,19]. The maximum surface adsorption (Γ_{max}) and the minimum area per surfactant molecule at the water–air interface (A_{min}) were calculated using the equation given below.

$$\Gamma_{max} = \frac{1}{n * R * T} * \lim_{c \to CMC} \frac{d\gamma}{dlnc} \qquad (3)$$

where n is the number of dissociated ions, equal to 2 and 3, respectively, for the salt of tetradecanoic acid with 1,2 diaminoethane and N -(2-aminoethyl)-1,2-ethanediamine, R is the universal gas constant (8.314 J /mol·K), T—absolute temperature;

$$\mathbf{A}_{min} = \frac{\mathbf{1}}{N_A * \Gamma_{max}} \qquad (4)$$

Referring to Table 1, it can be said that the product of tetradecanoic acid with N –(2-aminoethyl)-1,2-ethanediamine has a minimum maximum adsorption value (Γ_{max}), it has a large surface area per surfactant molecule

Table 1. Results of surface activity of synthesized surfactants

Surfactants	CMC*10^4 (mol/l)	γ_{cmc} (mN/m)	π_{cmc} (mN/m)	C_{20}*10^4 mol/l)	pC_{20}	CMC/C_{20}	Γ_{max}*10^{10} (mol/sm^2)	A_{min}*10^2 (mm^2)
Salt of tetradecanoic acid with 1,2 diaminoethane	1.46	28.12	19	0.0003	3.46	0.42	0.73	227.48
Salt of tetradecanoic acid with N -(2-aminoethyl)-1,2-ethanediamine	1.4	26.58	34.98	0.075	5.12	0.54	0.67	248.23

As shown in Table 1, the salt of tetradecanoic acid with N -(2-aminoethyl)-1,2-ethanediamine exhibits the lower critical micelle concentration (CMC) and the highest surface pressure (26 mN/m). In contrast, the salt formed with 1,2 diaminoethane shows low value maximum adsorption value (Γ_{max}), indicating that each surfactant molecule occupies a larger interfacial surface area.

Figure 6 presents the electrical conductivity measurements of concentrated solutions of the synthesized salts, along with the corresponding plots of conductivity as a function of concentration. Based on these plots, several thermodynamic parameters related to electrical conductivity were determined; the calculated values are summarized in Table 2.

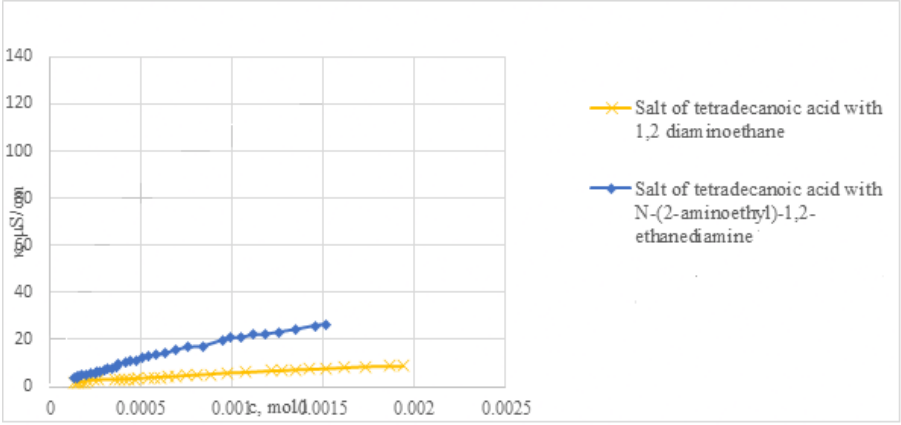

Fig. 6 Specific electrical conductivity of synthesized surfactants

The slopes of the linear regions before (S_1) and after (S_2) the critical micelle concentration (CMC) were determined. In addition, key thermodynamic parameters, including the Gibbs free energy of micelle formation (ΔG_{mic}) and the Gibbs free energy of adsorption (ΔG_{ads}), were calculated using the following equations

$$\Delta G_{mic} = (2-\alpha) * R * T * \ln(CMC)$$
$$\Delta G_{ads} = \Delta G_{mic} - 0.6023 * \pi_{CMC} * A_{min}, \quad (5)$$

where A_{min} represents the surface area of one surfactant molecule at the water-air interface at CMC [20].

Table 2. Parameters of the specific conductivity of the synthesized surfactants

Surfactans	α	β	Δ Gmic kJ/mol	Δ Gads, kJ/mol
Salt of tetradecanoic acid with 1,2 diaminoethane	0.84	0.13	-23.79	-26.6
Salt of tetradecanoic acid with N -(2-aminoethyl)-1,2-ethanediamine	0.45	0.54	-34.17	-39.49

As shown in Table 2, both the Gibbs free energy of micelle formation (ΔG_{mic}) and the Gibbs free energy of adsorption (ΔG_{ads}) are negative, indicating that these processes are thermodynamically spontaneous. Notably, for all three salts, ΔG_{ads} exhibits more negative values than ΔG_{mic}, suggesting a stronger thermodynamic preference for adsorption over micellization. This behavior is characteristic of surface-active substances, which tend to adsorb at interfaces prior to forming micelles [21,22].

In laboratory conditions, the petroleum-collecting ability of the synthesized surfactants was investigated, addressing the environmentally significant challenge of removing thin oil films from water surfaces. The experiments were conducted using a 0.17 mm Balakhan oil film in aqueous media with different degrees of mineralization, including distilled, fresh, and seawater. Salt of tetradecanoic acid with 1,2 diaminoethane, when applied in its undiluted form, exhibited petroleum-collecting activity in seawater for up to 6 days, with a collection coefficient of 13.51. The same surfactant, used as a 5 wt.% aqueous solution, also demonstrated oil-collecting

behavior, achieving a collection coefficient of 12.16. Salt of tetradecanoic acid with N-(2-aminoethyl)-1,2-ethanediamine showed superior petroleum-collecting performance, promoting more efficient oil film aggregation. In seawater, the maximum collection coefficient reached 20.26, and the retention time of the collected oil exceeded 6 days. These findings demonstrate the potential of the synthesized surfactants for mitigating oil contamination on water surfaces and highlight their prospective.

4. Conclusion

Tensiometric and conductometric methods investigations were employed to evaluate the properties of the surface-active substances in synthesized surfactants, and their key colloidal–chemical parameters were determined. Comparative analysis revealed the salt of tetradecanoic acid with N -(2-aminoethyl)-1,2-ethanediamine exhibits lower values of the critical micelle concentration, the minimum cross-sectional area of the polar group, surface pressure, and the efficiency parameter, as well as reduced surface tension at the CMC and lower maximum adsorption values. Laboratory experiments confirmed the effectiveness of the synthesized reagents in collecting thin oil films from water surfaces across a wide range of mineralization levels. Among the tested compounds, the salt of tetradecanoic acid with N -(2-aminoethyl)-1,2-ethanediamine demonstrated superior performance, highlighting its promise for the removal of environmentally hazardous oil films from natural water bodies. The obtained results support the feasibility of employing surfactants of this type in environmental protection

Acknowledgments.

This research was supported by the Azerbaijan Science Foundation Grant № AEF-MGC-2025-1(54)-20/15/4-M-15

LIST OF REFERENCES:

1. Bunton, C. A., Nome, F., Quina, F. H., & Romsted, L. S. (1991). Ion binding and reactivity in micellar solutions. *Accounts of Chemical Research*, *24*(12), 357–364.
2. Rosen, M. J. (2004). *Surfactants and Interfacial Phenomena* (3rd ed.). John Wiley & Sons.
3. Kresheck, G. S. (1975). Surfactants in water: A comprehensive treatise. In F. Franks (Ed.), *Water: A Comprehensive Treatise* (Vol. 4, pp. 95–107). Plenum Press.
4. Emerson, M. F., & Holtzer, A. (1967). On the hydrophobic bond in micellar systems: The effects of organic additives on the critical micelle concentration of dodecyltrimethylammonium bromide. *The Journal of Physical Chemistry*, *71*(10), 3320–3330.
5. Asadov, Z. H., & Zarbaliyeva, I. A. (2020). *New surfactants based on triglycerides, (ethanol)amines and orthophosphoric acid* (Monograph). Muallim Publishing House.
6. Ramadan, M. S., Evans, D. F., & Lumry, R. J. (1983). Role of hydrogen bonding in surfactant hydrophobicity. *The Journal of Physical Chemistry*, *87*(22), 4538–4543.
7. Ramadan, M. S., Evans, D. F., Lumry, R. J., & Philion, S. (1985). Influence of hydrogen bonding on the properties of surfactants. *The Journal of Physical Chemistry*, *89*(4), 3405–3410.
8. Bergenstähl, B., & Stenius, P. (1987). The mechanisms of the phase behavior of surfactants in water. *The Journal of Physical Chemistry*, *91*(23), 5944–5948.
9. Evans, D. F., Yamaguchi, A., Wei, G. J., & Bloomfield, V. A. (1983). Critical micelle concentrations in ethylammonium nitrate. *The Journal of Physical Chemistry*, *87*(3), 537–541.
10. Lattes, A., & Rico, I. (1989). Microemulsions in nonaqueous solvents. *Journal of Colloid and Interface Science*, *129*(2), 535–545. [Note: Source 10 title corrected based on journal archives for Lattes/Rico 1989].

11. El-Sharaky, E.-S. A., El-Tabey, A. E., & Mishrif, M. R. (2019). Novel star polymeric nonionic surfactants as crude oil emulsion breakers. *Egyptian Journal of Petroleum*, *22*(4), 779–793.
12. Greber, K. E. (2017). Synthesis and surface activity of cationic amino acid-based surfactants in aqueous solution. *Journal of Surfactants and Detergents*, *20*(1), 1189–1196.
13. Abo-Riya, M., Tantawy, A. H., & El-Dougdoug, W. (2016). Synthesis and evaluation of novel cationic Gemini surfactants based on guava crude fat as petroleum-collecting and dispersing agents. *Journal of Molecular Liquids*, *221*, 642–650.
14. Ao, M., Xu, G., Zhu, Y., & Bai, Y. (2008). Synthesis and properties of ionic liquid-type imidazolium surfactants. *Journal of Colloid and Interface Science*, *326*(2), 490–495.
15. Bergenstahl, B., & Stenius, P. (1987). The Journal of Physical Chemistry, *91*(23), 5944–5948.
16. Evans, D. F., Kaler, E. W., & Benton, W. J. (1983). Liquid-liquid phase separation in surfactant-oil-water systems. *The Journal of Physical Chemistry*, *87*(3), 533–537.
17. Chatterjee, A., Moulik, S. P., Sanyal, S. K., Mishra, B. K., & Puri, P. M. (2001). Thermodynamics of surfactant aggregation. *The Journal of Physical Chemistry B*, *105*(1), 128–139.
18. Zhang, T., Cao, X., Wang, X., & Changchun, S. (2017). Synthesis, surface activity and thermodynamic properties of cationic Gemini surfactants with diester and rigid spacers. *Journal of Molecular Liquids*, *230*, 505–510.
19. Galán, J. J., González-Pérez, A., Seijas, J. A., Uriarte, E., & Rodríguez, J. R. (2005). Physicochemical study of the self-aggregation of alkylpyridinium surfactants. *Colloid and Polymer Science*, *283*, 456–460.
20. Alimova, A. N., Zarbaliyeva, I. A., Nabiyeva, H. T., Ahmadbayova, S. F., & Aliyeva, N. M. (2025). Synthesis and research of surfactants based on dodecanoic acid with n,n`-bis(2aminoethyl)-1,2-ethanediamine and 1,2 epoxypropane. *Journal of Processes of Petrochemistry and Oil Refining*, *26*(3), 848–857.
21. Humbatov, H. H., & Dashdiyev, R. A. (1998). *Liquidation of accidental petroleum spills using surfactants*. Elm.
22. Zarbaliyeva, I. A., Nabiyeva, H. T., Alimova, A. N., Ahmadbayova, S. F., & Mammadov, A. M. (2024). Thermogravimetric and petrocollecting and petrodispersing study of the surfactants synthesized from the reaction of N1-(2-aminoethyl)ethane-1,2-diamine with fatty acids having different carbon chain length. *Azerbaijan Oil Industry Journal*, *8*, 38–44.

INSTRUCTIONS FOR AUTHORS

1. "The Baku Engineering University Journal-Chemistry and Biology" accepts original unpublished articles and reviews in the research field of the author.
2. Articles are accepted in English.
3. File format should be compatible with **Microsoft Word** and must be sent to the electronic mail (**journal@beu.edu.az**) of the Journal. The submitted article should follow the following format:

- Article title, author's name and surname
- The name of workplace
- Mail address
- Abstract and key words

4. The title of the article should be in each of the three languages of the abstract and should be centred on the page and in bold capitals before each summary.
5. **The abstract** should be written in **9 point** type size, between **100** and **150** words. The abstract should be written in the language of the text and in two more languages given above. The abstracts of the article written in each of the three languages should correspond to one another. The keywords should be written in two more languages besides the language of the article and should be at least three words.
6. . **UDC** and **PACS** index should be used in the article.
7. The article must consist of the followings:

- Introduction
- Research method and research
- Discussion of research method and its results
- In case the reference is in Russian it must be given in the Latin alphabet with the original language shown in brackets.

8. **Figures, pictures, graphics and tables** must be of publishing quality and inside the text. Figures, pictures and graphics should be captioned underneath, tables should be captioned above.
9. **References** should be given in square brackets in the text and listed according to the order inside the text at the end of the article. In order to cite the same reference twice or more, the appropriate pages should be given while keeping the numerical order. For example: [7, p.15].

Information about each of the given references should be full, clear and accurate. The bibliographic description of the reference should be cited according to its type (monograph, textbook, scientific research paper and etc.) While citing to scientific research articles, materials of symposiums, conferences and other popular scientific events, the name of the article, lecture or paper should be given.

Samples:

a) ***Article:*** Demukhamedova S.D., Aliyeva İ.N., Godjayev N.M.. *Spatial and electronic structure af monomerrik and dimeric conapeetes of carnosine üith zinc,* Journal of structural Chemistry, Vol.51, No.5, p.824-832, 2010

b) ***Book:*** Christie ohn Geankoplis. *Transport Processes and Separation Process Principles*. Fourth Edition, Prentice Hall, p.386-398, 2002

c) ***Conference paper:*** Sadychov F.S., Aydın C., Ahmedov A.İ.. Appligation of Information – Commu-nication Technologies in Science and education. II International Conference."*Higher Twist Effects In Photon- Proton Collisions", Bakı, 01-03 Noyabr, 2007, ss 384-391*

References should be in 9-point type size.

10. The margins sizes of the page: - Top 2.8 cm. bottom 2.8 cm. left 2.5 cm, right 2.5 cm. The article main text should be written in Palatino Linotype 11 point type size single-spaced. Paragraph spacing should be 6 point.
11. The maximum number of pages for an article should not exceed 15 pages
12. The decision to publish a given article is made through the following procedures:

- The article is sent to at least to experts.
- The article is sent back to the author to make amendments upon the recommendations of referees.
- After author makes amendments upon the recommendations of referees the article can be sent for the publication by the Editorial Board of the journal.